Characterization of Centreline Segregation of Continuously Cast Microalloyed Pipeline Steel

by

Pusong Wang

A thesis submitted in partial fulfillment of the requirements for the degree of

Master of Science

in
Materials Engineering

Department of Chemical and Materials Engineering
University of Alberta

Abstract

Quantitative electron microprobe analysis (EMPA) was used in this study to quantify the segregation of alloying elements (e.g., Mn, Si, etc.) at the centreline for continuous cast slabs and pipes of microalloyed steel exhibiting different Mannesmann Ratings. Elemental segregation levels at the centreline region were compared to the microhardness readings. Mn levels at the centreline were studied at various homogenization temperatures for a variety of times.

An EMPA elemental mapping technique was developed to quantify elemental distributions over a relatively large region of the centreline segregation band for continuous cast slab samples. Line scans for slab samples were conducted based on the EMPA maps. Segregation ratio (S.R.) was used to evaluate the level of elemental segregation in the centreline region. Peak Mn levels of 2.6 wt% (S.R. = 1.65) and 2.67 wt% (S.R. = 1.53) were found for Mannesmann 3 samples in the as-cast and pipe conditions, respectively. The peak Mn levels for Mannesmann 2 samples were 2.32 wt% (S.R. = 1.47) and 2.30 wt% (S.R. = 1.32). Image analysis showed that both slab and pipe samples have wider centreline segregation bands in Mannesmann 3 steels than in Mannesmann 2 steels.

Microhardness testing across the segregation band showed higher hardness values for the Mannesmann 3 samples relative to the Mannesmann 2 samples. In addition, the Mannesmann 3 samples had a higher hardness peak to average hardness ratio (P/A) than the Mannesmann 2 samples. The maximum microhardness values for slabs were 263 HV and 289 HV, with average values of 241 HV and 251 HV for Mannesmann 2 and Mannesmann 3 steels, respectively. This gives a P/A ratio as 1.09 and 1.15 for Mannesmann 2 slab and Mannesmann 3 slab respectively. For pipes, the Mannesmann 2 samples had a maximum microhardness value of 250 HV (P/A was 1.16), while the Mannesmann 3 samples had a maximum microhardness value of 303 HV (P/A was 1.55).

Homogenizations (1100 ˚C, 1200 ˚C, and 1300 ˚C) reduced Mn segregation at the centreline for both Mannesmann 2 and Mannesmann 3 slab samples. For the Mannesmann 2 samples, the Mn S.R. decreases most (from 1.54 to 1.08) at 1300˚C for 2 h, with average microhardness decrease from 241 HV to 208 HV. For the Mannesmann 3 samples, the Mn

S.R. decreases most (from 1.69 to 1.36) at 1100˚C for 16 h, with average microhardness decrease from 251 HV to 205 HV. S.R. decreased dramatically for single segregation band samples, while there was only a slight reduction for multiple segregation bands.

A macro analysis was used to distinguish the difference of segregation behaviour between Mannesmann 2 and Mannesmann 3 samples. The sum seg (SS) number was applied to microhardness, ferrite grain size, prior austenite grain size (PAGS), image analysis and Mn composition for slab samples, pipe samples and as-homogenized samples. The SS number indicates an increase level of segregation from Mannesmann 2 to Mannesmann 3 sample. In the future, a SS number database could be developed with more samples analyzed. This database provides a fast and easy way (using image analysis) to diagnose the casting process parameters for both research and industrial use.

Acknowledgements

First, I would like to express my thanks to my supervisor Professor Hani Henein and Professor Douglas Ivey for their continuous support of my Master study and relate research. Besides my supervisor, I would also like to thank Dr. Barry Wiskel. This thesis would not have been possible without his comments and inputs through the entirety of my research. Thanks to all post-doctoral fellows and students in the Advanced Materials and Processing Laboratory (AMPL) for guidance and discussions.

Special thanks to the sponsors including Evraz Inc. NA, Trans-Canada Pipelines, Enbridge Pipelines Inc., UT quality Inc. and Alliance Pipeline Ltd. along with the Natural Sciences and Engineering Research Council (NSERC) of Canada.

Last but not the least, thanks to my family: my parents and my wife for supporting and encourage me through this study.

Table of Contents

List of Tables

List of Figures

1. Introduction

Microalloyed steel is a low alloy steel (including niobium(Nb), vanadium(V), titanium(Ti), molybdenum(Mo), etc.) widely applications requiring good strength, toughness, and weldability. (Degarmo, 2003) The steel is produced using continuous casting, followed by homogenization and thermomechanical controlled processing (TMCP). These process steps yield the desired mechanical properties.

For continuous casting, solidification begins on the outside of the slab and proceeds inwards. Due to the greater solubility of the solute in the liquid than in δ iron, the liquid becomes enriched in solute atoms. The localized concentration differences between dendrite arms are called microsegregation. (Campbell, 2003) At the final stage of solidification, the enriched liquid will flow into the center of the slab due to convection. The combination of the porosity and elemental segregation at the end of solidification results in a phenomenon called macrosegregation known as centreline segregation. (Reger, 2014) The macrosegregation usually has a larger scale (in mm) than microsegregation (in μm).

Various slab rating systems are used to assess centreline segregation. The Mannesmann rating system is one method used to assess the quality of the continuous cast slabs. The Mannesmann rating is based on visual examination of HCl etched slab surfaces and is related to the size and continuity of dark dots. (Rapp, 2010) Lower Mannesmann rating is given for fewer dots have been found in the test samples, and represents a lower level of macrosegregation. Mannesmann 2 and Mannesmann 3 steels were interested in this work because they have similar properties and difficult to distinguish in the Mannesmann rating system.

Following continuous casting, a homogenization process is used to remove microsegregation developed in the continuous casting stage. (Fredriksson, 2006) During homogenization, alloy solutes will redistribute themselves in the slab by a diffusion controlled process. Microsegregation can be removed during homogenization treatment due the small distances, while macrosegregation could not. (Campbell, 2003) Temperature and time are the two major

factors in the homogenization process. (Lynch, 2011) Homogenization temperature affects diffusivity during the process and time controls the diffusion distance along with temperature.

Macrosegregation is the most important ones since it is hard to eliminate during homogenization. Also, it is known increasing number of alloying elements have a significant impact on the mechanical properties of pipe steel. For example, Mn is known to segregate to the centre of the slab. Beidokhti's research shows that a higher Mn content results in a higher sulfide stress cracking susceptibility due to harder phase forms during welding. (Beidokhti, 2009)

The aim of this work is to quantify the centreline segregation band and to establish and optimize a quantitative element detection method using electron microprobe analysis (EMPA). Samples with different Mannesmann ratings are compared in terms of appearance (width of the centreline segregation band), microhardness and elemental segregation. Comparison between different temperature and time combinations for both Mannesmann 2 and 3 slabs are done using homogenization experiments. Finally, the Sum Seg (SS) analysis compares the difference between Mannesmann 2 and 3 samples in microhardness, ferrite grain size, prior austenite grain size, image analysis and Mn composition.

2. Literature Review

As introduced in the previous chapter, centreline segregation has a significant impact on the mechanical properties of microalloyed pipeline steels. This chapter will review the role of manganese (Mn) in microalloyed steels, centreline segregation of continuous cast slabs of microalloyed steel, the Mannesmann rating system used for evaluating centreline segregation of continuous casting slabs, the effect of homogenization on reducing centreline segregation, and the methodology and application of electron microprobe analysis (EMPA) for quantifying elemental segregation.

2.1 Role of Mn in Microalloyed Steel

This section introduces the effect of additional Mn on microalloyed steels. Microalloyed steel is a type of low carbon steel (less than 0.1 wt% C and 2 wt% Mn) with minor amounts (less than 0.15 wt%) of alloying elements, e.g., niobium, vanadium, titanium and others. (Degarmo E. P., 2003) The additional alloying elements play the important role of refining the grain size during thermomechanical controlled processing (TMCP) and enhance the strength of the steel by precipitation hardening. These improvements benefit both the strength and toughness of the steel. (Siwecki, 1995) (Zajac, 1991)

Mn is the alloying element with the highest mass in microalloyed steels. Mn affects the mechanical properties in multiple ways. The addition of Mn (and Ni) decreases the austenite-ferrite transformation temperature during solidification. (Bain, 1939) However, the Mn in excess of ~1 wt% may increase the level of centreline segregation for continuous casting. (Williams, 1995) Mn increases the strength of the steel and is an important element in solid solution strengthening. (Zhao, 2003) A phenomenon connected to “uphill diffusion theory” indicates that higher Mn concentration results in lower carbon activity and affects the diffusion of carbon. This phenomenon explains possible carbon segregation at the centreline region and confirms chemical potential is the driving force for diffusion. (Krauss, 1990) This segregated carbon at the centreline could change the path during solidification, and effect mechanical property. As shown in Figure 2.1, Mn increases ferrite microhardness values significantly for Mn levels exceeding 1 wt%. (Thelning, 1984) As a result of all the above

phenomena, microhardness values for ferrite increase from 80 HV to 165 HV as Mn increases from 1 wt% to 4 wt%. (Thelning, 1984)

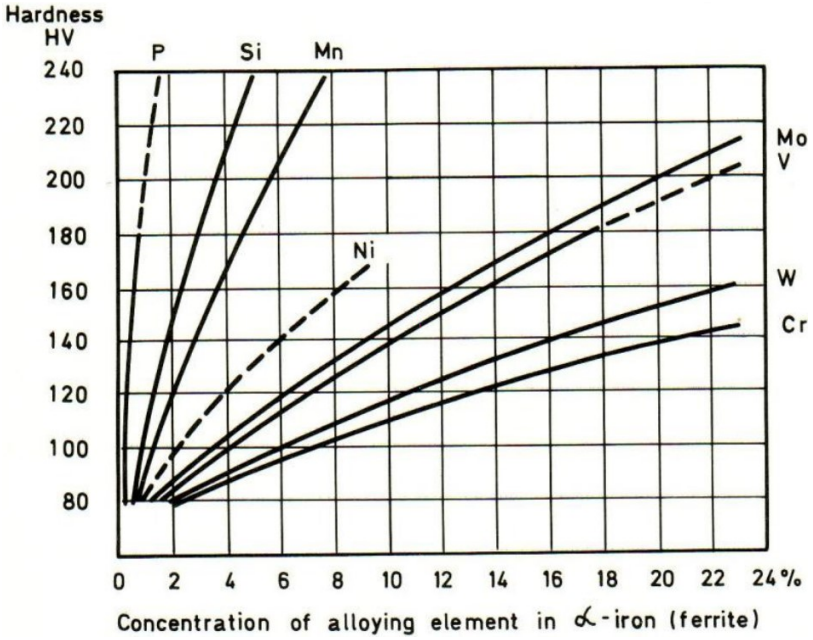

Figure 2.1 Effect of substitutional alloying element additions on ferrite hardness. (Thelning, 1984)

2.2 Continuous Casting of Microalloyed Slabs

Microalloyed pipeline steels are typically produced using continuous casting process. Segregation of solutes occurs in continuous casting of microalloyed steels. There are two types of segregation in continuous cast steel slabs, microsegregation, and macrosegregation. Continuous casting process, centreline segregation phenomena, and consequences of the centreline segregation for pipeline steels will be introduced and discussed in this section.

2.2.1 Continuous Casting

Continuous casting is a well-known steelmaking process. As shown in Figure 2.2, the molten metal flows from the ladle into the tundish and then into the water mold. The molten steel starts solidifying in a water-cooled mold and forms a solid shell at the outside of the slab. The liquid with the solid shell continues solidifying through the support rolls as water is

sprayed on both sides of the slab. Casting speed refers to the slab velocity. At the cut-off point in Figure 2.2, a torch is used to cut the slabs to desired lengths.

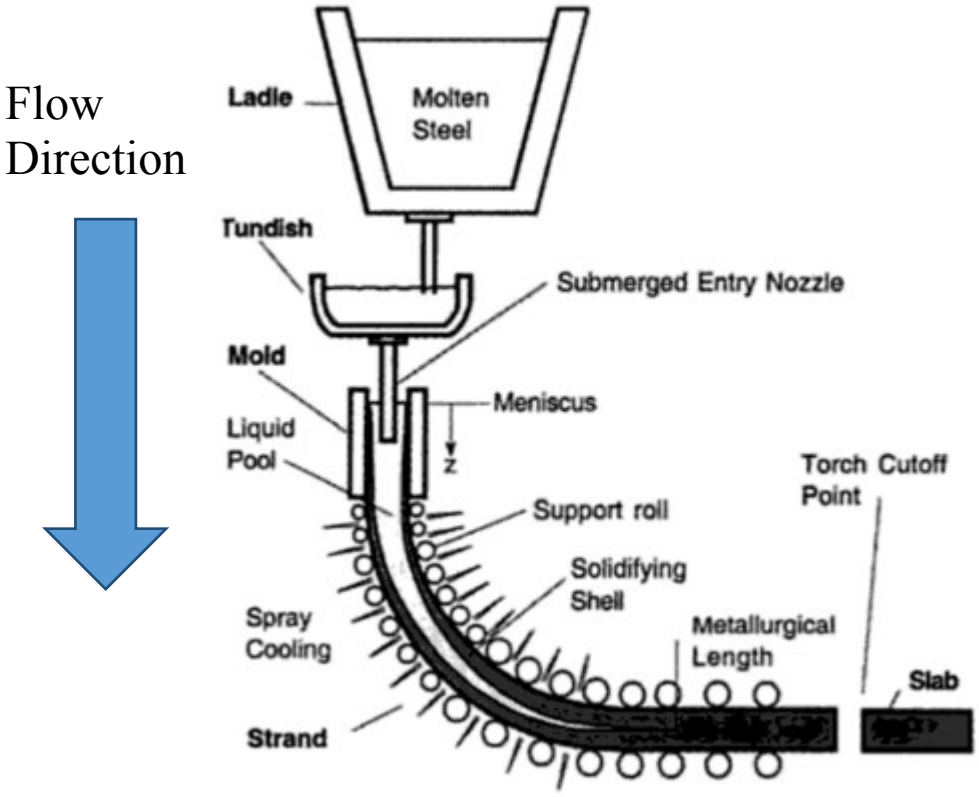

Figure 2.2 Schematic of continuous casting. (Thomas, 2001)

2.2.2 Centreline Segregation in Continuous Cast Slabs

The basic principles of the formation of microsegregation in cast alloys are well known. During solidification, crystals are formed and solute elements are rejected from the crystals into the liquid, due to their low solid solubility. As the temperature decreases, the solubility of solute elements also decreases in the solidified crystal. The solute enriched liquid in the interdendritic regions is solidified and is referred to as microsegregation. For the solute enriched liquid in front of the solid-liquid interface, macrosegregation appears as a result of diffusion and convection (physical movement of the liquid). (Ghosh, 2001) Centreline segregation in continuous cast slabs is a typical example of macrosegregation and is an important indicator of the quality of steel products. Macrosegregation, thus, manifests itself

in the variation in the composition of alloying elements on the scale of several millimeters to centimeters within a slab. The segregation ratio (S.R.) is used to indicated the level of segregation. This S.R. equals to the detected peak wt% divided by the nominal wt%.

A Thermo-Calc prediction calculation of alloying element composition during solidification was done by Davis using a version Q on the pipeline steel (Fe-0.03C-0.25Si-1.70Mn-0.008P-0.005S-0.052Al-0.082V-0.063Nb). (Davis, 2009) The maximum ratio (same as S.R.) of these elements between last liquid and the first solid during solidification in this pipeline steel were compared in Table 2-1. Mn and Si have an S.R. of 1.69 and 2.57, respectively. (Davis, 2009) Another prediction model gives a Mn S.R. of 1. 38. (Won, 2010) Won predicted this Mn S.R. using a finite difference model based on a Fe-0.13C-0.35Si-1.52Mn-0.016P-0.002S system. This model assumed complete mixing of solute in the liquid and local equilibrium at the liquid/δ, liquid/γ, and δ/γ interface.

C and Nb have larger S.R. than Mn and Si and they tend to form precipitates. The large Nb (C, N) precipitates in Figure 2.3 were observed in the centreline region. Energy dispersive x-ray spectroscopy (EDS) was used to identify the precipitates. (Davis, 2009)

Table 2-1 Thermo-Clac simulation results (in wt%) and maximum ratio. (Davis, 2009)

Elements	Nominal Concentration (wt%)	First Solid	Last Liquid	Max. Ratio
C	0.03	0.0043	0.2022	47.02
Si	0.25	0.159	0.408	2.57
Mn	1.7	1.471	2.491	1.69
Nb	0.082	0.0128	0.3113	24.32

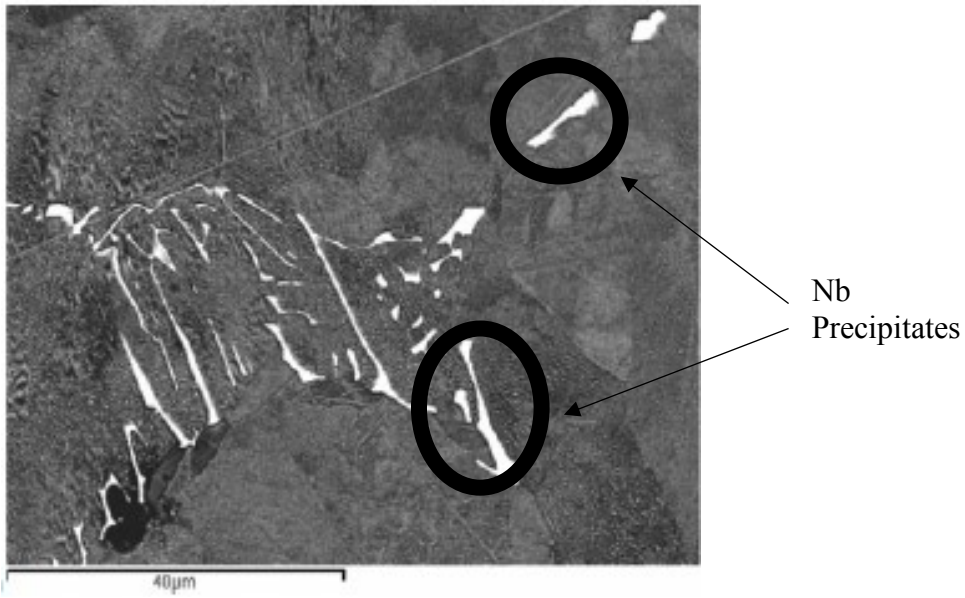

Figure 2.3 Large Nb(C,N) particle at the centreline position. (Davis, 2009)

Microstructure inhomogeneity at the centreline region has also been reported for this pipeline steel. As shown in Figure 2.4, there is approximately 10% volume fraction (arrow pointed) of pearlite found at the centreline segregation region (middle thickness of the slab). For rest of the slab, there is 2-4% pearlite (circled) founded. (Davis, 2009) This additional pearlite at the centreline segregation region is expected to increase the microhardness value at the centreline.

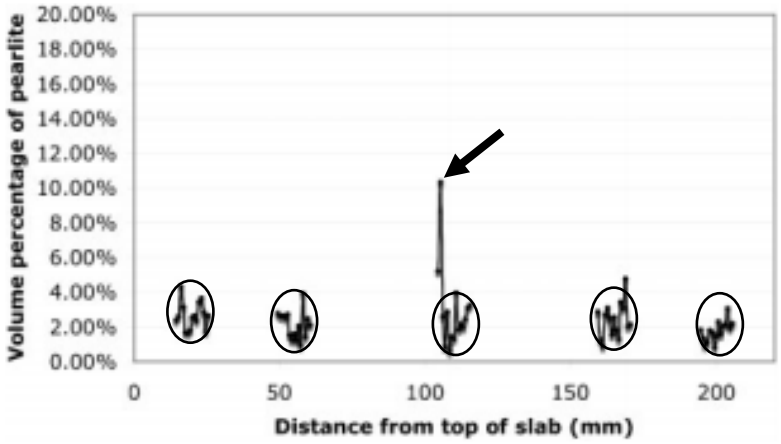

Figure 2.4 Pearlite volume fraction in steel slab. (Davis, 2009)

The formation of hard phases and those precipitates can arise from this centreline segregation and may result in a greater hydrogen induced cracking and/or sulfide stress cracking susceptibility. (Lesoult, 2005) Beidokhti's research showed that 2 wt% Mn results in higher SSC susceptibility than the 1.4 wt% Mn samples in weld condition due to the higher hardness values resulting in the welds. (Beidokhti, 2009)

2.2.3 Consequence of Segregation

As discussed above, macrosegregation occurs during continuous casting of microalloyed steel. The formation of hard phases can arise from this centreline segregation and may result in a greater hydrogen induced cracking and/or sulfide stress cracking susceptibility. (Beidokhti, 2009) (Tsuchida, 1984) (Lesoult, 2005) Also, weldability, impact strength, and toughness are effected by the level of macrosegregation. (Devillers, 1988)

Si segregation has an impact on CCT diagram. Figure 2.5 shows the change in CCT diagram as Si increases from 1.0 wt% to 2.0 wt% based on the Fe-0.2wt%C-1.5wt%Mn system. The transformation from austenite to pearlite has been delayed by increasing Si from 1.0 wt% to 2.0 wt% (Tsukatani, 1991) Bainite start temperature increase as Si wt% increases. This change in CCT diagram is due to the increase in carbon activity of ferrite with increase Si. (Tsukatani, 1991)

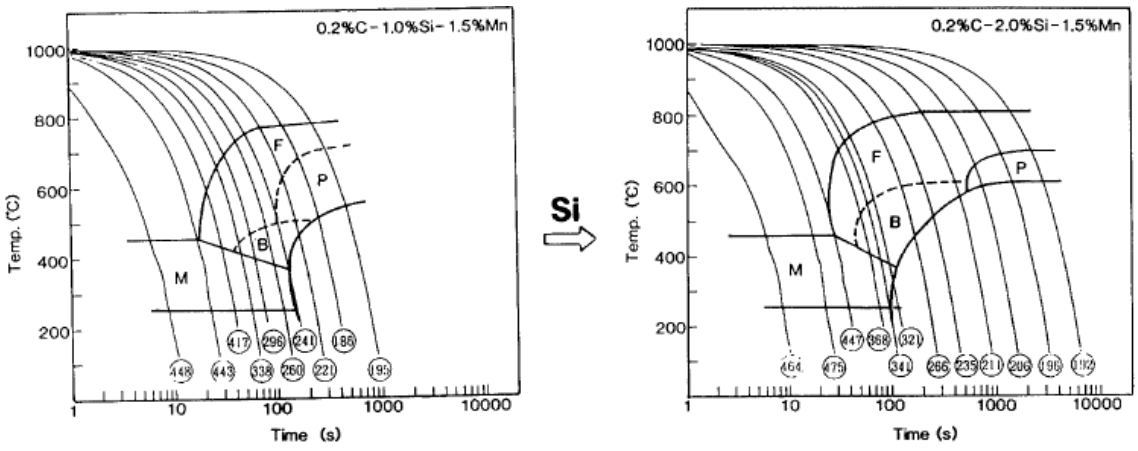

Figure 2.5 Change in CCT diagram as Si increase from 1.0 wt% to 2.0wt% on Fe-0.2wt% C-1.5wt%Mn system. (Tsukatani, 1991)

Figure 2.6 presents chemical composition and mean microhardness values of a base metal and several weld metals prepared for SSC test. Highlighted in Figure 2.6 are Mn wt% in these steels and correspond microhardness values. There are two groups of the weld metal, group L and group H with Mn wt% around 1.4 and 2.0 respectively. (Beidokhti, 2009) Figure 2.7 is the summary results of SSC tests, and in general, the group H (2.0 wt% group) has higher SSC susceptibility than the group L (1.4 wt% group). These results reflect the additional solute at the centre of the slab could increase cracking susceptibility. Evaluation of the slab segregation level could be critical to ensure pipe quality.

Composition (%)	C	Si	Mn	P	S	Cr	Ni	Mo	V	Ti	Nb	Hardness (HV)
Base metal	0.08	0.23	1.55	0.025	0.013	0.17	0.02	0.01	0.005	0.03	0.03	190
Weld No. L00	0.03	0.17	1.32	0.021	0.009	0.09	0.02	0.25	0.005	0.009	0.01	198
Weld No. L10	0.03	0.20	1.35	0.013	0.010	0.09	0.03	0.28	0.005	0.03	0.01	209
Weld No. L20	0.04	0.23	1.40	0.016	0.011	0.10	0.03	0.24	0.008	0.08	0.01	222
Weld No. L30	0.05	0.25	1.42	0.019	0.010	0.10	0.04	0.28	0.008	0.11	0.02	255
Weld No. L40	0.06	0.27	1.48	0.017	0.008	0.09	0.03	0.29	0.010	0.17	0.02	268
Weld No. H00	0.04	0.20	1.90	0.025	0.011	0.08	0.02	0.29	0.008	0.004	0.01	214
Weld No. H10	0.05	0.27	1.92	0.024	0.010	0.08	0.02	0.28	0.010	0.02	0.01	226
Weld No. H20	0.05	0.25	2.00	0.022	0.010	0.08	0.02	0.28	0.010	0.05	0.01	233
Weld No. H30	0.07	0.30	2.14	0.020	0.013	0.08	0.03	0.29	0.009	0.11	0.02	288
Weld No. H40	0.07	0.33	2.15	0.022	0.012	0.09	0.02	0.28	0.010	0.16	0.02	307

Figure 2.6 The chemical composition and mean hardness values of the base metal and weld metals for SSC test. (Beidokhti, 2009)

Group L				Group H			
	80% YS	110% YS	Max. hardness (HV)		80% YS	110% YS	Max. hardness (HV)
L00	P*	P	202	H00	P	FN	218
L10	P	P	211	H10	P	P	232
L20	P	P	225	H20	P	FN	240
L30	P	P	260	H30	FN	CF	292
L40	FN	FN	275	H40	FN	CF	323

* P: pass; FN: failure by NACE criterion; FI: failure by internal investigation; CF: complete fracture.

Figure 2.7 The results SSC test for group L and group H weld metals on X70 pipe steel. (Beidokhti, 2009)

2.3 Evaluation of Macrosegregation

As discussed in the previous section, the centreline segregation has a huge impact on the mechanical properties of steels. This section will introduce the method used to evaluate centreline segregation in the industry now.

In production, steelmaking companies use a method called “Mannesmann Rating System” (MR) to evaluate the amount of centreline segregation for their cast slabs. This assessment is used to meets specifications of pipe quality. To assess a cast slab, macroetching is required for Mannesmann ratings (MR). Hot HCl acid is typically used as the macro etchant. (Rapp , 2010) Figure 2.8 shows an example of centreline segregation in a continuous cast slab. According to Fumio and Isamu, the black dots (circled) shown in Figure 2.8 may be phosphides that contain Fe, Mn and P. (Kurosawa, 1990)

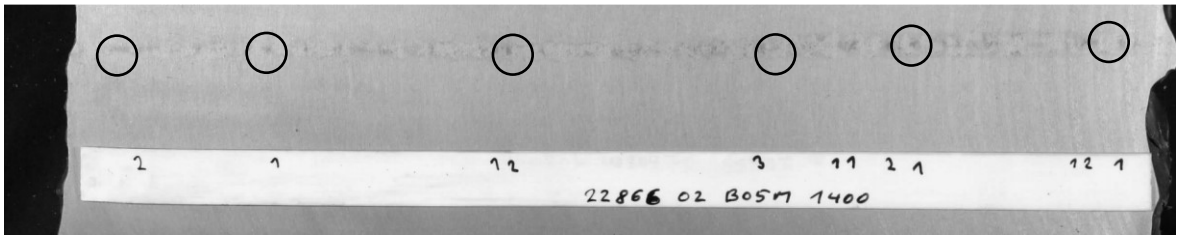

Figure 2.8 Example of visual inspection of centreline segregation. (Valek, 2011)

Dots like those seen in Figure 2.8 are measured for size and continuity. These measurements are then used to determine a Mannesmann rating for the steel in industry. There are 4 different classes in the MR rating system. Areas with high numbers have a higher amount of centreline segregation. The assessment method for different classes, specified by Spectra Energy, is shown in Table 2-2. (Rapp, 2010)

Table 2-2 Assessment method for Mannesmann rating system. (Rapp, 2010)

MR	Continuity	Density	Dot Size
		Dots Per 100 mm	
1	Not Continuous	10 or less	1mm to 3mm
2	Not Continuous	11 to 18	1mm to 5mm
		Maximum 5	3 mm to 5mm
	Not Continuous	At least 1	≥5mm
3	Not Continuous	19	All Sizes
	Not Continuous	6	3mm to 5mm
4	Continuous	Continuous dots more than 10 mm in length and 1mm in thickness.	

2.4 Homogenization

Method used to evaluate the centreline segregation for pipeline steels was reviewed. Homogenization is widely used in the steel industry as one of the major tools to minimize inhomogeneity of segregated elements that developed during casting. In this section, the role of the homogenization process in steel processing will be discussed in more detail. Then, the effect of homogenization temperature on Nb precipitates dissolution for microalloyed steels will be reviewed.

2.4.1 The Role of Homogenization

The major objective of the homogenization process is to reduce the amount of segregation. The austenite grain size increases and solutes redistribute during homogenization process.

Table 2-3 shows the effect of homogenization on the austenite grain size. The austenite grains grow after homogenization at 1200 °C for various times. The grain size increases from 1.02 mm to 1.13 mm after 3 hours and reaches 2.6 mm after 13 hours. The microhardness

values decrease as the austenite grain size increases. Figure 2.9 (a) compares the average austenite grain size and average ferrite grain size for microalloyed steel. Ferrite grain size increases as austenite grain size increases at the same retained strain and accelerated cooling rate. Figure 2.9 (b) is the microhardness value as a function of ferrite grain size. The Petch relationship is found, and microhardness decreases as ferrite grain size increases. Thus, microhardness value will decrease after homogenization due to the increasing size of austenite grain size.

Table 2-3 Austenite grain size after homogenization at 1200 °C from 3 to 13h. (Eskandari, 2008)

Sample Condition	As-cast	Homogenized					
		3h	5h	7h	9h	11h	13h
Grain Size (mm)	1.02	1.13	1.46	1.74	2.28	2.46	2.60

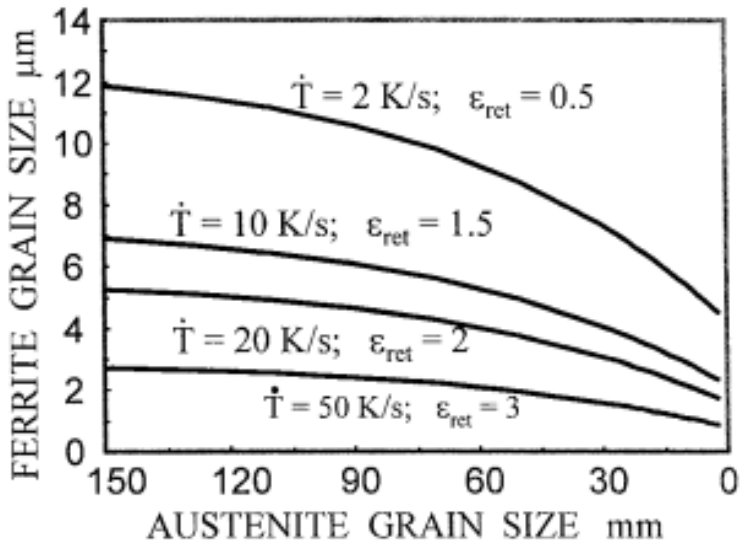

(a)

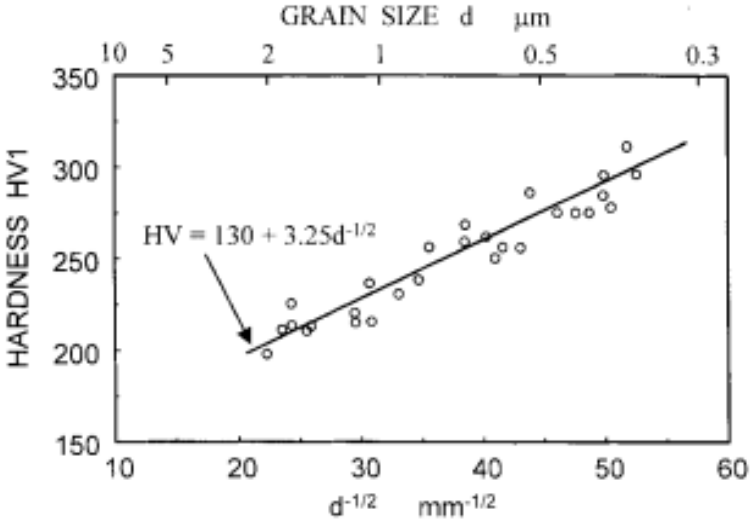

(b)

Figure 2.9 (a) Predictions of ferrite grain size as a function of austenite grain size and (b) Measured Microhardness as a function of ferrite grain size for microalloyed steel. (Priestner, 2000)

Elemental segregation occurs during continuous casting, and enriched areas are found within the interdendritic regions and centreline of the slabs. (Aboutalebi, 1995) The homogenization process is used to reduce elemental segregation within the interdendritic regions but does not affect the regions affected by macrosegregation. (Lippard, 1998) Figure 2.10 shows the level of segregation reduction for Ni, Mo, and Ti in the steel during homogenization. The

approximate segregation ratio reductions after 4 hours of homogenization at 1232 °C for Ni, Mo and Ti are 32%, 45%, and 60%, respectively. (Cox, 1967)

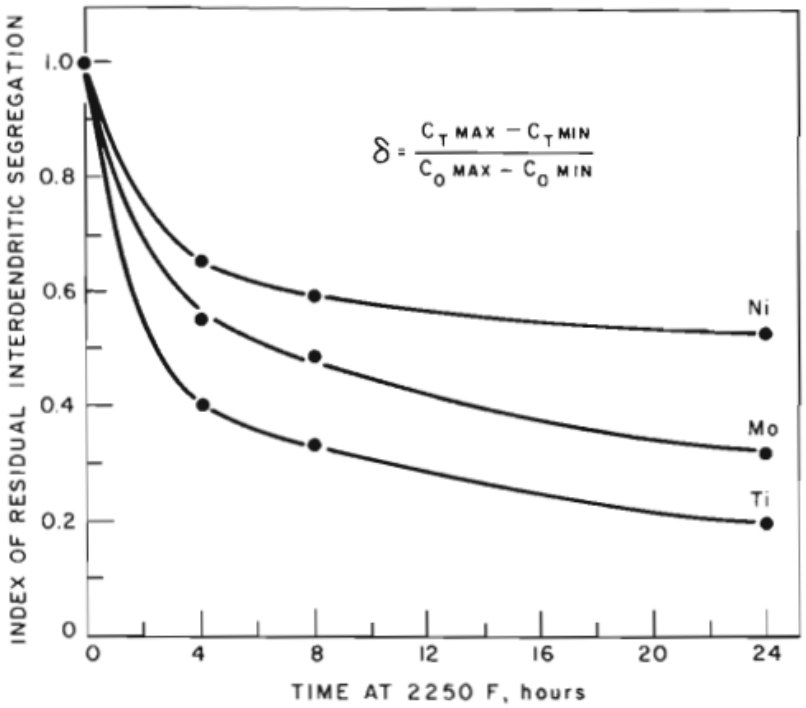

Figure 2.10 Example of reduction of elemental segregation after homogenization at 1232 °C for 4 h. (Cox, 1967)

2.4.2 Nb Precipitates Dissolution

Nb affects the three critical temperatures of austenite, T_{GC} (grain-coarsening temperature), T_{RXN} (the recrystallization-stop temperature), and Ar_3 (the transformation temperature). (Palmiere, 1994) Figure 2.11 summarizes the steel bulk wt%, precipitate composition, T_{DISS}^{OBS}(oberserved dissolution temperature), T_{DISS}^{CALC} (calculated dissolution temperature), and T_{GC}. Steel E4 (highlighted) has similar chemistry than the one used in this study. NbC precipites were observed for steel E4, with possible N presented noted as $NbC_{0.8}$. The calculated dissolution temperature for E4 is 1321 ˚C which agrees observed temperature. (Palmiere, 1994) 1300 ˚C will be the target temperature to dissolve Nb precipitates in this study.

Present Study							
	Bulk Compositions (Wt Pct)			Precipitate	T_{DISS}^{OBS}	T_{DISS}^{CALC}	T_{GC}
Steel	Nb	C	N	Composition	(°C)	(°C)	(°C)
E1	0.049	0.090	0.008	$NbC_{0.8}$ NbC	~1300	1247	1100
E2	0.048	0.080	0.024	$NbC_{0.67}N_{0.33}$ $NbC_{0.8}N_{0.07}$	>1300	—	1150
E3	0.020	0.080	0.008	$NbC_{0.8}$ NbC	1100	1107	1000
E4	0.090	0.080	0.008	$NbC_{0.8}$ NbC	>1300	1321	1200

Figure 2.11 Summary of grain-coarsening temperature, precipitate composition, and dissolution temperature for microalloyed steel during homogenization. (Palmiere, 1994)

2.5 Electron Microprobe Analysis (EMPA)

As discussed segregation conditions above, the elements segregation needs to be quantified in this study. There are several techniques could evaluate the level of the centreline segregation.

Mannesmann rating system is a qualitative method to evaluate the level of the centreline segregation. Energy dispersive X-ray analysis (EDX) and electron microprobe analysis (EMPA) can be used to quantify centreline segregation and, from the EMPA data, a segregation ratio (S.R.) can be determined. (Tsuchida, 1984) (Davis., 2009) EMPA is commonly used to quantify elemental segregation at the centreline due to its lower detection limit and higher detection accuracy than EDX. (Goldstein, 2012) The electron probe microanalyzer (EPMA or EMPA) is an analytical element detection tool carried out on a smooth surface (fine polished). The EPMA can provide both quantitative and qualitative wavelength dispersive spectroscopy (WDS) and energy dispersive spectroscopy (EDS) for elements from C to U. (Laboratory, 2015)

In this section. EMPA setup, major parameters, coating method, mapping method, and elements detection in previous researches for microalloyed steels were reviewed.

2.5.1 EMPA

Similar to an SEM, EPMA uses a filament to generate an electron beam as shown in Figure 2.12. The distinguishing difference between an EPMA and SEM is that the EPMA has an adjustable beam current. The energy detection is located below liquid nitrogen container. (squared in Figure 2.12) The wavelength detector is based on the dispersed wavelength of the analyzed specimen as shown in the right lower corner (circled) in Figure 2.12. (Hall, 1966) Electrons are generated from the filament at the top of the instrument. Electrons hit the sample surface and emit X-rays at specific or characteristic wavelengths (energy). (Birks, 1971) This emitted X-ray wavelength (energy) is collected by a wavelength dispersive X-ray spectrometer (WDS) or an energy dispersive X-ray spectrometer (EDS), respectively, as shown in Figure 2.12. (Verlt, 1994)

EDS collects all energies of the emitted X-rays produced from the sample. EDS has a lower detection range than WDS, due to the poor X-ray peak energy resolution and peak overlap. (Martiny, 2008) WDS selects the X-ray wavelength of interest by using a designated diffraction crystal and collects using a sealed detector (circled in Figure 2.12). (Reed, 1996) WDS has a relatively higher detection limit (0.01 wt%) (Goldstein, 1992), while EDS typically has its limit at 0.08 wt%. (Reed, 1996)

The chemical composition is calculated from the ratio of the counts of characteristic X-rays from the tested material (unknown concentration) to the counts of standards (known concentration). (Kuisma-Kursula, 2000) The accuracy of the detection depends on the experimental parameters and sampling, which will be discussed in the next following two sections.

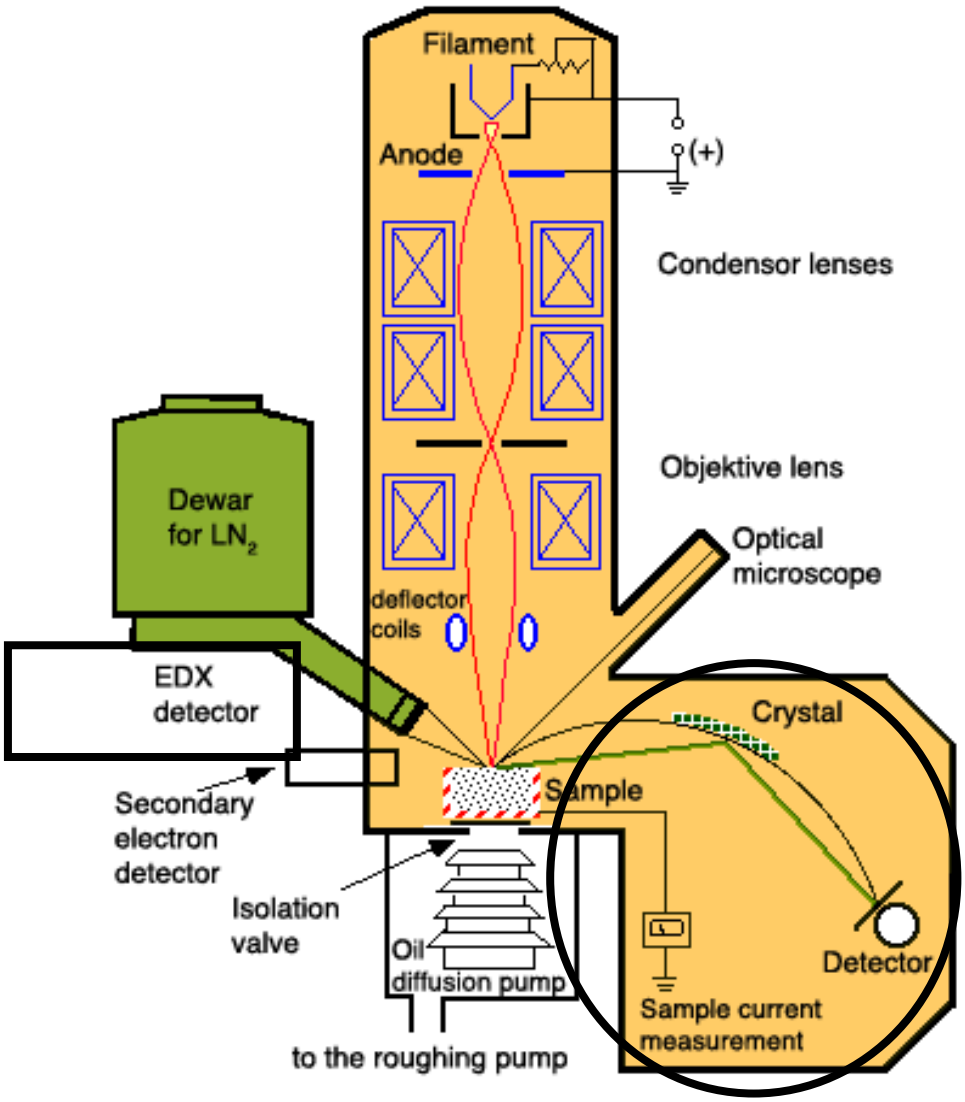

Figure 2.12 Schematic diagram of EPMA. (Meyer, 2015)

2.5.2 Major Parameters

Three major parameters, voltage, current and peak counting time, will be discussed in this section. Voltage determines the interaction volume as shown in Equations 2-1 and 2-2. (Everhart, 1972) The explanation of the interaction volume could be found in the Appendix H.1 Interaction Volume. Electron beams penetrate into the sample surface, and the width and depth of the effective beam are related to the accelerating voltage and an atomic number of the solid. (Hafner, 2007)

$$x\ (\mu m) = \frac{0.1\ E_0^{1.5}}{\rho} \qquad 2\text{-}1$$

$$y\ (\mu m) = \frac{0.077\ E_0^{1.5}}{\rho} \qquad 2\text{-}2$$

Where E_0 is voltage, ρ is material density.

Equation 2-1 and 2-2 provide the depth and width of the effective beam size, respectively, (Potts, 1987) where x is the depth of electron penetration and y is the width of the excited volume E_0 is the accelerating voltage of the electron beam (keV) and ρ is the density of the solid being analyzed (g/cm^3).

Both current and peak counting time affect the detection limit using EMPA, which also controls the accuracy of the measurement. Equation 2-3 shows the relationship between detection limit (DL) and net peak counts (N_{np}), which increase with both of increasing current and peak counting time. (Potts, 1987). As shown in Equation 2-3, higher net counts decrease detection limit. As a result, higher current and longer peak count time help improve accuracy using EMPA. The example of detection limit for the real situation on Mn is shown in Chapter 4 (Table 4-3).

$$DL = \sqrt{2} * \frac{3 * \sqrt{N_b} * C_{std}}{N_{np}} \qquad 2\text{-}3$$

Where DL is detection limit, N_b is the net background counts, N_{np} is the net peak counts, and C_{std} is concentration in standard (wt%)

2.5.3 Sample Coating

To achieve the best results from EMPA, samples require a thin film coating of electrically conductive material on a polished surface. As discussed before, the detection limit is controlled by counts that received, which will be affected by the thickness of coating layer. Same thickness of the coating is critical between standard material and known samples. The polishing must be finer than 1 μm for microprobe analysis. Studies have found that quantitative analysis can be inaccurate due to a variation in the thickness of the carbon

coating; therefore, all analyzed samples including standard blocks need to have equal coating thicknesses.

The variation of coating thickness has effects on the collection of X-rays when low count rates occur due to the low concentration of microalloying elements. (Kerrick, 1973) As established in previous research, the percent X-ray intensity loss is proportional to the product of the density of the coating (mg/cm^3) of the thickness of the film (cm). (Sweatman, 1969) Reed gives an Equation 2-4 for the X-ray intensity loss (ΔI) as follows:

$$\Delta I = \frac{8.3 * 10^4 * (\rho z)}{V_0^2 - V_c^2} \qquad 2\text{-}4$$

where ρ is the density of the film (mg/cm^3), z is the thickness of the film (cm), V_0 is acceleration voltage (keV) and V_c is critical excitation voltage for the target element (keV).

2.5.4 Elemental Mapping

Elemental mapping is done by sweeping a focused electron beam across an area of the specimen. The First X-ray "dot map" was introduced in 1956. WDS is used to generate the x-ray maps in 1968. (Cosslett, 1956) (Fitzgerald, 1968) The spatial resolution for X-ray mapping is the X-ray excitation region or the electron beam interaction volume as discussed above. According to previous research, the spatial resolution is expressed by the following Equation 2-5. (Anderson, 1966)

$$R_x\,(\mu m) = \frac{0.064 * \left(E_0^{1.68} - E_c^{1.68}\right)}{\rho} \qquad 2\text{-}5$$

where R_x is the spatial resolution, E_0 is the electron accelerating voltage, E_c is the critical excitation voltage and ρ is the density of the solid.

Since the pixel number of each line is selected by the operator of the machine, the magnification of the map is calculated from Equation 2-6 (Friel, 2006),

$$M = \frac{L}{R_x N_p} \qquad 2\text{-}6$$

where M is the magnification, L is the width of the image, R_x is the spatial resolution and N_p is the number of pixels in a line.

Undersampling occurs when the pixel size is large and this results in a pixelated image. To avoid undersampling, Friel suggested a higher magnification for the best quality map unless large-scale trends are the purpose of the mapping of a small region. (Friel, 2006) For a large field of view, a vertical WDS spectrometer usually suffers from a defocusing problem, which leads to significantly fewer counts received. (Marinenko, 1987) This can be eliminated by using an auto-focus function in the software, although it is a very time-consuming process. (Newbury, 1990)

Since mapping technique uses less peak counting time (5ms) than quantitative analysis (80s), the detection limit for maps is more than 10 times worse than that using single point analysis. (Friel, 2006) According to Goldstein, a minimum of 250,000 total counts is required for a high-quality dot map. (Goldstein, 1992) The detection limits for most elements are 0.5-1 wt% for bulk material with WDS and 2-5 wt% for EDS. (Goldstein, 1992)

2.5.5 Element Detection Using EMPA

Figure 2.13 compares the segregation ratios (S.R.) for Mn and P for micro and macro levels at the centreline position by EMPA. The nominal concentrations of Mn for steel high and low are 1.55 wt% and 0.4 wt%, respectively, with corresponding phosphor concentrations of 0.024 wt% and 0.07 wt%, respectively. These elements at the given concentration levels are detected successfully in the research. (Tsuchinda, 1984)

Figure 2.14 shows the elemental mapping of Mn, P, Cr and Ti at the centreline segregation region using EMPA. The nominal Mn concentration is 1.5 wt% with 0.02 wt% P added in the examined steel. The mapping technique in EMPA detected elements at the given concentration successfully and the maximum segregation ratio for Mn is 1.69. (Preblinger, 2006)

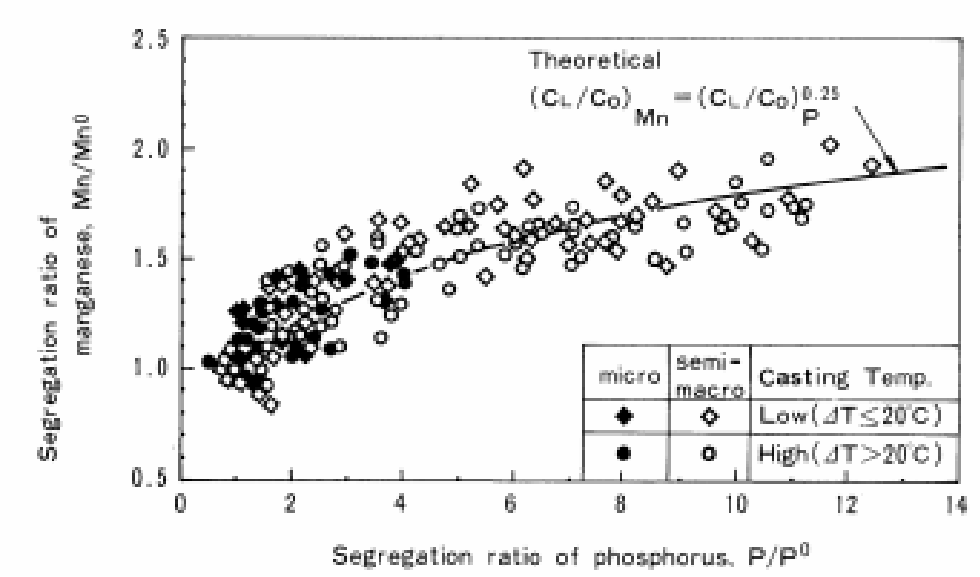

Figure 2.13 Solute concentration profile for micro and semi-macrosegregation using EPMA. (Tsuchinda, 1984)

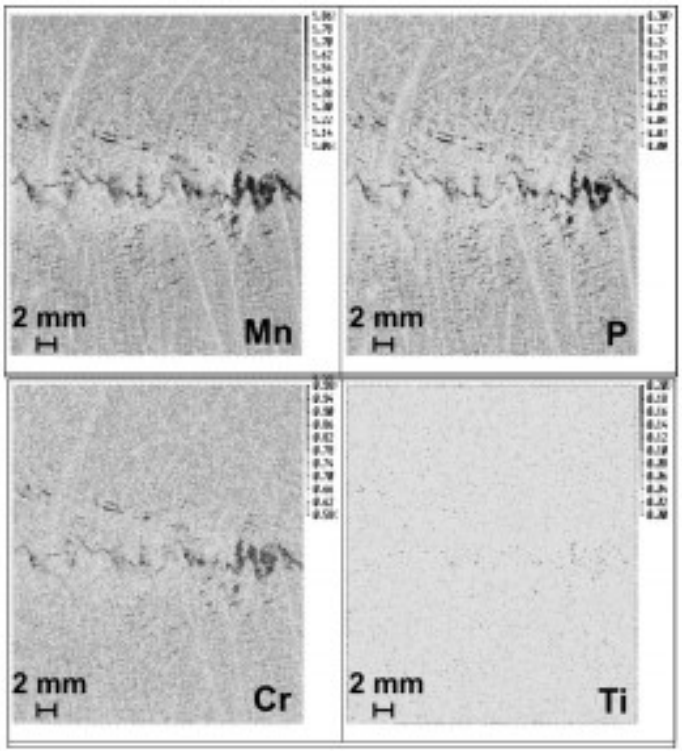

Figure 2.14 Elemental mapping at centreline in wt%. (Preblinger, 2006)

Figure 2.15 shows a line scan of a carbon concentration profile through a martensite structure using EMPA. The high carbon region is identified as martensite and regions besides it is ferrite. The nominal concentration of carbon in the steel is 0.64 wt%, and a higher carbon concentration is found for the martensite structure at a distance from 5 to 9 μm as shown in Figure 2.15 (two vertical dashed lines) than surrounding ferrite. The average carbon concentration in the martensite structure for this image is around 0.72 wt%, while for ferrite it is less than 0.1 wt%.

Figure 2.16 shows EMPA results for a line scan through a bainite structure, with carbon concentration levels at 0.45 wt%. There are several spikes in Figure 2.16, which are confirmed as retained austenite laths. (Pinard, 2013) This study verified that EMPA is accurately able to detect light elements like carbon at levels higher than 0.1 wt%.

The previous researches discussed in this section confirms the ability of EMPA on segregation analysis at the low concentration level (~0.1 wt%). These comparisons prove C segregation will be hard to determine since it is relying on the microstructure and inclusions. There is too less C in the solution that showing the C centreline segregation. Thus, C segregation is not included in this study.

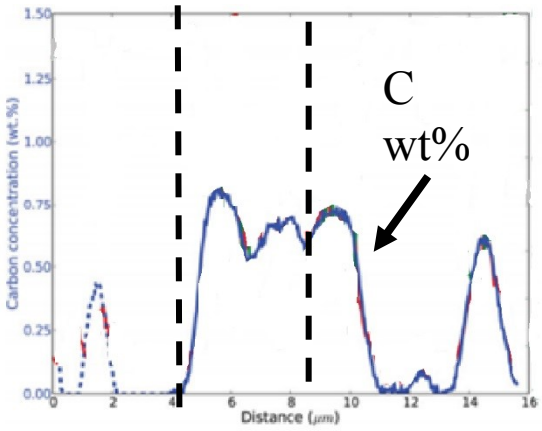

Figure 2.15 C concentration line scan through martensite using EMPA on C steel. (Pinard, 2013)

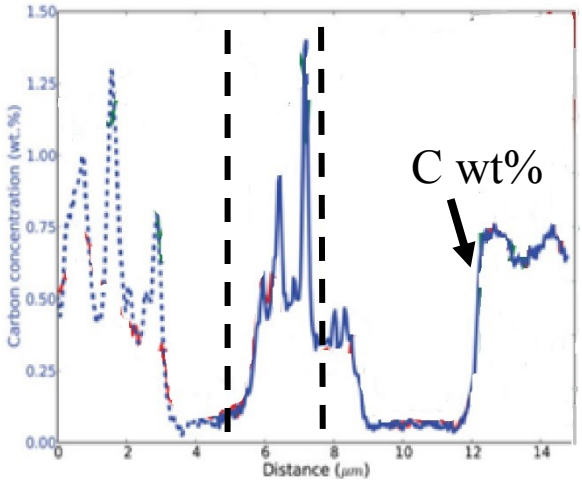

Figure 2.16 C concentration line scan through bainite using EMPA on C steel. (Pinard, 2013)

2.6 Summary

The centreline segregation of Mn in continuous cast microalloyed steel was reviewed. The segregation ratio of Mn was found to be approximately 1.7 in the previous research. The effect of homogenization process on elements segregation and precipitates dissolution was discussed. Increasing homogenization temperature and time were found to reduce segregation. At a temperature above 1300 °C, Nb precipitates are thermodynamically unstable. Previous work using EMPA of centreline segregation confirmed that the level of elements in the microalloyed were above the detection limit of EMPS.

The goal of this work is to develop a methodology (apply EMPA, optical microscopy and hardness tests) to distinguish the difference between Mannesmann 2 and 3 readings for both as-cast and pipe steel; conduct experimental homogenization tests to assess the effect of temperature and time on the Mn segregation reduction and hardness profile; and undertake a macro analysis to quantify and difference the centreline segregation for Mannesmann 2 and Mannesmann 3 samples.

The next two chapters of the thesis will introduce experimental methods and results including optical microscopy inspection, imaging analysis, microhardness test, and the EMPA analysis.

3. Experimental Methods

This chapter introduces the steels (composition, location, sample preparation) studied in this work, followed by detailed description of the homogenization tests conducted, the metallurgical analysis, the electron microprobe analysis, and the image analysis method.

3.1 Steels Studied

The steels studied in this work are introduced in Table 3-1 with their Mannesmann Rating (MR), type, thickness and elemental compositions that are different. The steel compositions are very similar; thus, only the major elemental chemistries of the steels are listed in Table 3-1.

Two pipe steels, A and B, having different Mannesmann ratings (2 and 3) and three as-cast slabs, C, D, and E were studied. Steels A, B, and C were used to establish and optimize a methodology of quantitative alloy element analysis of centreline segregation. Steels D and E were used to perform a homogenization simulation process and to detect elemental concentration at segregation region for as-cast and homogenized conditions. Comparison of segregation level and metallurgy and mechanical behaviours between Mannesmann 2 and 3 slab samples were done based on steels D and E. Same comparison between Mannesmann 2 and 3 pipe samples were done based on steels A and B.

All samples were derived from commercial steels provided by Evraz Inc. NA. Samples A and B, when fully processed, are pipe steels used in the current oil industry. After casting, all slab samples were macroetched using hydrochloric acid to reveal the centreline segregation. Etching was done by Evraz personnel at their own facility.

Table 3-1 Selected nominal chemistries (wt %) of steels used in this work.

Sample	MR	Type	Thickness (mm)	C	Mo	Ti	P	Mn	Nb	Cu
A	2	Pipe	12.5	0.04	0.14	0.02	0.01	1.59	0.09	0.30
B	3	Pipe	12.5	0.05	0.14	0.02	0.01	1.58	0.09	0.31
C	3.9	As-cast	200	0.06	0.04	0.02	0.01	1.47	0.07	0.21
D	2	As-cast	200	0.04	0.14	0.02	0.01	1.59	0.09	0.30
E	3	As-cast	200	0.05	0.14	0.02	0.01	1.58	0.09	0.31

3.2 Sample Locations

In this section, sample preparation methods will be introduced for each type of steel, and the shape and size of the analyzing samples will be provided. The sectioning locations will be discussed in this section.

3.2.1 Pipe Steels A and B

Sample A and B were cut from the pipe. To obtain these samples, a rectangular section of the ring was first cut from the pipe as illustrated in Figure 3.1. Samples for pipes were taken 180° away from the weld on the pipe.

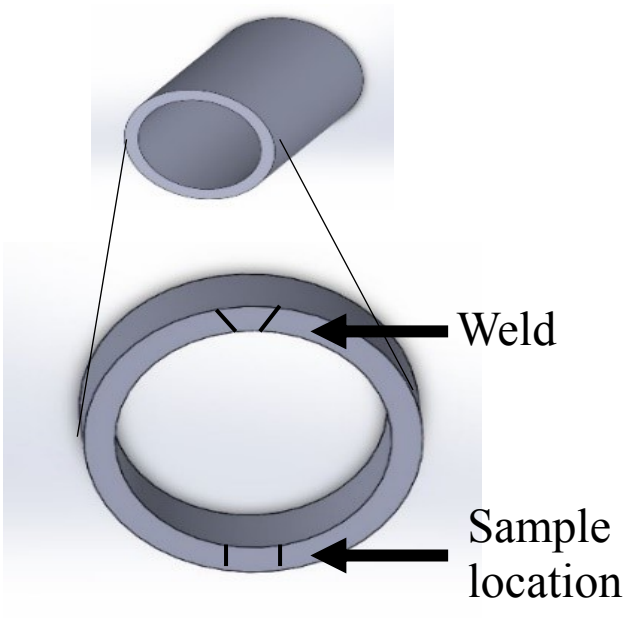

Figure 3.1 Sectioning position example of pipe samples.

3.2.2 Sample C

Sample C was obtained as a cast slab, which had been given a Mannesmann rate of 3.9. The flat block was cut from a cast slab 254 mm away from the left edge, and the through thickness was analyzed as shown in Figure 3.2.

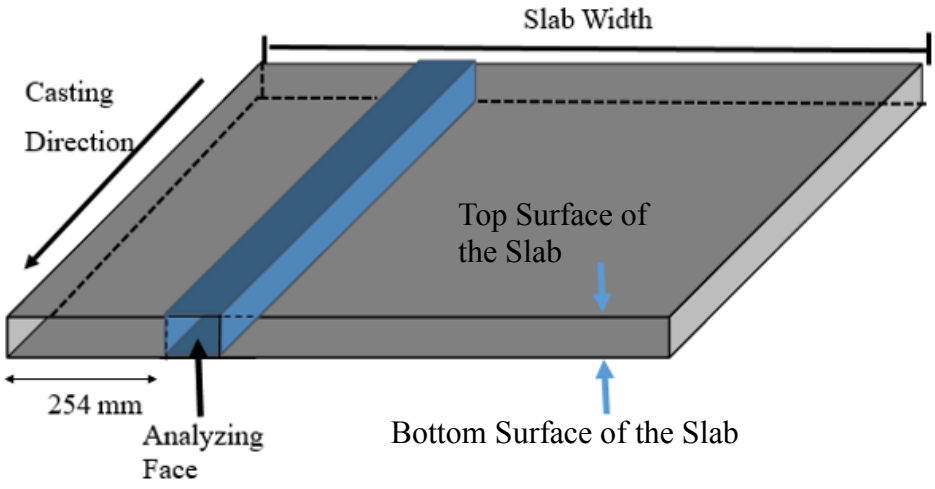

Figure 3.2 Location of flat block in cast slab.

The surface shown in Figure 3.3 was the analyzing face, which was indicated in Figure 3.2. In order to study this cast steel, small sample blocks were cut through slab thickness of the flat block in sizes of 0.5 in (12.7 mm) × 0.75 in (19.1 mm) × 0.75 in (19.1 mm) (w × l × t) as A1 block shown in Figure 3.3. Samples were labeled from A1 to A16, with A1 and A16 were the bottom and top surfaces of the slab, respectively. The dark line appearing in Figure 3.3 (circled) was suspected to be the centreline band from macroetching by the hot HCl solution. A cutting mark was left on block A8 as an indication to the centreline band for further study.

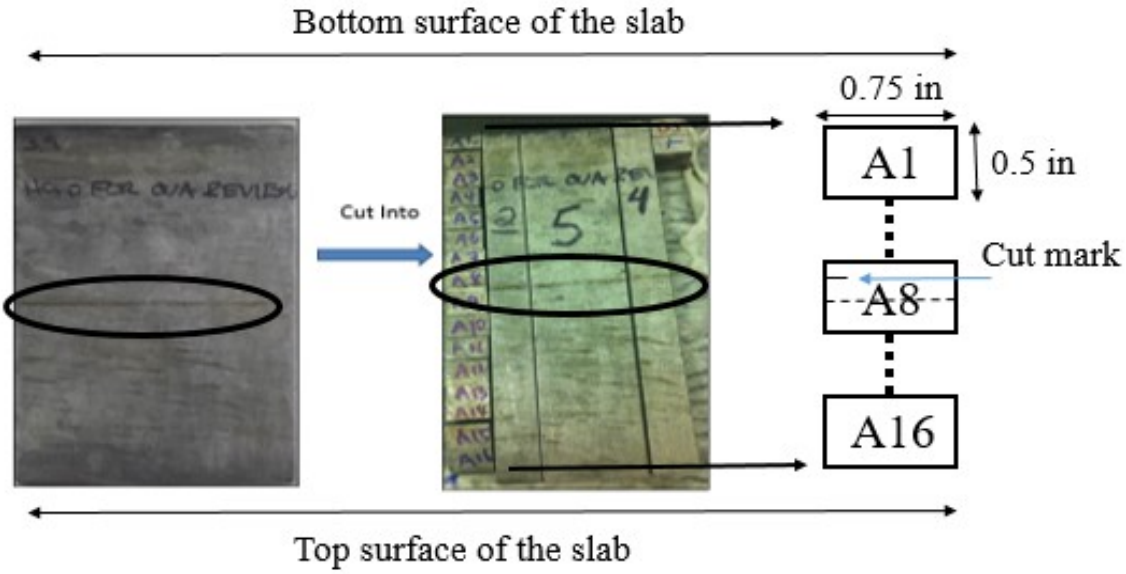

Figure 3.3 Sample locations and labels through the slab thickness for slab C.

3.2.3 Homogenization Slabs D and E and Mirror Analyzing Surface

Figure 3.4 is showing the two different views of slab samples for a better explanation in future discussion. The front view is the view of the analyzing face and against the cast direction. The top view looks at the top surface of the slab as shown in Figure 3.5.

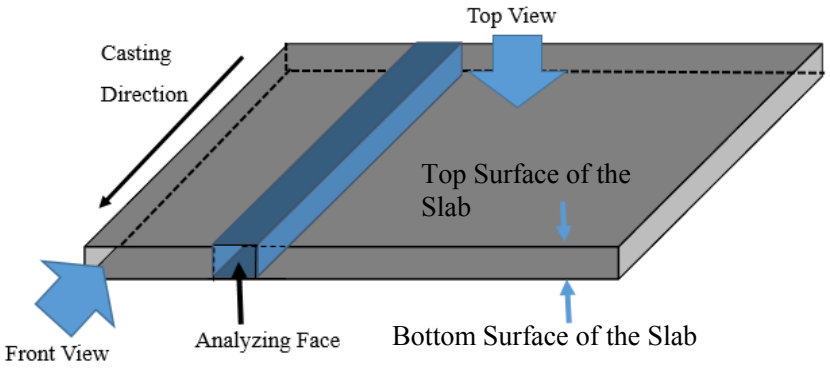

Figure 3.4 Top view and front view schematic diagram of the analyzed slab.

A front view of the sample was shown in Figure 3.5. Homogenization experiments were performed on the as-cast slab samples, D and E. Two slab samples were received and prepared in this study. Sample D was used as an example in this section to show the locations of samples taken from the slab. From the as-cast slab, the centreline segregation bands were revealed by macroetching, as shown in Figure 3.5. The dark line was the centreline segregation band and the two dashed lines separated by 0.5 in (12.5 mm) indicate the location where the samples were cut from the slab and evaluated in a homogenization experiment.

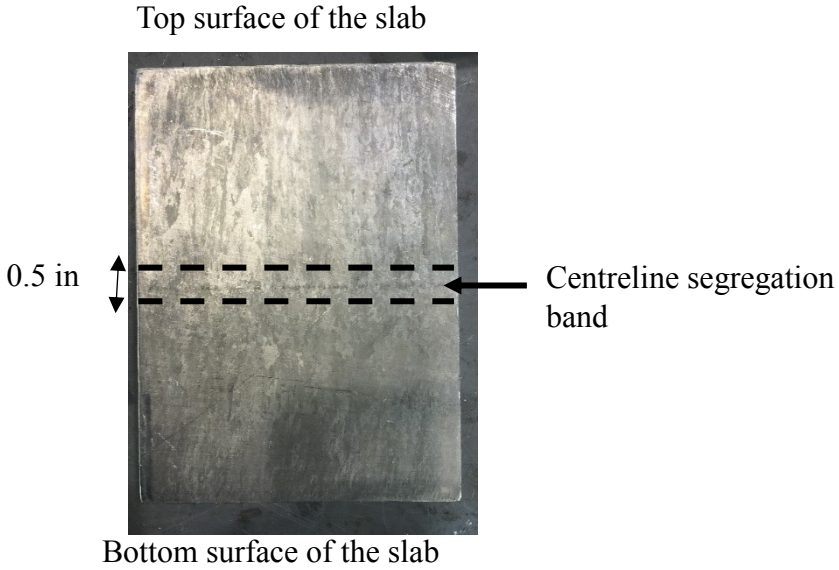

Figure 3.5 Image of macroetched as-cast slab D (MR=3) for homogenization experiment.

A top view of the slab was shown in Figure 3.6. Samples with 0.5 inch (12.5 mm) wide were cut from the slabs for both slab D (MR=2) and slab E (MR=3). The centreline segregation band was located in the middle of the sample from the front view (could not see from top view). Since the segregation behavior is complex, mirror surfaces (as arrow indicated in Figure 3.5) were analyzed for the homogenization simulation. This mirror analyzing surface ensured homogenized samples (before homogenization) have same segregation behaviours (and location) with as-cast samples. To create a mirror surface, strips were cut from the middle of the thickness (Figure 3.5). Analyzing surface had an area of 0.5 inches (12.7 mm) by 0.5 inches (12.7 mm). Sample blocks in Group 1 were used as as-cast samples and sample blocks in Group 2 were used for homogenization and placed in a furnace.

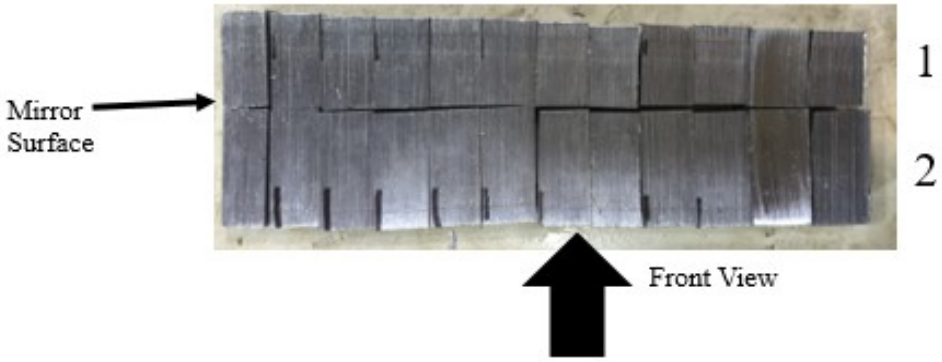

Figure 3.6 Mirror sample surface preparation for slab D (MR=2).

3.3 Homogenization Experiments

Homogenization experiments were performed to determine whether centreline segregation may be reduced. Several homogenization temperature and time combinations were selected to find the optimal homogenization conditions that reduced segregation most effectively. Included in this section were the homogenization plan and the experimental procedure. Rounded corner for indication was introduced in the procedure.

3.3.1 Homogenization Plan

The homogenization temperatures and times used in this study were shown in Table 3-2. There were two groups of samples for homogenization experiments. To obtain multiple time

and temperature combinations, four different homogenization times and three different homogenization temperatures were selected. Due to the limited availability of equipment, homogenization times were set at 1 hr, 4 h, 8 h and 16 h. At 1300 °C, the 4 h sample for Mannesmann 3 was disintegrated due to a high degree of oxidation in the furnace. Thus, at 1300 ˚C, the homogenization times were set at 1 hr, 2 h and 4 h.

Table 3-2 Homogenization times and temperatures.

Sample	MR	Temperature (°C)	Time (hours)
Slab D	2	1100, 1200	1, 4, 8, 16
		1300	1, 2, 4
Slab E	3	1100, 1200	1, 4, 8, 16
		1300	1, 2, 4*

* The sample with 4 h homogenization disintegrated when taken out of furnace due to excessive oxidation.

3.3.2 Homogenization Experimental Procedure

After all samples had a corner grounded off to identify a top surface (of the slab) direction for samples as shown in Figure 3.7 (a). This corner helped to identify the orientation of the sample after taken out of the furnace. Samples were labeled with an engraver on the analyzing surface, as shown in Figure 3.7 (b). The downwards pointing arrow on the sample surface was indicating cooling direction during the solidification. The letters on the surface represent Mannesmann rating of the sample.

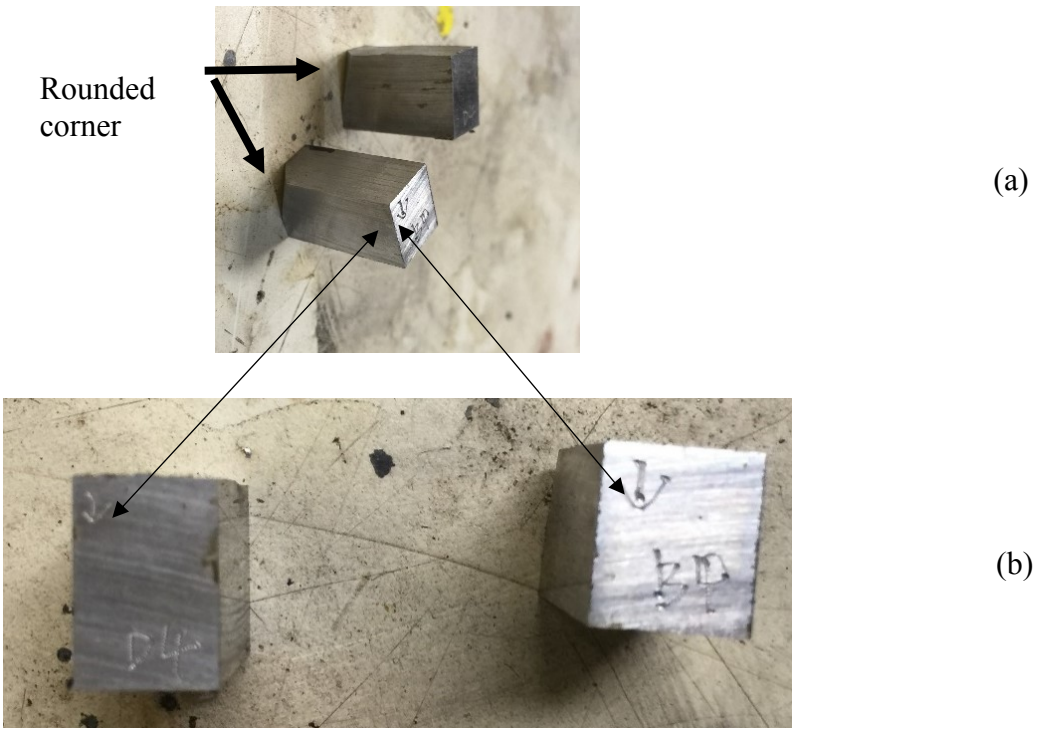

Figure 3.7 Example of homogenization sample with (a) rounded corner and (b) sample label on analyzing surface.

Samples were placed into a resistance furnace after the desired temperature was reached and stabilized. Time measurements began once the temperature was stable for 3 minutes after inserting the sample in the furnace. Samples were removed when the desired homogenization time was reached. During cooling, a tong was used to remove the oxidation layer which formed during homogenization. Samples were relabeled on the both sides of the analyzed face after the samples completely cooled. The labeled samples were mounted and prepared for metallurgical analysis.

3.4 Metallurgical Analysis

After samples had been prepared, they were analyzed using optical microscopy inspection and microhardness test. Different metallurgical analysis methods were discussed in Table 3-3 for all 5 steels with different techniques.

Both pipe samples, A and B, were microetched with 2% Nital and Vickers microhardness tests were performed through the centreline segregation band. Slab C was both micro and macroetched and microhardness tests were performed through the centreline segregation band. The comparison could be found in section 4.1. Saturated piciric acid method requires a fine polishing after etch, the comparison of the polishing results could be found in Appendix A. Thus, 4% Picral was used for the analysis in this study for convenience. PAGS and allomorphic ferrite grain size were measured based on the macro etched images. The method could be found in Appendix B. Slabs C and D were macroetched and microhardness tests were done through the 12.5 mm thickness.

Table 3-3 Metallurgical analysis for all 5 Steels.

Sample	MR	Macroetching		Microetching	Microhardness
		4% Picral Acid	Saturated Picric Acid	2% Nital	Vickers
Pipe A	2	-	-	Yes	Yes
Pipe B	3	-	-	Yes	Yes
Slab C	3.9	Yes	Yes	-	Yes
Slab D	2	Yes	-	-	Yes
Slab E	3	Yes	-	-	Yes

3.5 Electron Microprobe Analysis

Electron microprobe analysis (EMPA) was performed on all 5 steels to quantify the centreline segregation after metallurgical analysis. The setup, sample preparation methods, and the detailed procedure of line traverses and mapping analysis will be described in this section. Running conditions for each experiment are tabulated and presented in this section. Detailed results and analysis will be presented in the next two chapters.

3.5.1 Microprobe Equipment

EMPA in this study was conducted using a Cameca SX 100 instrument and controlled by Probe for EPMA (PFE) software. The microprobe made by Cameca can generate an electron beam size from 0.1 to 10 μm, while the current ranges from 10 to 200 nanoamps (nA). Five elements could be detected at a time, since there were five detectors on the Cameca microprobe.

3.5.2 Sample Preparation

Samples were mounted in 1 inch (25.4 mm) of epoxy, polished and etched to prepare them for microhardness tests. After microhardness testing, the mounted samples were cut to a thickness of 0.173 inches (4.4 mm) to match the standard block thickness in our electron microprobe laboratory (EML). The location of the line scan for pipe samples according to the microhardness locations could be found in the Appendix C. The line scans for slabs were based on the Mn maps. Then fine polishing with 1 μm diamond suspension was applied to remove the etched layer without removing the microhardness indentation markers. Quantitative microanalysis requires a relatively flat surface with fine polishing to a 0.05 μm level. All samples and standard blocks were coated with carbon, at the same time, to ensure uniformity of the coating thickness, followed by insertion of the samples into the analyzing stage. The samples were then examined by EMPA.

3.5.3 Line Traverse Procedure

EMPA standardization started with peaking procedure for the wanted elements on the standard block. The peaking procedure was performance on known material that includes analyzing element. This gave peak position of wavelength scan. The peaking process was running at 20 nA and 15 keV with a 10 μm beam. A lower operating energy could help reduce X-ray emission and provide better results. Based on the peak wavelength, linear backgrounds were selected for both lower and higher positions.

An example setup of elements on the spectrometer with peak positions was shown in Table 3-4. After all wavelengths had been selected, a standardization process was developed. For each element, 5 points were chosen for running the standards. The setup for the

spectrometers and peak positions for each element is shown in Table 3-4. The details about diffraction crystals could be found in the Appendix H.2 Diffraction Crystal.

Table 3-4 Microprobe spectrometer setup with peak wavelength.

Spectrometer	Element	Crystal	Peak Position	Higher Background	Lower Background
Sp1	Cr	PET	26206	750	-900
Sp2	P	PET	70322	400	-700
Sp3	Mn	LLIF	52189	1600	-1200
Sp4	Si	TAP	27741	800	-760
Sp5	Cu	LLIF	38274	1000	-1000

After all the elements had been assigned with standard analyzing elements conditions (include peak position, peak counts etc.), operating conditions for microprobe analysis were selected. Conditions other than those in Table 3-5 were also used. The example results of EMPA line scans could be found in Appendix D. A comparison and decision of operational conditions for line scans will be discussed in Chapter 4.

Table 3-5. Microprobe elements quantitative running condition comparison.

	Voltage (keV)	Current (nA)	Count Time (s)	Beam Size (μm)	Point Spacing (μm)	Detection Limit for Mn (wt%)
A	15	100	20	0.1	4 μm	0.018
B	15	100	20	10	4 μm	0.018
C	15	200	80	10	10 μm	0.005

3.5.4 Element Mapping Procedure

For element mapping, the center of the sample needed to be identified first. The coordinates of four corners of analyzing sample were used to estimate the center of the sample. Based on the size of the sample, the size of the map was determined by selecting the size of each pixel.

The size of the maps was slightly less than the size of the analyzed sample. This avoided having the current beam hitting the epoxy, since the high current could damage the epoxy.

The pixel size was chosen as 10 μm by 10 μm for maximum efficiency. The detection time for each pixel was 5 ms. The acquisition voltage was 15 keV as same as line traverse condition. Condition E in Table 3-6 corresponds to an increase in current from 200 nA to 400 nA for better results than condition D.

Table 3-6 EMPA mapping conditions comparison.

Conditions	Voltage (keV)	Current (nA)	Count Time (ms)	Pixel Size (μm)
D	15	200	5	10x10
E	15	400	5	10x10

To analyze the image, the free software program ImageJ was used. A *.tif file of the raw maps without a scale bar was opened in ImageJ and saved to another file type (tiff). Then the image was converted to a colour image using Image/Type/16-bits, and enhanced contrast for better quality. Once the image was coloured, it was saved and labeled appropriately. The detailed macro could be found in Appendix EMPA MapsJ Macro.

3.6 Image Analysis

Both the macroetched slab surface and EMPA Mn maps revealed the centreline segregation band from optical microscopy images. Enable to compare the segregation level in numbers between different Mannesmann rating samples, image analysis was used based on macro images and EMPA Mn maps. Using image analyzing software, ImageJ, optical micrographs and EMPA maps were translated into the grey level. A MATLAB code (in Appendix F was used to calculate the number of counts and percentage of each grey level class. The results were compared in Chapter 5.

3.6.1 Macro Image Analysis

For macro images, they were taken based on the etched slab surface as shown in Figure 3.8 (a). The blue square was the analyzed area with 5 mm in height. Then cleared outside of the blue square and obtained Figure 3.8 (b). Using ImageJ, original centreline macro images were transferred and inverted into a binary black and white image as shown in Figure 3.8 (c). The bright/white spots in Figure 3.8 (c) were the segregated points. The macro image analysis was done based on these binary images.

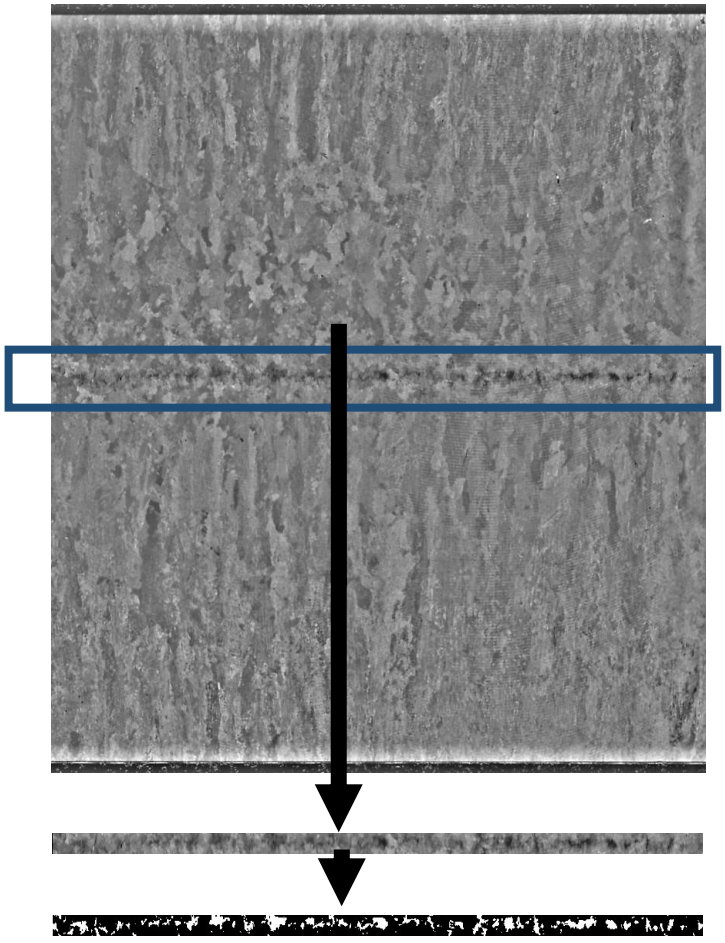

Figure 3.8 (a) Macro image MR=2 with the blue squared analyzing area, (b) original analyzing area, and (c) binary analyzing image with the white part as segregated region.

3.6.2 EMPA Mn Maps Analysis

Similar to macro image analysis, EMPA Mn maps analysis was done based on original Mn maps. Colored and enhanced contrast images were used in this section for demonstration purpose. The blue square in Figure 3.9 (a) represents the 5 mm height analyzing area. Using ImageJ, Figure 3.9 (b) were transformed into the grey level and analyzed in MATLAB.

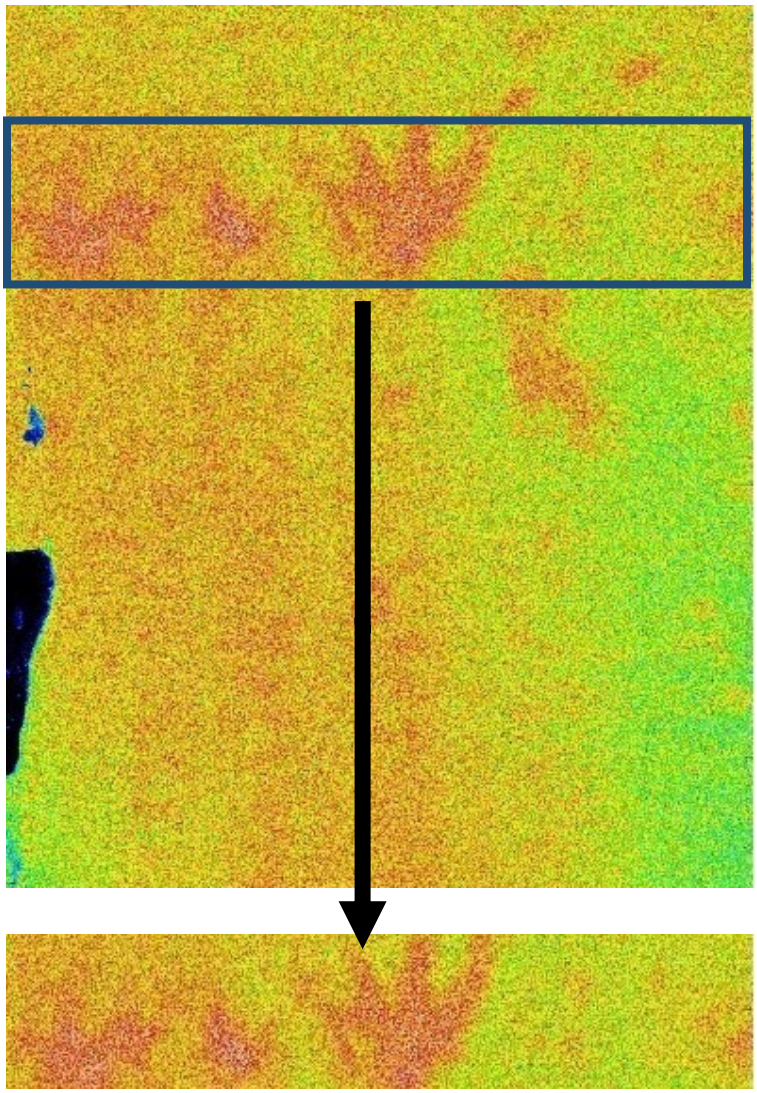

(a)

(b)

Figure 3.9 (a) Mn maps of slab D (MR=2) with the blue squared analyzing area and (b) analyzing area with a height of 5 mm for slab D.

3.7 Summary

The sampling method and experimental procedure for characterizing centreline segregation for microalloyed steels were presented in this section. There are three different major techniques used to characterizing the centreline segregation, optical microscopy inspection, microhardness test, and electron microprobe analysis. In next chapter, the quantify methodology will be discussed first, followed by results and discussions on the difference between Mannesmann 2 and Mannesmann 3 samples, the effect of homogenization temperature and time for Mn segregation reduction, and the macro analysis results between Mannesmann 2 and Mannesmann 3 samples.

4. Results and Discussions

The experimental methods for characterizing centreline segregation in microalloyed steels were reviewed in Chapter 3. This Chapter presents the results and discussion for the following: 1) optimization of conditions for etching and EMPA mapping and lines scans; 2) differences in segregation level between Mannesmann 2 and 3 as-cast and pipe samples, using optical microscopy inspection, microhardness testing, and EMPA analysis; 3) the effect of the homogenization process (i.e., temperature and time) on both Mn segregation reduction; and 4) the macro analysis on different Mannesmann rated samples comparison.

4.1 Optimization of Etching Conditions and EMPA Mapping and Line Scans

This section presents and discusses the results of four approaches used in this work to quantify the microstructure and/or the degree of segregation at the centreline: 1) macroetching, 2) microetching, 3) microhardness, and 4) EMPA used to quantify the microstructure and/or degree of segregation at the centreline.

4.1.1 Macroetching Method

This section compares micrographs resulting from two types of macroetchants used to reveal the prior austenite grain boundaries (PAGB) at the centreline. A comparison of the two etching conditions is provided in Table 4-1.

Table 4-1 Comparison between PAGB etchants.

Etchant Name	Content	Time mins	Temperature °C	Cycles
Bechet and Beaujard	saturated picric acid in water (~2%) + 1% HCl + Teepol	20-40	70	multiple
4% Picral	picric acid + ethanol + 1% HCl	1	25	1

These two etchants have similar formulas but differ in the etching procedure. The 4% Picral etchant uses less time at a lower temperature than the Bechet and Beaujard method. The 4%

Picral etchant is more practical because the Bechet and Beaujard method require multiple etching-polishing cycles as discussed in Chapter 2. (Purdy, 2004) Examples of etched surfaces are shown in Figure 4.1. Both etchants successfully reveal the PAGB. Based on the quality of the images and the simplicity of the process, the 4% Picral etch was used in this study to reveal the PAGB. For the as-cast samples, macroetching for PAGB reveals a segregation zone, which is located along the centreline band.

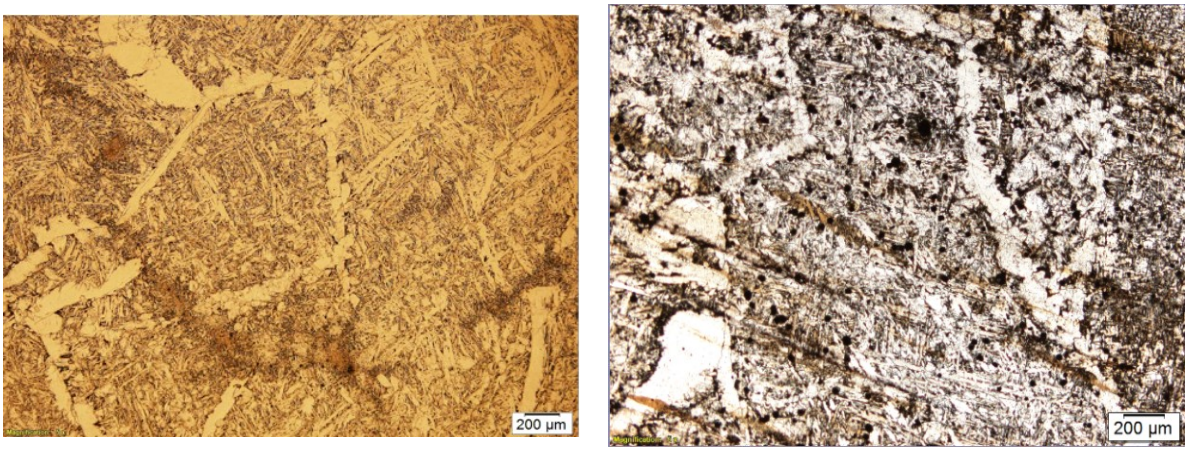

(a) (b)

Figure 4.1 Optical micrographs of etched PAGB (a) Slab D - 4% Picral for 1min and (b) slab C - Bechet and Beaujard for 20mins.

To find the optimal etching time, experiments were conducted with various etching times on the as-cast samples. As shown in Figure 4.2 (a), ferrite grains (indicated by the arrow) begin to be revealed at 30 s (Figure 4.2 (a)). At 45 s (Figure 4.2 (b)), the detailed structure inside the prior austenite grain and grain boundary lines (arrow in Figure 4.2 (e)) start to appear. Finally, at 60 s (Figure 4.2 (c)), a segregation zone (slightly darker, circled) appears at the centreline region. The dark regions in all the images are porosity near the centreline region. Based on these tests, 4% Picral with 60 s etching was used in this study for further analysis to image the PAGB and the segregation zone. As will be discussed later, the width of this segregation zone was measured using ImageJ software.

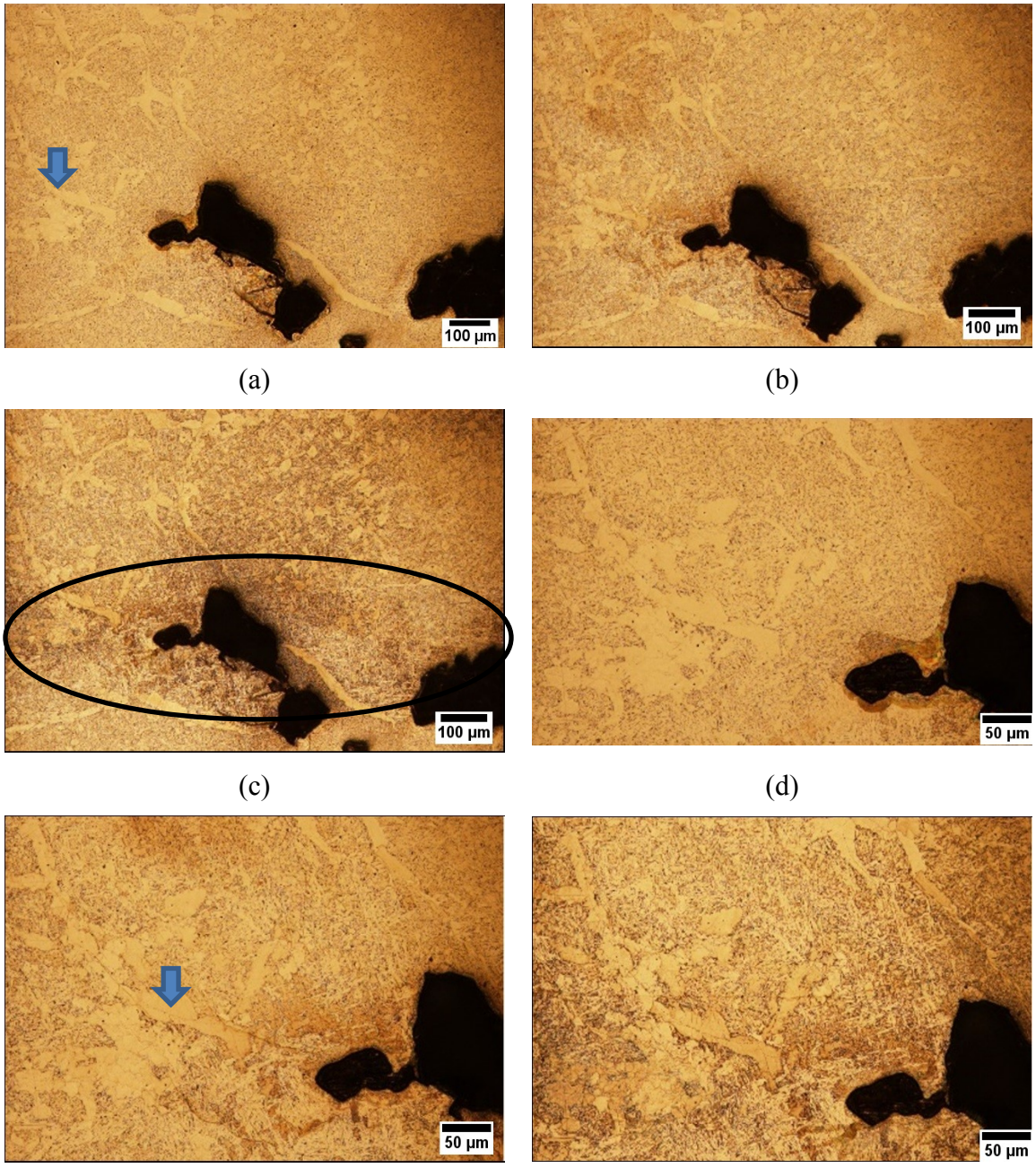

Figure 4.2 Optical micrographs after of 4% Picral etching for slab D (MR=2) at different times. (a) 30s, (b) 45s, (c) 60s, (d) 30s, (e) 45s, and (f) 60s.

4.1.2 Microetching Method

A 2% Nital (Samll, 2008) etchant was also used to analyze the microstructure at the centreline band for pipe steel samples. A set of experiments was performed to determine the optimal etching time. As shown sequentially in Figure 4.3, etching time was varied from 5 s to 30 s. Included in the figures are black arrows that indicate the suspected centreline segregation band. The centreline segregation band is revealed at 5 s (Figure 4.3 (a)) into the etching process. At 15 s (Figure 4.3 (c)), detailed features of the microstructures appear, and the centreline segregation line darkens with increasing time. For 30 s (Figure 4.3 (e)), the lines appear black and distinct, which allows for band width measurement. Also, multiple bands were observed on the pipe samples, indicated by black arrows in Figure 4.3. The width of the segregation bands was measured and are discussed later.

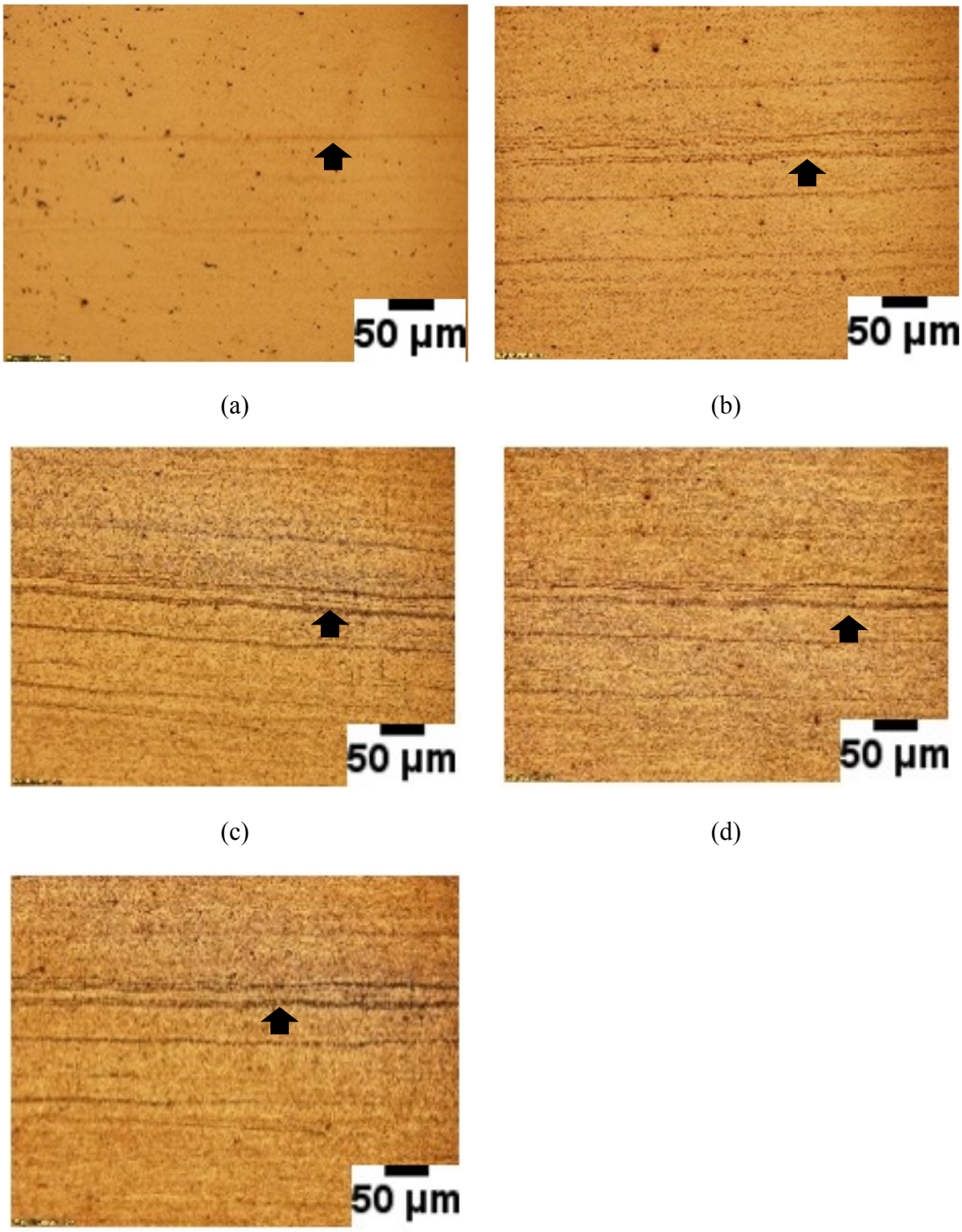

(a) (b)

(c) (d)

(e)

Figure 4.3 Optical micrographs after 2% Nital etching of pipe B (MR=3), with arrows pointing to segregation bands, (a) 5s, (b) 10s, (c) 15s, (d) 20s, and (e) 30s.

At the stage finished in this study, the detail microstructure of the dark bands is not clear. The microstructure analysis was based on the literature. From Nayak's image (Figure 4.4), similar segregation bands were found for HSLA pipeline steel. (Nayak, 2008) As shown in Figure 4.4, the centreline segregation band (along with rolling direction) of this pipe steel were magnified (circled), and pearlite was observed at the centreline segregation band.

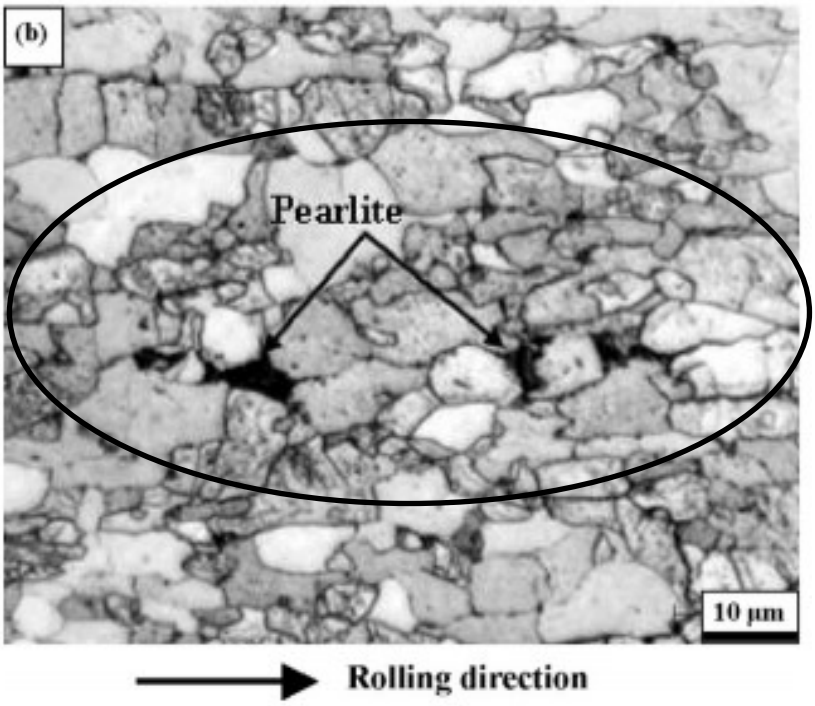

Figure 4.4 Centreline segregation band and pearlite for HSLA pipeline steel. (Nayak, 2008)

4.1.3 Microprobe Mapping Method

Mn is the easiest alloy element in the steel to detect using EMPA since it has the highest concentration of the alloying elements in the steel. As discussed in Chapter 2, elemental area mapping with EMPA uses a small amount of counting time on each point compared with quantitative point analysis. This provides an efficient measure of the elemental concentration.

Two different EMPA mapping conditions were done (Table 4-2). A pixel size of 10 μm by 10 μm was selected for both. The pixel size was decided by the size of the region to be analyzed at the centreline segregation region. The segregation region in this study for slab

samples has its dimension of around 10 mm by 10 mm. The detection time was selected as 5 ms with high scanning currents of 200 nA and 400 nA for Conditions 1 and 2, respectively.

Table 4-2 EMPA mapping conditions.

Condition	Voltage	Current	Counting Time	Pixel Size
1	15 keV	200 nA	5 ms	10 X 10 μm
2	15 keV	400 nA	5 ms	10 X 10 μm

For microprobe mapping, images were built based on count intensity. The maximum and minimum counts (detected by line scans) were then converted to wt% values based on EMPA line scans. Higher count intensity regions (which correspond to a higher concentration of Mn) are shown as red colours and the nominal composition as yellow/green. Specific values of wt% Mn for each map described in Table 4-2 are labeled on Figure 4.5 (a) and (b).

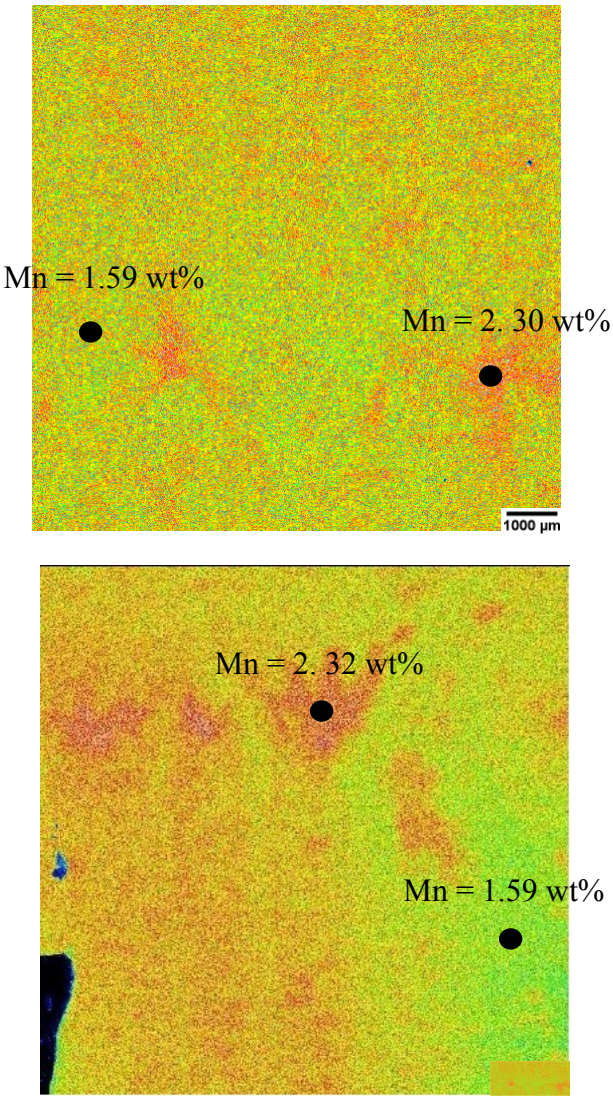

Figure 4.5 Mn maps for slab D (MR=2) at (a) 200 nA and (b) 400 nA.

Based on Equation 2-3, a higher current will increase the net peak counts. (Potts, 1987) For materials with low concentrations, the higher scanning current (Friel, 2006) for Condition 2 (Table 4-2) produces maps of better quality with better colour contrast for the Mn segregated regions (Figure 4.5 (b)), including centreline segregation and interdendritic microsegregation, than the lower current. For better imaging results, 400 nA maps were used in this study.

The mapping procedure for the same area in slab E used Condition 2 for Mn, Nb, Si, Cr, and Mo (Figure 4.6 (a), (b), (c), (d), and (e), respectively). The black area in all the maps is porosity in the steel. Included in each image is the maximum and minimum (detected by line

scans) element levels associated with the mapping counts. These are indicated by arrows. The maps were built based on the detected intensity at each pixel. Maps were processed into colour images to enhance the contrast based on the concentration difference. The colour contrasts are the indication of the level of composition difference for each element. The darker colour (smaller in grey level) in the processed images represents lower detected intensity.

As shown in Figure 4.6 (a), Mn segregation in the centreline area is highlighted. The dark orange region corresponds to the highest Mn concentration of 2.66 wt%. Figure 4.6 (b) reveals the Nb concentration for the same area. Bright areas in the map show high Nb content close to 1.39 wt%, with 0.09 wt% as the nominal concentration, which is blue on the map. Si segregation in Figure 4.6 (c) occurs in the same regions as with Mn. Si has a nominal composition of 0.30 wt%, which is blue in Figure 4.6 (c). The bright point indicates Si enrichment with a peak value of 0.76 wt% detected from line scans. Cr and Mo segregation were not found under these detection conditions, as shown in Figure 4.6 (d) and (e).

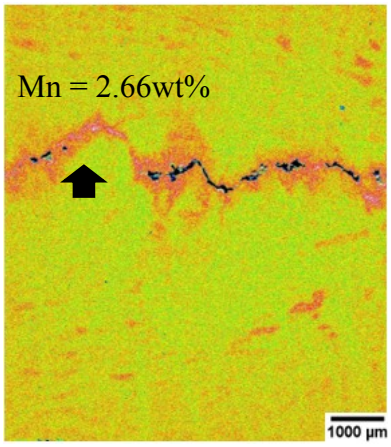

(a)

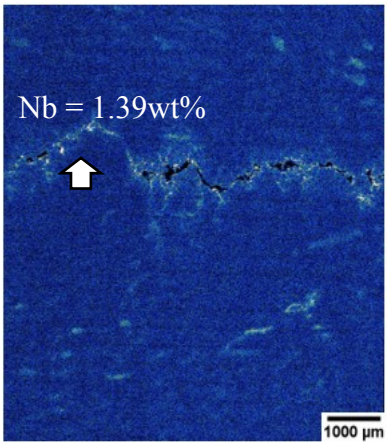

(b)

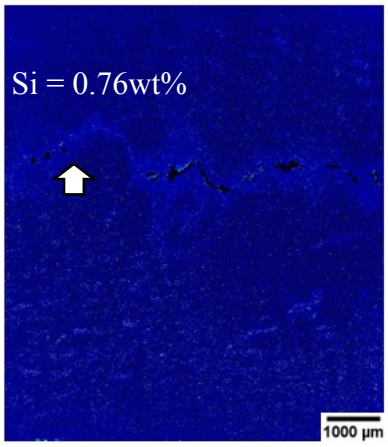

(c)

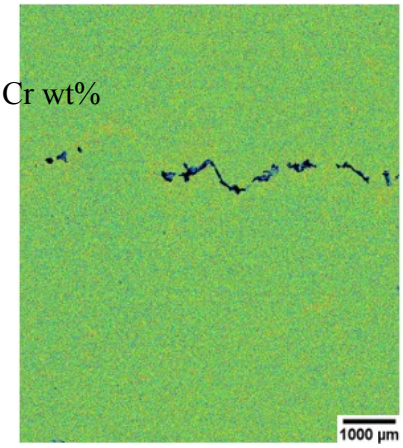

(d)

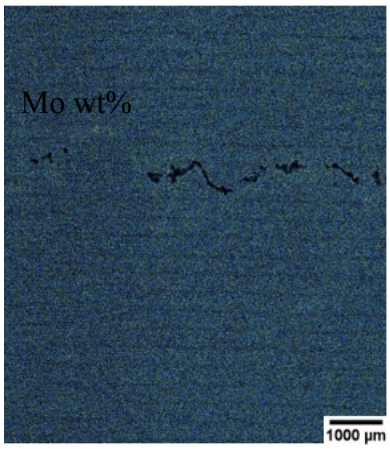

(e)

Figure 4.6 Elemental maps of slab E (MR=3) for (a) Mn, (b)Nb, (c) Si, (d) Cr, and (e) Mo.

From the preliminary mapping results, Mn, Nb, and Si are segregated to the same locations. A more significant colour difference is shown on the maps for higher levels of segregation (higher S.R.). Cr and Mo do not show segregation effects in the maps. From quantitative point analysis, Cr shows slight segregation, following the same pattern as Mn. A peak Cr concentration of 0.32 wt% was found compared with the nominal 0.24 wt% Cr composition. This segregation ratio is close to the literature findings in the past. For a cast AerMet 100 steel, Cr segregation at the centreline has also been reported as 3.55 wt% with a nominal concentration of 3.0 wt%. (Lippard H. E., 1998) Increasing counting time in Condition 2 (Table 4-2) could help reveal the segregation pattern for Cr and Mo mapping.

4.1.4 Microprobe Point Analysis (Line Scan) Conditions

Current and counting time are two of the variables of the microprobe analysis that effect the detection accuracy, as previously discussed in Chapter 2. Other variables to be considered include beam energy, beam current, counting time, beam focusing size and distance between analysis points on a sample. Each of these will be discussed in turn in this section.

Simulations were carried out on steel with 10 μm beam and 20,000 electrons using three beam energies, 10 keV, 15 keV and 20 keV. The results of the beam energy effect on the interaction volume are shown in Figure 4.7. Blue lines in Figure 4.7 (a) (b) and (c) represent simulated electron interaction under 10 keV, 15 keV and 20 keV respectively. Both width and depth of the beam increase as voltage increases. It can be seen in Figure 4.7, as the electron beam energy increases from 10 keV to 20 keV, the interaction depth increases from the maximum of 0.4 μm to a maximum of 14.2 μm. However, the increase in interaction o the width of the beam is not as significant with the width increasing from a maximum of 17.5 μm to 22.5 μm as the beam energy increases from 10 keV to 20 keV, respectively.

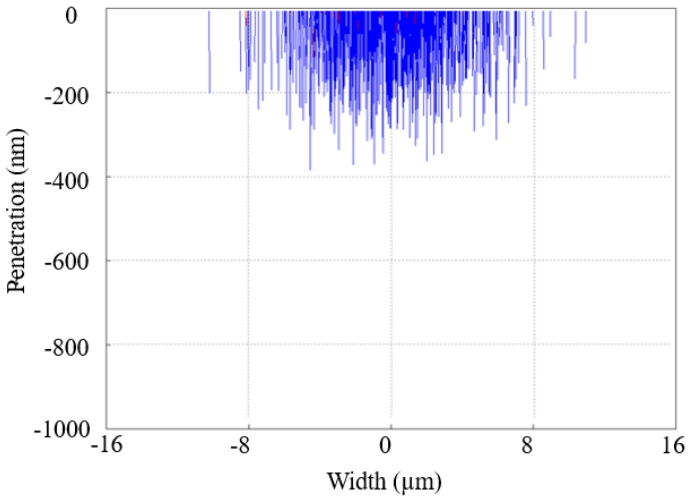

(a)

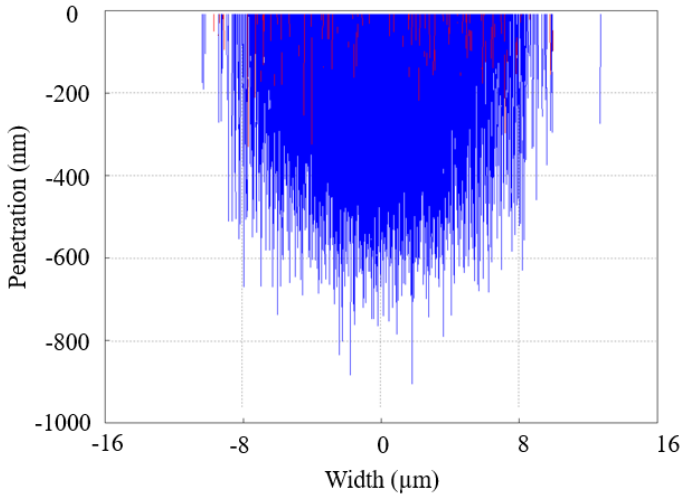

(b)

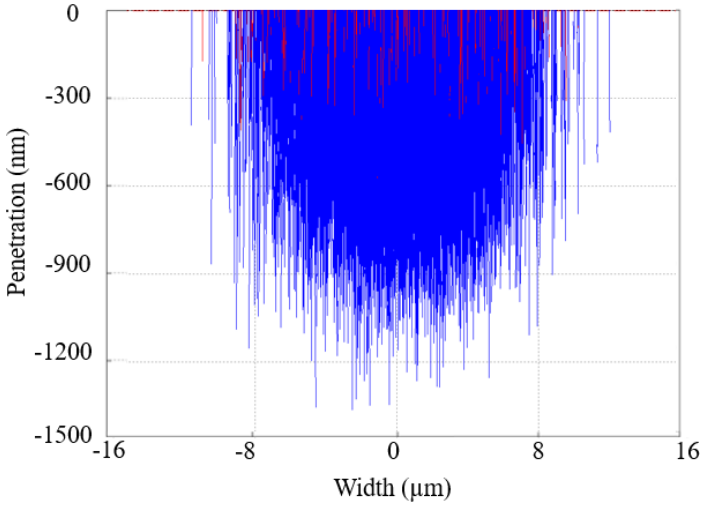

(c)

Figure 4.7 Interaction volume simulation using Monte Carlo method with different voltage (a) 10 keV, (b) 15 keV, and (c) 20 keV.

To determine the optimum combination of beam size, current and counting time to be used for microprobe analysis, pipe B sample was used. Two different beam sizes (0.1 and 10 μm) were used under similar current and counting times as shown in A and B in Table 4.3. The energy emitted from the sample under these conditions was measured in the microscope. This was then used in Equation 2.3 to calculate the detection limit of Mn. Comparing setup A to setup B, an increase in beam size yields a larger detection area but similar detection limit for Mn. Setup C has a higher current and counting time than setup B, and leads to a lower statistical detection limit for Mn at a 99% confidence level than setup B. The effect of beam size should be further discussed.

Table 4-3 Microprobe quantitative operating conditions comparison.

	Voltage (keV)	Current (nA)	Count Time (s)	Beam Size (μm)	Point Spacing (μm)	Detection Limit for Mn (wt%)
A	15	100	20	0.1	4 μm	0.018
B	15	100	20	10	4 μm	0.018
C	15	200	80	10	10 μm	0.005

An electron beam size of 0.1 μm is also known as a "fully focused beam". The fully focused beam was required to use for EMPA maps. Line scans could vary in beam size. Samples analyzed were focused optically and electronically for both beam sizes. As shown in Figure 4.8, 10 μm beam has larger scanned area than 0.1 μm beam. However, the scanned area with the 0.1 μm beam would yield a high resolution with respect to the microstructural features to be analyzed. Thus, for a given microstructure the optimum beam size needs to be determined that will provide a balance between the area to be analysed and the resolution of the microstructure. To determine this optimum beam size for the samples to be analyzed in this work, a comparison of Mn composition was analyzed using 0.1 μm and a 10 μm beam was conducted on pipe sample B (due to its smaller segregation band width compared with the as-cast sample) to determine the optimal point analysis conditions.

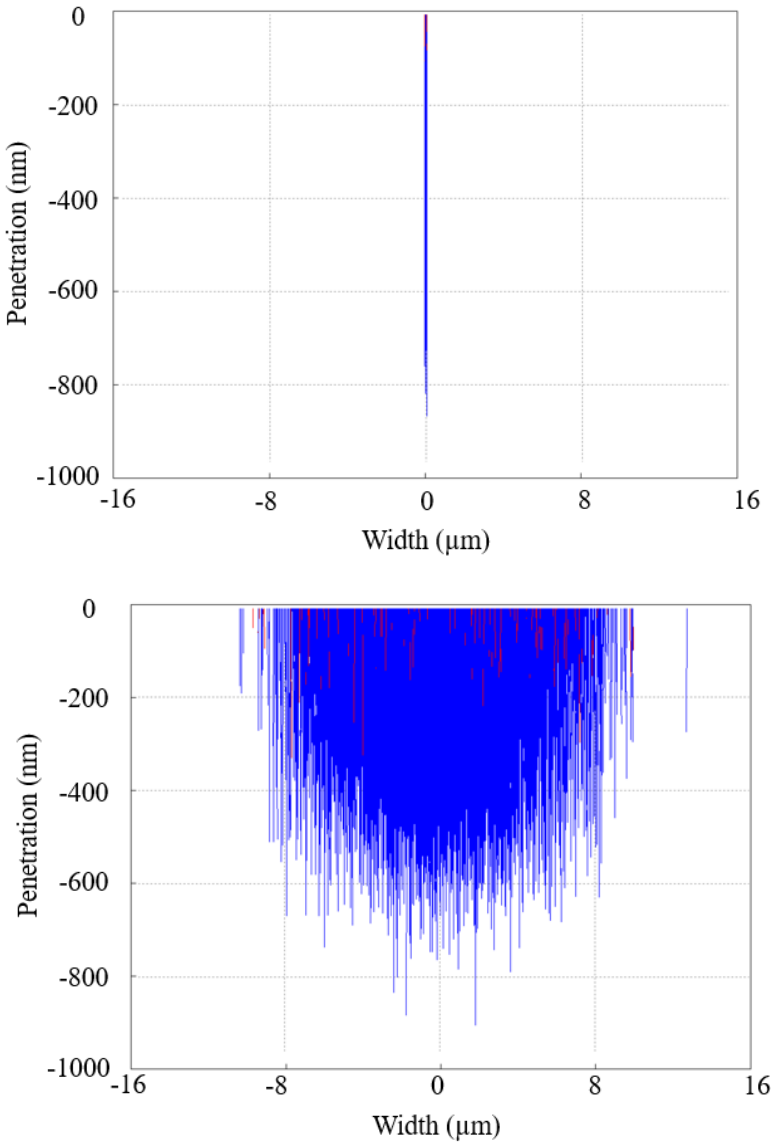

Figure 4.8 Interaction width comparison for (a) 0.1 µm and (b) 10 µm.

Figure 4.9 shows Mn composition profiles for 0.1 and 10 µm beam sizes for pipe sample B. It is evident that both beam sizes are providing similar detection of Mn in the steel sample. Thus, the 10 µm beam size was selected for microprobe analysis in this study for quantitative analysis. Using such a larger beam size, it is expected that, the number of detection points for the same scanning distance will decrease.

The distance between detection points will now be discussed. The smallest spacing between two detection points is determined by the effective beam size. A larger distance between two

detection points reduces the number of points needed in a line traverse and increases efficiency. However, more widely spread detection points have the concern of missing sections of the segregation band. A comparison between 4 µm and 10 µm spacing for pipe sample A is shown in Figure 4.10. There is no difference between the results for the 4 µm and 10 µm point spacing. Even though the 4 µm point spacing profile has a slightly smoother curve, the 10 µm beam was selected due to its better time efficiency.

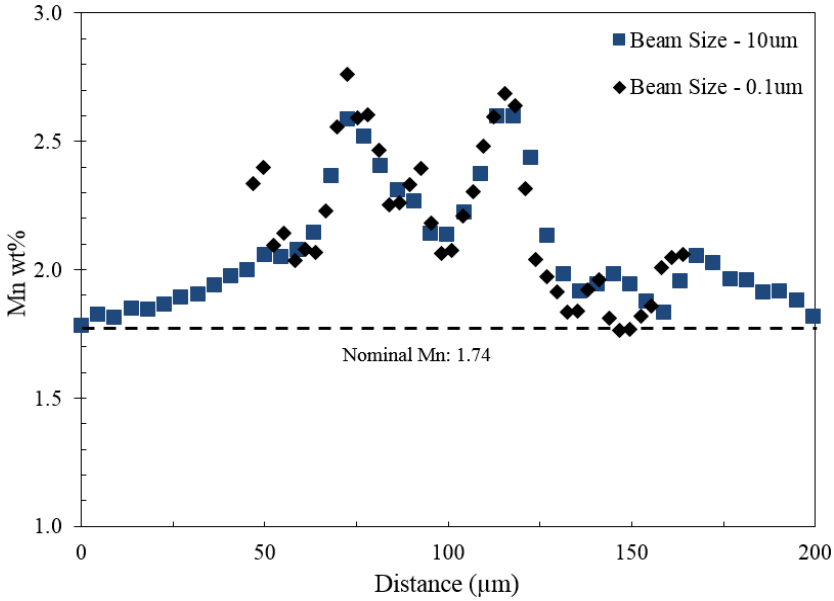

Figure 4.9 EMPA line scan for Mn for two beam sizes for pipe B (MR=3).

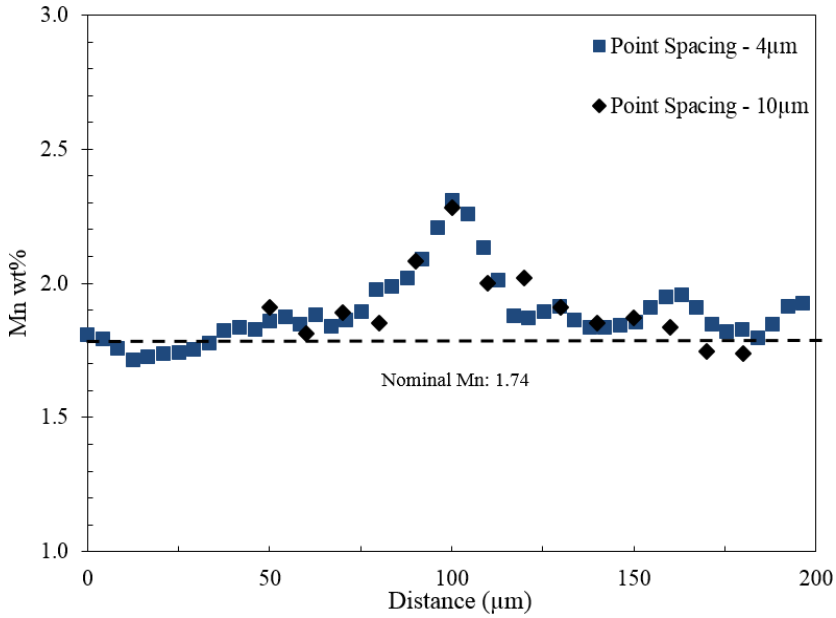

Figure 4.10 Comparison of point spacing variation for Mn detection for pipe A (MR=2).

In summary, Setup C was used with an accelerating voltage of 15 keV, 200 nA current, 80 s peak counting time, a 10 µm electron beam size, and a 10 µm point spacing. This setup was optimized for Mn. For other elements, the process described for Mn must be repeated to determine the optimum operating conditions of the microscope to yield the desired accuracy . For example, longer analysis times would be needed for lower concentration elements such as P. and lower voltage and current would be necessary for C detection to avoid high heat input.

4.2 Mannesmann Comparison

As discussed in Chapter 2, the Mannesmann rating number might represent the level of centreline segregation for cast slabs. There is no connection between Mannesmann rating values and Mn composition. In this section, Mannesmann 2 and 3 slabs and pipes were compared using optical microscopy, EMPA and Vickers microhardness testing. Image analyses were performed base on the Mannesmann rating images and EMPA Mn maps, and the difference between Mannesmann 2 and 3 slab samples will be discussed.

4.2.1 Optical Microscopy Comparison

Comparison of both as-cast and pipe samples using optical microscopy was performed. PAGS, allotriomorphic ferrite along the austenite grain boundaries, and width of the segregation zone were compared for all as-cast samples subjected to 4% Picral etching.

4.2.1.1 Cast Sample Comparison

The PAGS (outlined in Figure 4.11) and allotriomorphic ferrite size (indicated by arrow) were measured on the etched slab surfaces at the centreline region. For each Mannesmann rating, 10 images at the centreline region were captured and analyzed.

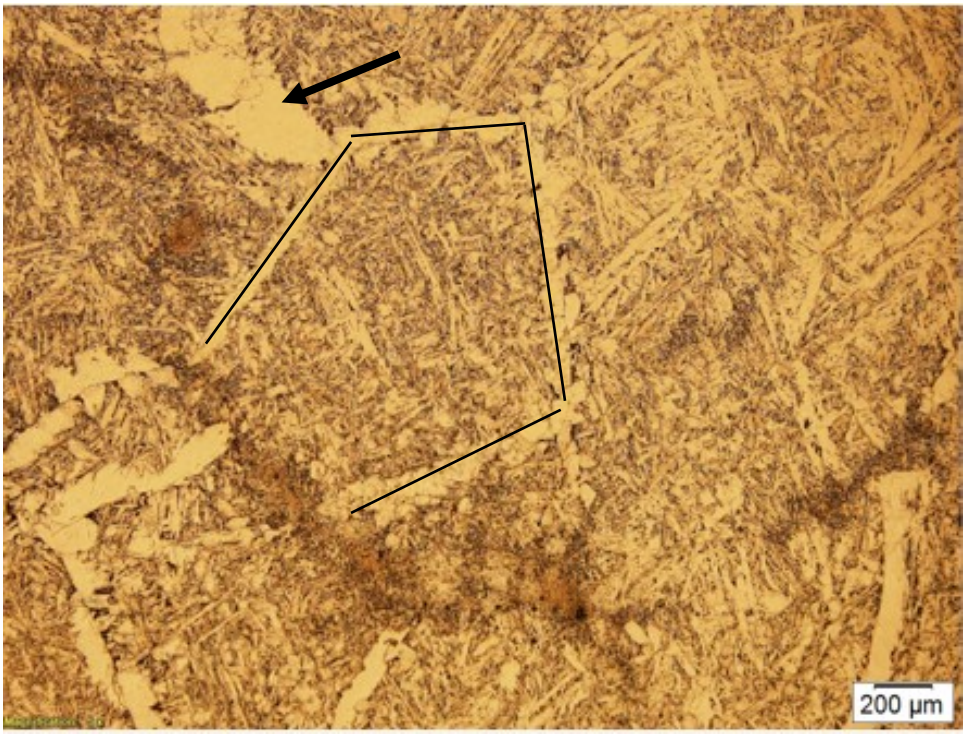

Figure 4.11 Optical micrograph of the prior austenite grains (PAG) of slab D (MR=2).

Table 4-4 summarizes the average austenite and allotriomorphic ferrite grain sizes along the austenite grain boundaries. The Mannesmann 2 slabs have average PAGS of 705 µm with a standard deviation of 321 µm, while Mannesmann 3 slabs have average PAGS of 773 µm with a standard deviation of 402 µm. The average ferrite grain size (standard deviation) for

the Mannesmann 2 and Mannesmann 3 slabs are 63.1 μm (28.7 μm) and 58.5 μm (23.6 μm) respectively.

Table 4-4 PAGS and ferrite size comparison for Mannesmann 2 and 3 slab samples.

	Average PAGS (Standard Deviation) (μm)	Average Ferrite Grain Size (Standard Deviation) (μm)
Mannesmann 2	705 (321)	63.1 (28.7)
Mannesmann 3	773 (402)	58.5 (23.6)

The PAGS has a wide size range from 16 μm to 1.02 mm for Nb-Ti microalloyed cast steel in previous research. (Femandez, 2003) (Eskandari, 2008) The detected PAGS falls within the range of the literature values. Due to the complexity of the solidification in continuous casting of slabs, there is a large standard deviation for the austenite and ferrite grain sizes.

The size of the allotriomorphic ferrite on the prior austenite grain boundary depends on the PAGS. (Capdevila, 2003) The difference between the two samples was small compared with the large standard deviation as the small difference (also large standard deviation) of PAGS. Thus, there is no significant difference for PAGS and allotriomorphic ferrite grain size between Mannesmann 2 and 3 slab samples.

A segregation zone (mostly ferrite) was observed at the centreline segregation band region (circled in Figure 4.12). The black areas are the porosities. Fujda reported (Fujda, 2005) that the pearlite content in the segregation zone for a continuous cast microalloyed steel has a higher carbon content than the slab surface. For a steel having 0.1 wt% C, the maximum value of pearlite reported at the centreline was 24% with11% at the slab surface and 13% at the sub-surface of the slab. (Fujda, 2005) Davis reported a higher amount of pearlite at the centreline as well as the presence of bainite and martensite for a continuous cast pipeline steel slab. The volume fraction of pearlite was reported to be 10 % at the centreline segregation zone, while the rest of the slab had 2-4% volume fraction of pearlite. (Davis,

2009) All observations made in this work of the microstructure of the centreline did not reveal any pearlite.

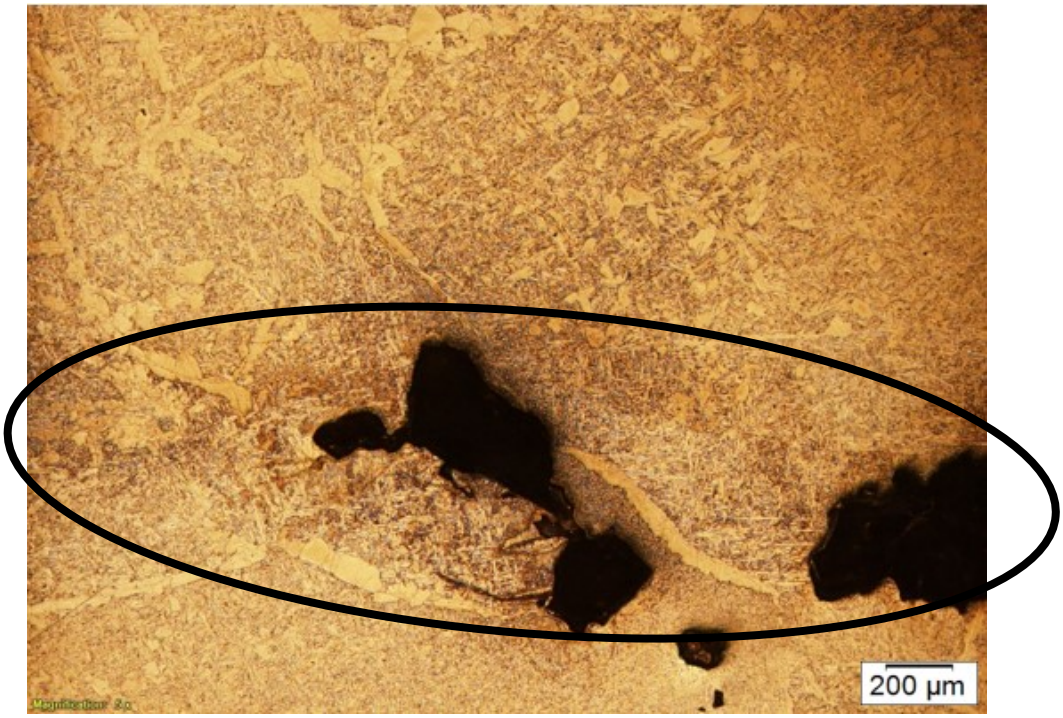

Figure 4.12 Optical micrograph of the segregation zone (circled) in slab D (MR=2).

From the images of optical micrographs, the width of the dark regions in the slabs were measured. The results shown in Table 4-5 indicate that Mannesmann 2 and 3 slabs have average segregation zone sizes of 514 µm and 644 µm, respectively, and standard deviations of 256 µm and 117 µm, respectively. There is no significant difference in the average segregation zone size for the two samples. Based on the Mannesmann rating method, Mannesmann 2 and 3 slabs have similar black dot sizes, this is in agreement with Rapp, 2010.

Table 4-5 Segregation zone width comparison for Mannesmann 2 and 3 slab samples.

	Average Segregation zone Size (µm)	Standard Deviation (µm)

Mannesmann 2	514	256
Mannesmann 3	644	117

The standard deviation for the Mannesmann 3 sample is significantly smaller than the standard deviation for Mannesmann 2 sample. From the standard Mannesmann centreline segregation charts, the major difference between Mannesmann 2 and Mannesmann 3 is that Mannesmann 3 slabs have the continuous black dots. (Su, 2013) Small segregation zones (black dots on the analyzing images) will be invisible for Mannesmann rating system. A smaller variation in the size of the segregation zone makes more continuous black dots are visible from the images. The smaller standard deviation of the segregation zone size for Mannesmann 3 slabs indicates a more uniform size of black dots found on the macro images.

4.2.1.2 Pipe Sample Comparison

For pipe samples, the segregation band was revealed using a 2% Nital etch. The segregation band is relatively uniform and smaller in width than in the slabs, since the sample has been rolled. Higher Mannesmann rated samples show a darker band colour as pointed out in Figure 4.13.

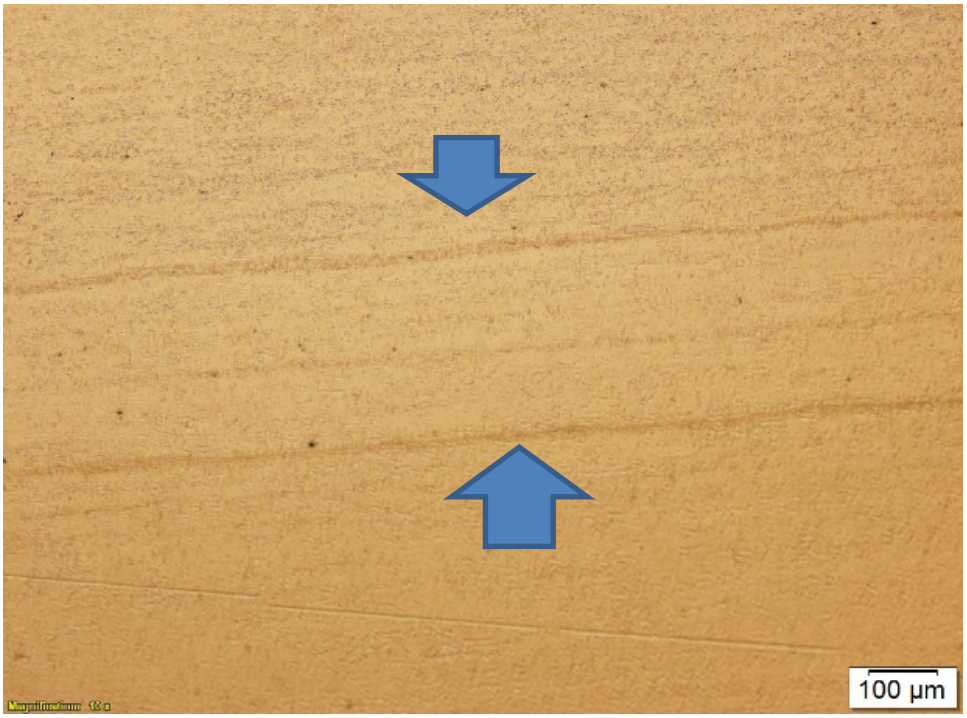

Figure 4.13 Optical micrograph of segregation bands (arrow pointed) of Nital etched pipe B (MR=3).

The measured segregation band widths are presented in Table 4-6. The Mannesmann 2 sample has an average segregation band width of 33.2 µm with a standard deviation of 0.16 µm, while the Mannesmann 3 sample has an average of 39.5 µm with a standard deviation of 0.22 µm. This is in agreement with the larger/wider segregation band for higher Mannesmann rating slab samples, as discussed above. The formation of this high hardness band will be discussed later in Section 4.2.3.

Table 4-6 Comparison of segregation band width for pipe Mannesmann 2 and 3 samples.

	Average Segregation Band Width (µm)	Standard Deviation (µm)
Mannesmann 2	33.2	0.16
Mannesmann 3	39.5	0.22

4.2.1.3 Summary

The steel pipe wall thickness is reduced during the rolling process. The pipe samples underwent a reduction ratio of 16 to 1 during rolling. The reduction ratio is the ratio reduced during TMCP from slab to pipe. The reduction ratio for the slab segregation band width is essentially the same as the rolling reduction ratio.

The segregation band width was measured using optical microscopy images and Mn line scan results. The results were tabulated and compared in Table 4-7. All measurements corroborate that the centreline segregation band is wider in the Mannesmann 3 steels than the Mannesmann 2 steels. From the optical microscopy measurements, the steel thickness is reduced by a factor of 15.7 during the rolling process in steel making (from the slab (200 mm) to pipe (12.7 mm)). The reduction ratios for Mannesmann 2 and 3 samples are 15.5 and 16.3, respectively. There is a minor effect due to the microstructure (segregation zone measured before) during homogenization for both Mannesmann 2 and 3 samples since the measured segregation band width reduction is similar to the steel thickness reduction.

Table 4-7 Segregation band width comparison between Mannesmann 2 and 3 samples.

	Optical-Slab (μm)	Optical-Pipe (μm)	Reduction Ratio
Mannesmann 2	514	33.2	15.5
Mannesmann 3	644	39.5	16.3

4.2.2 Mn Composition (EMPA) Comparison

4.2.2.1 Cast Sample Comparison

To compare the Mn segregation results of different Mannesmann rated as-cast samples, Mn concentrations were plotted and compared with microhardness values in Figure 4.14. For the Mannesmann 2 cast sample, the width of a major segregation band was 1600 μm. The Mn

segregation ratio was calculated to be 1.35 at the highest Mn concentration of 2.14 wt% with 1.59 wt% nominal Mn concentration. There is no peak in microhardness at the same location.

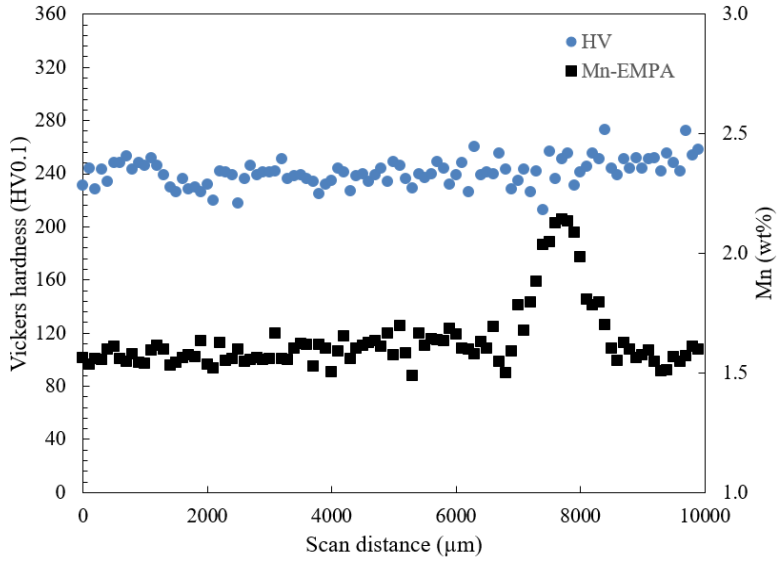

(a)

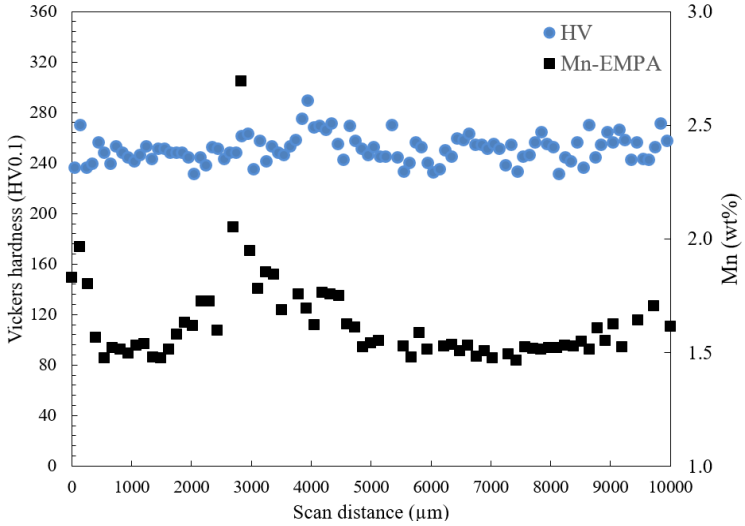

(b)

Figure 4.14 Comparison between microhardness and Mn composition for (a) slab D (MR=2) and (b) slab E (MR=3).

For the Mannesmann 3 cast sample, a large Mn peak was found with a segregation band width of 2000 μm. The Mn S.R. was calculated as 1.7 with 2.69 wt% as the highest value detected and 1.58 wt% as the nominal composition. The literature simulated Mn segregation at the centreline on continuous cast pipeline steel has an S.R. of 1.69. (Davis, 2009) This is the same region with EMPA detected Mn S.R. and microhardness tests on the Mannesmann 3 slab samples. The microhardness tests locations were selected to be close to the EMPA line scan location. There are small shifts in the test location.

The Mn segregation band has a similar shape and width with the corresponding microhardness peak for the Mannesmann 3 sample. There was a peak shift (between the microhardness peak and Mn peak) as shown in Figure 4.14 (b). This is because the analyzed locations were not exactly the same as discussed in the previous paragraph. The Mn segregation and microhardness results for the cast samples suggest that the higher Mannesmann rating samples have higher Mn segregation ratios with larger segregation zones. A critical segregation level is required to reveal any microhardness differences for the cast samples, such as the Mannesmann 3 sample.

Figure 4.15 shows a typical microprobe line scan at the centreline of a cast HSLA steel from the literature. Mn is segregated at the centreline in the Figure with a S.R. of 1.33 and a band width of approximately 10 mm. (Den Boer, 2013) The literature reported segregation band is wider than the segregation bands measured in this work. The average bands have size around 1-2 mm based on the EMPA Mn line scan results. The measured segregation width in the literature varies from 1 mm to 10 mm depending on different chemistry and cast conditions. The detected Mn in this study shows a smoother and more continuous Mn composition change within the segregation band than the literature profiles.

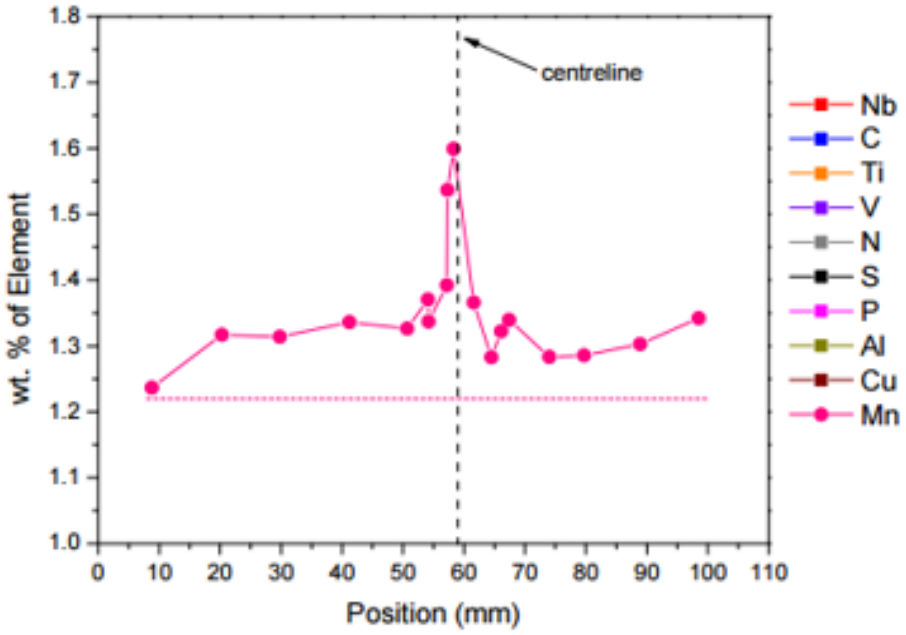

Figure 4.15 Typical EMPA line scan results at the centreline segregation region of a continuous cast HSLA steel. (Den Boer, 2013)

4.2.2.2 Pipe Sample Comparison

The Mn concentration at the centreline is reported here and is used to compare Mn segregation behavior between Mannesmann 2 and Mannesmann 3 pipes at this segregated zone. As shown in Figure 4.16, there is a single segregation band for the Mannesmann 2 pipe sample, while multiple bands exist for the Mannesmann 3 pipe sample.

For the Mannesmann 2 pipe sample, the highest Mn concentration detected was 2.31 wt% compared with the nominal Mn concentration of 1.74 wt%. The segregation band is 42 µm thick, and the Mn segregation ratio is 1.33. For the Mannesmann 3 pipe sample, the Mn peak occurs at 2.47 wt% with 1.74 wt% being the nominal Mn concentration in the steel. The major segregation band width is 50 µm, and the Mn segregation ratio is 1.44.

Compared with the Mannesmann 2 pipe sample, the Mannesmann 3 pipe sample has a higher Mn segregation ratio at the centreline region with a slightly wider segregation zone. It is evident that the higher Mannesmann rating sample corresponds to higher elemental concentration at the centreline segregation zone.

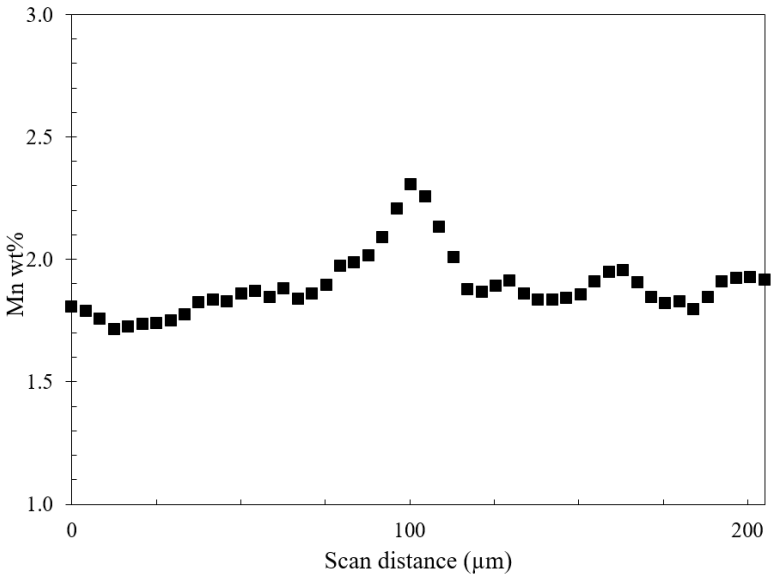

(a)

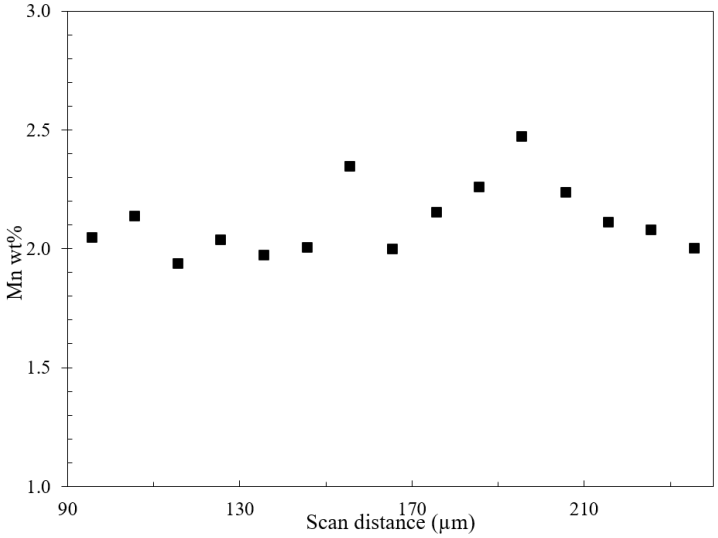

(b)

Figure 4.16 Mn composition determined using EMPA though the segregation band of (a) pipe A (MR=2) and (b) pipe B (MR=3).

4.2.2.3 Summary

The Mn S.R. for both Mannesmann 2 and 3 samples are provided in Table 4-8. For both as-cast and pipe samples, the Mn segregation ratio for Mannesmann 3 samples is higher than that for Mannesmann 2 samples. The corresponding microhardness ratios at the same location exhibit similar behaviour.

Table 4-8 Segregation ratio (S.R.) comparison for Mannesmann 2 and 3 samples.

	As-cast Segregation		Pipe Segregation	
	Mn Ratio	HV Ratio	Mn Ratio	HV Ratio
Mannesmann 2	1.35	1.09	1.33	1.16
Mannesmann 3	1.70	1.15	1.44	1.55

4.2.3 Microhardness Comparison

4.2.3.1 Cast Sample Comparison

The microhardness tests were performed across the centreline segregation zone at a total distance of 10 mm (with zone size of around 1 mm). As shown in Table 4-9, the Mannesmann 2 sample has an average microhardness of 241 HV with a standard deviation of 10.2 HV. The Mannesmann 3 sample has an average microhardness of 250 HV at the centreline segregation region with a standard deviation of 10.9 HV. The highest microhardness values detected for Mannesmann 2 and Mannesmann 3 are 263 HV and 289 HV, respectively. The difference between Mannesmann 2 and 3 slab sample is not significant consider one standard deviation.

Table 4-9 Microhardness comparison for Mannesmann 2 and 3 slab samples.

	Average Microhardness (HV0.1)	Peak Value (HV0.1)	Standard Deviation (HV0.1)
Mannesmann 2	241	263	10.2
Mannesmann 3	250	289	10.9

With respect to the average values, the microhardness of Mannesmann 3 slab samples appears to be slightly higher than the values in Mannesmann 2 slabs. Figure 4.17 compares the microhardness versus the scan distance for slab D and E. Included in the figure is a horizontal dashed line representing the sample average microhardness value of the centreline

region. Unlike Mn composition profile (Mn segregation peak), both microhardness profiles show a relatively constant values of microhardness over the 10 mm thickness in the slab centreline.

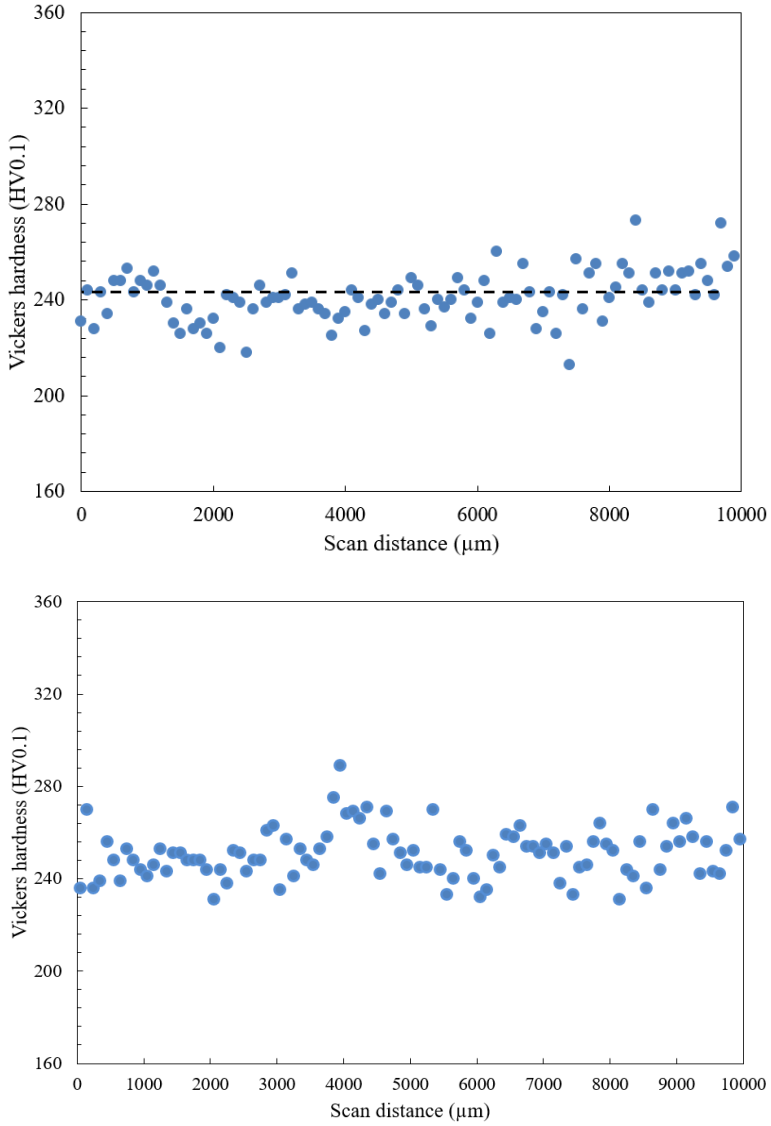

Figure 4.17 Microhardness across the segregation band for (a) slab D (MR=2) and (b) slab E (MR=3).

The experimental P/A ratio is 1.09 and 1.15 for Mannesmann 2 and 3 respectively. From EMPA line scan results at the close position (more detail in section 4.2.3), Mn S.R. are found to be 1.58 and 1.70 for Mannesmann 2 and Mannesmann 3 respectively (see section 4.2.2.1)

According to Thelning (Thelning,1984), microhardness of ferrite increases 1.37 times when Mn increase from 2 wt% to 4 wt%. It is seen from Figure 2.1 that over small ranges of Mn content in solid solution (<3wt%), the relationship between Mn content and microhardness can be approximated using a linear relationship. Thus, a S.R. of 1.58 for Mannesmann 2 should yield a P/A ratio of 1.08. For the Mannesmann 3 slab a Mn S.R. of 1.70 should yield a P/A of 1.16. The Mn S.R. and microhardness P/A found in this work were also follow a similar linear relationship. These values are in agreement with the measured P/A values of 1.09 and 1.15 for Mannesmann 2 and 3 respectively. Thus, for the region of centreline segregation, the microstructure is likely most affected by the solute solution of Mn. Other effects that could contribute to these P/A values could be the presence of pearlite, bainite and/or martensite. (Davis, 2009) (Howe, 1991) Although these phases were not identified in the sample, their presence would be expected to result in a greater value of the P/A.

There is only less than 10 % increase for mannesmann 2 sample when Mn increase from nominal to its peak value. The increase of Mn within the segregation zone (small increase between each analyzing location) is not big enough to reflect on the microhardness change. The Mn segregation does not translate into an increase in microhardness might be due to the other factors that need to be analyzed in the future work.

4.2.3.2 Pipe Sample Comparison

The hardness values for the segregated area, and the average hardness values for both Mannesmann 2 and 3 pipe samples are shown in Table 4-10. The highest Vickers microhardness value for the Mannesmann 2 sample is 250 HV with an average value of 215 HV. The Mannesmann 3 sample has a peak microhardness value at 304 HV with an average value of 196 HV.

Table 4-10 Microhardness comparison for Mannesmann 2 and 3 pipe samples.

	Average Microhardness (HV0.1)	Peak Value (HV0.1)	Standard Deviation (HV0.1)
Mannesmann 2	215	250	5.42
Mannesmann 3	196	304	4.83

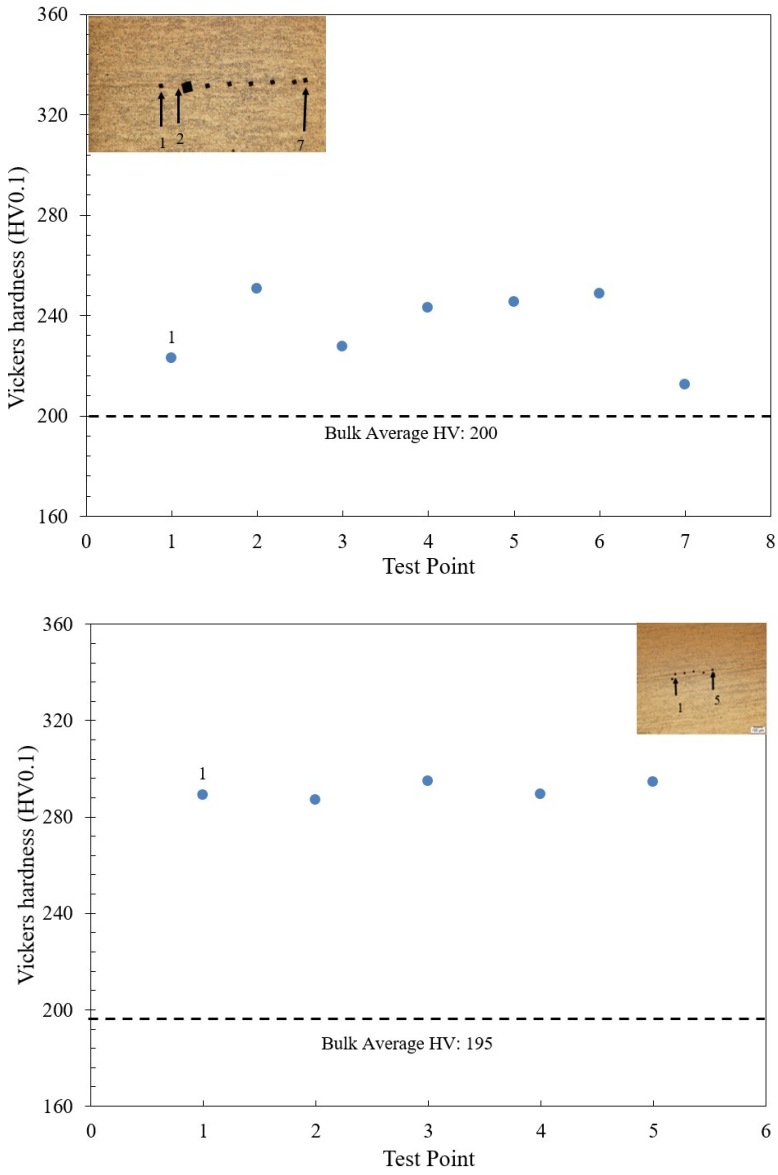

Figure 4.18 Microhardness along the segregation band for (a) pipe A (MR=2) and (b) Pipe B (MR=3).

The reason for the larger peak hardness difference is due to solute strengthening and precipitation hardening. Acicular ferrite and bainite were found in the middle of the pipe. (Reip, 2006) The two phases have higher microhardness values than ferrite. Mn provides solution strengthening at compositions over 1 wt% at the centreline (Beidokhti, 2009) and Nb provides strengthening at the centreline by decreasing the grain size during hot rolling (Hashemi, 2009) and providing precipitation strengthening. (Kostryzhev, 2010) Due to a

higher level of segregation behaviour at the centreline for the Mannesmann 3 sample than the Mannesmann 2 sample, the Mannesmann 3 sample had a higher peak microhardness of the segregation band.

4.2.4 Image Analysis

Although there is only a slight difference in microstructures, the Mannesmann 3 sample exhibits a higher level of segregation than the Mannesmann 2 sample in terms of Mn composition and microhardness but there is a large standard deviation. Indeed, these comparisons were based on local segregation (micro view), and the results depend on the location in the analyzed sample.

A macro analysis was used to determine the segregation level for a 5 mm wide area at the centreline of the slab. This analysis involves microhardness tests results, metallurgical measurments, microprobe anlaysis results and image analysis results. The image analysis connect the Mn segregation with Mannesmann rating numbers and provides metallurgical meaning (Mn segregation level) for the Mannesmann system.

In order to compare the Mannesmann rating system with Mn segregation at the centreline, a comparison of the segregation difference between Mannesmann 2 and 3 samples was done using image analysis based on the macro images and Mn EMPA maps. Image analysis for both macro images and EMPA Mn maps was done to compare the different Mannesmann samples. Image analysis was done based on grey level differences.

4.2.4.1 Macro Image Analysis

From MATLAB (v. 2016b) calculations, the percentage of different grey levels for slab D using macro image are tabulated in Table 4-11. The analysis was based on the image has a width of 5 mm around the centreline segregation as motioned in section 3.5. Grey levels represent the brightness of the original photo image. A pixel with a higher brightness as shown in Section 3.6.1, has a higher level of segregation. The first row in Table 4-11 lists the grey level classes from 10 to 230 and the second row the percentage of pixels at the corresponding grey level for the analyzed sample. The 0-10 interval is 0. For the

Mannesmann 2 slab sample using a macro image, the highest portion of grey levels falls in 150-170 range.

Table 4-11 Macro image analysis results for slab D (MR=2).

Grey level classes	10-30	30-50	50-70	70-90	90-110	110-130	130-150	150-170	170-190	190-210	210-230
Count %	0	0	0.01	0.14	2.62	13.22	30.39	31.56	14.57	5.86	2.20

4.2.4.2 EMPA Mn Mapping Analysis

From the MATLAB calculations, the percentage of different grey levels for slab D using the EMPA Mn maps is tabulated in Table 4-12. The analysis was conducted based on the 5 mm wide region, which is the same as macro image analysis (section 4.2.4.1). Grey level here represents the signal intensity of Mn in microprobe mapping analysis. A grey level of 0 represents no Mn had been detected at the pixel. Higher values of grey levels correspond to higher values of Mn content . For the Mannesmann 2 slab sample, the highest frequency of grey level class falls in 10-30 grey level. While each pixel in the Mn map corresponds quantitatively to a weight percent of Mn, the conversion of pixel grey values to Mn content would require calibration which was not done in this work.

Table 4-12 EMPA Mn maps analysis results for slab D (MR=2).

Grey level classes	0-10	10-30	30-50	50-70	70-90	90-110	110-130	130-150	150-170	170-190	190-210	210-230
Count %	5.30	79.6	20.2	0.22	0.01	0	0	0	0	0	0	0

4.2.4.3 Mannesmann Comparison

The grey level data from macro images and Mn maps were tabulated and compared for both Mannesmann 2 and 3 slabs. Figure 4.19 and Figure 4.20 compared the percentage distribution of grey levels from image analysis on macro images and EMPA Mn maps, respectively. A higher grey level might represent a higher level of segregation (macro images) and amount of Mn composition (Mn maps).

For macro images, the Mannesmann 3 sample has its two highest grey level classes as 190-210 and 210-230 (190-230), while Mannesmann 2 has its two highest grey levels at 130-150 and 150-170 (130-170). For EMPA Mn maps, the Mannesmann 3 sample has its two highest grey level classes at 30-50 and 50-70 (30-70), while Mannesmann 2 has its highest two grey levels at 10-30 and 30-50 (10-50). Both methods show that the Mannesmann 3 slabs have higher levels of segregation and Mn composition at the centreline segregation region than Mannesmann 2 slabs.

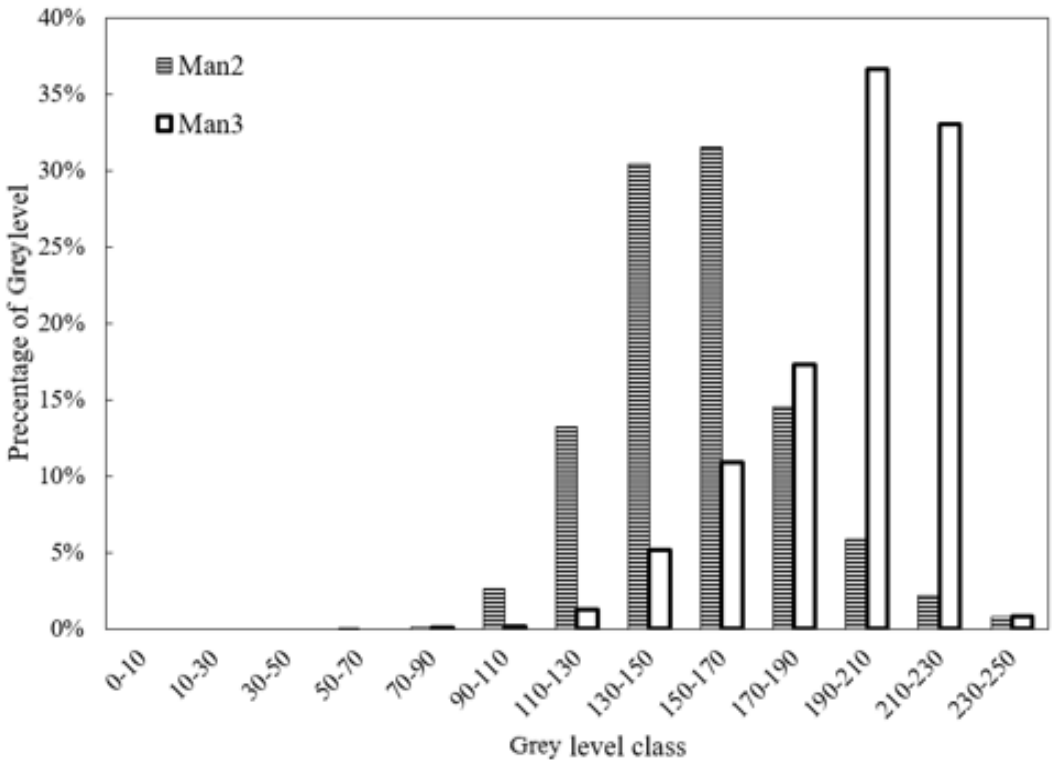

Figure 4.19 Percentage of grey levels for Mannesmann 2 and 3 samples using macro images.

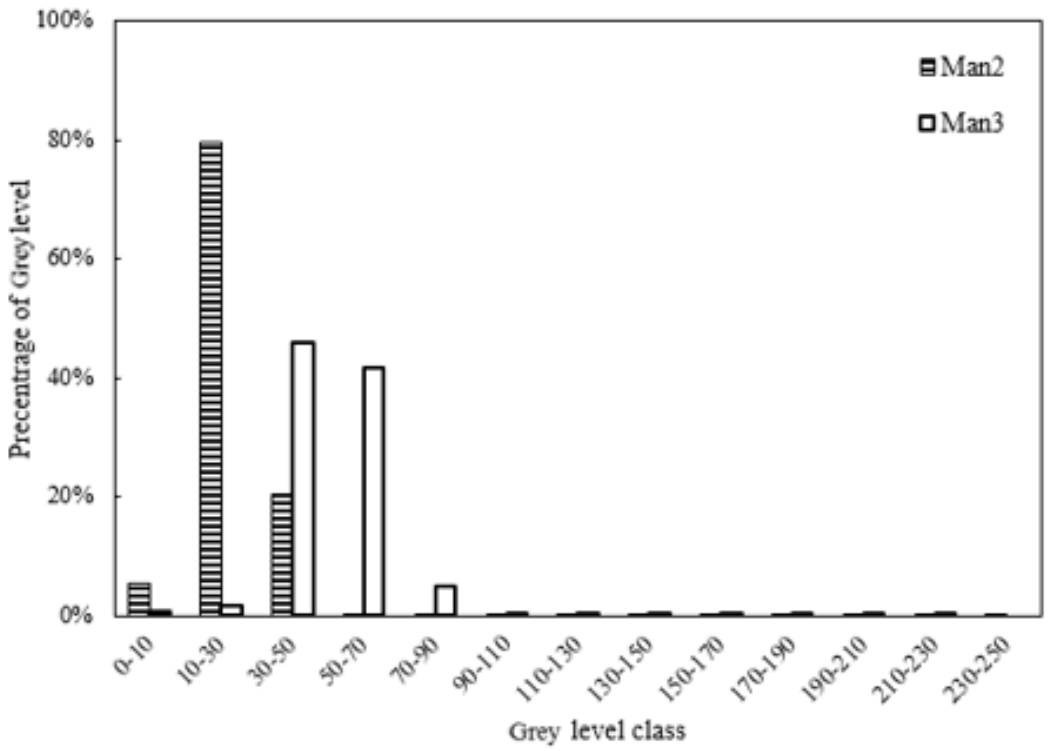

Figure 4.20 Percentage of grey levels for Mannesmann 2 and 3 samples using EMPA Mn mapping.

Figure 4.19 and Figure 4.20 show the distribution of different class of grey levels from two different sources. To compare the results from two different types of images (optical and EMPA Mn intensity), sum seg (SS) number was calculated for both Mannesmann 2 and 3 slabs. Also, this number was calculated using microhardness results, Mn composition form EMPA line scans, etc. This SS number connects the macro image directly to Mn composition and microhardness, and express the level of the segregation at the centreline region in a macro view. The sum seg number was calculated using Equation 4-1.

$$SS = \sum_{j=a}^{b} (P_j \times i)_j \qquad 4\text{-}1$$

where i is the average value at the jth class, a is the lowest value in the category, b is the highest value in the category, and Pj is the percentage of counts at the jth class.

Using image analysis results as an example, j is the grey level class, and Pj is the percentage of the grey level of jth class. Figure 4.21 compares the SS numbers for Mannesmann 2 and 3 based on image analysis results. Both methods (optical and Mn maps) show a higher SS number for Mannesmann 3 slabs than Mannesmann 2 slabs. From the previous research on the image analysis of the macro images, Mannesmann 3 pipeline steel slab samples had a larger number of black dots at the centreline segregation region based on macro image analysis. The total number of black dots increased from 33 to 50 for Mannesmann 2 and 3 sample respectively. (Su, 2013) This agrees with higher the image analysis results and the calculated SS number for Mannesmann 3 slabs than Mannesmann 2 slabs. To complete the analysis of the relationship between SS number and Mannesmann rating number, Mannesmann 1, 4, and 5 samples need to be analyzed in future work. The difference of SS number on microhardness and Mn composition between Mannesmann 2 and 3 slabs will be discussed in section 4.4.

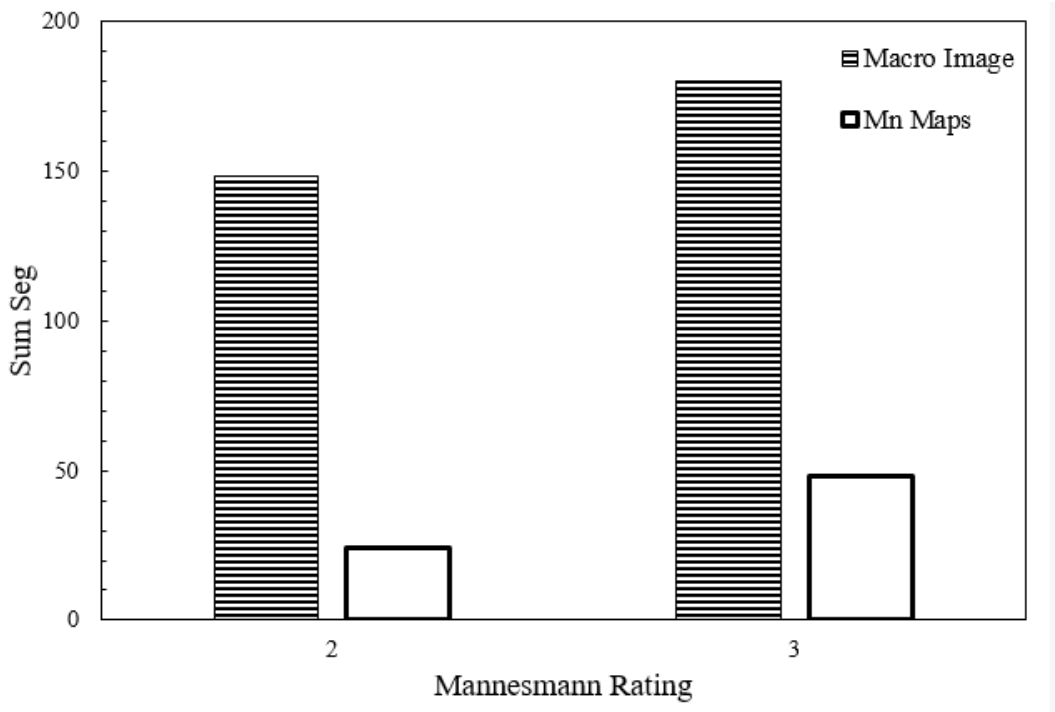

Figure 4.21 Sum seg number for Mannesmann 2 and 3 slab samples using image analysis.

4.2.5 Summary

To compare the Mannesmann 2 and 3 sample, Mn segregation ratio (S.R.), microhardness peak to average ratio (P/A) and width of the segregation band were used. Table 4-13 summarizes S.R. and P/A numbers for Mannesmann 2 and 3 samples. For both as-cast and pipe samples, the Mn S.R. for Mannesmann 3 samples is higher than that for Mannesmann 2 samples. The corresponding P/A at the same location exhibit similar behaviour.

Table 4-13 S.R. and P/A comparison for Mannesmann 2 and 3 samples.

	As-cast Segregation		Pipe Segregation	
	Mn S.R.	HV P/A	Mn S.R.	HV P/A
Mannesmann 2	1.35	1.09	1.33	1.16
Mannesmann 3	1.70	1.15	1.44	1.55

The width of the segregation band for both slabs and pipes were measured using optical images and EMPA Mn line scans. Reduction ratio was calculated （the band width of slab over the band of pipe）for each type (optical and EMPA). As shown in Table 4-14, the reduction ratio for the segregation band width decreased by a factor of ~16 based on the etched images and by a factor of ~40 based on Mn segregation profiles. The reduction ratio during rolling process is 16. Thus, the heat treatment has an effect on the microstructure, but not on Mn segregation. A homogenization experiment was done to study the change in Mn segregation and microhardness during homogenization.

Table 4-14 Segregation band width comparison between Mannesmann 2 and 3 samples.

	Optical-slab (μm)	Optical-pipe (μm)	Reduction Ratio	Mn Measured-slab (μm)	Mn Measured-pipe (μm)	Reduction Ratio
Mannesmann 2	514.4	33.2	15.5	1600	42	38
Mannesmann 3	644.5	39.5	16.3	2000	50	40

4.3 Homogenization Effects

The homogenization experiments were done on both Mannesmann 2 and 3 samples. As described in Chapter 3, a mirror samples for surface analysis were produced. The rounded off corner indicated the direction of the sample in the whole slab. These marking processes ensured the same location was analyzed for both as-cast samples and homogenized samples. Although cutting, grinding, and polishing can result in small displacements (several microns) between the two surfaces analyzed, the segregation behavior on the two faces should be similar.

Vickers microhardness tests were performed to examine the mechanical properties at the centreline segregation region for both the as-cast and homogenized samples. Microprobe analysis (maps, line scans, and shot gun analysis) was used to distinguish the Mn segregation level after homogenization. The effect of homogenization on complex Mn segregation profiles is discussed. Microhardness, EMPA line scan and shot gun analysis results will be discussed in this section.

4.3.1 Microhardness Comparison

Figure 4.22 (a) and (b) show the microhardness variation through the centreline segregation band for both as-cast and homogenized samples (at 1100°C and 16 h) for Mannesmann 2 and Mannesmann 3 steels. The microhardness values at the segregation band region do not differ significantly from the average microhardness for the as-cast Mannesmann 2 sample. The average Vickers microhardness values decrease after the homogenization treatment, from 238.7 HV to 210.3 HV. This reduction in microhardness is the result of the homogenization treatment, as evident by the grain growth discussed in Chapter 2. The standard deviation for the homogenized Mannesmann 2 sample also decreased from 9 HV for the as-cast condition to 7.5 HV.

The Mannesmann 3 samples in Figure 4.22 (b) show similar behaviour as the Mannesmann 2 samples. There is no significant difference for the slab samples. The average microhardness decreased after homogenization from 250.8 HV to 205.4 HV, with standard deviations of 9.5 HV and 7.6 HV, respectively.

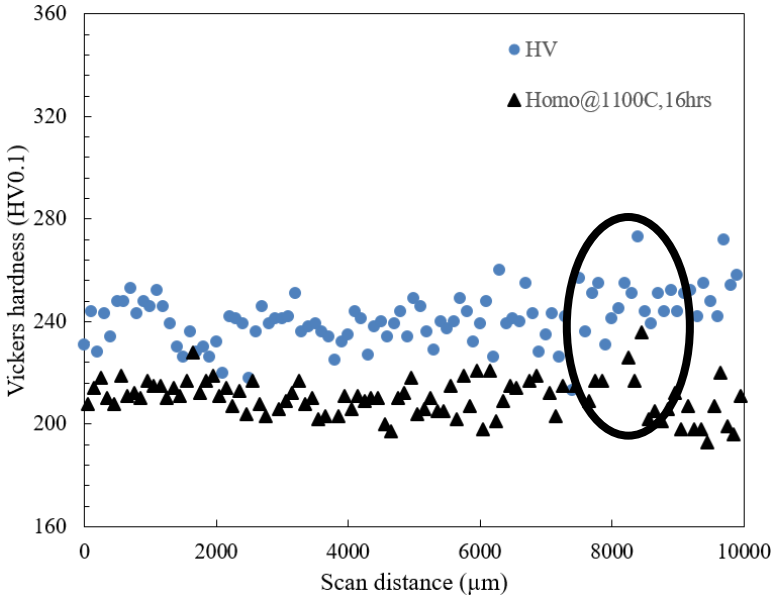

(a)

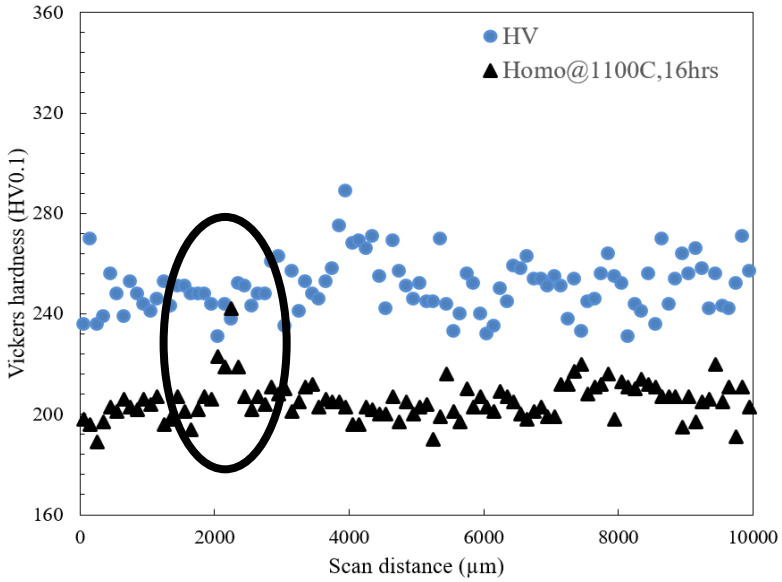

(b)

Figure 4.22 Microhardness before and after homogenization at 1100°C for 16 h: (a) D (MR=2) and (b) E (MR=3).

Both Mannesmann 2 and 3 samples show a decrease in average microhardness values after homogenization. The reason for the decrease in average values is an increase in prior austenite grain size during homogenization. With the preliminary measurement results, the PAGS before and after homogenized at 1100°C for 16 h were tabulated in Table 4-15. After

homogenized at 1100°C for 16 h, the average PAGS increases for both Mannesmann 2 and Mannesmann 3 slabs. Although the standard deviation is large compared to the grain size, there is an increasing in average grain size.

Table 4-15 PAGS measurement before and after homogenization at 1100°C for 16 h.

	Before (μm)	Standard deviation (μm)	After (μm)	Standard deviation (μm)
Mannesmann 2	705	321	874	222
Mannesmann 3	773	402	907	357

Using the parabolic grain growth formula, the final grain size after homogenization at 1100°C for 16 h is 806 μm compared with the as cast size of 707 μm. (Azizi, 2015) Both simulation and preliminary measurement results confirm the growth of the PAGB. Verification of grain growth needs to be completed on the homogenized samples. The complete measurement of the PAGB size needs to be done for future work.

The segregation band is more evident for the Mannesmann 3 slab sample in Figure 4.22(b) than in the Mannesmann 2 slab sample, with a clear microhardness peak due to more pronounced segregation behaviour. There is a 50 HV difference for the Mannesmann 3 slab sample between peak and average microhardness values and a 30 HV difference for the Mannesmann 2 slab sample. As discussed in Chapter 2, microhardness decreases as austenite grain size increases during the homogenization process.

The presence of hardness peaks (circled in Figure 4.22) for both samples is due to precipitates. As shown in Figure 4.23 (a), Nb nitride/carbide precipitates are present in both as-cast and homogenized samples. The EDX scan (Figure 4.23 (b)) indicates that the bright rod shaped precipitates are Nb-rich with Ti included. C and N were not displayed on the spectrum due to the detection limit on the machine. The EDX detector used was only able to pick up the element has an atomic number over 20. As discussed in Section 4.2.3 Nb precipitates at the centreline provide precipitation hardening.

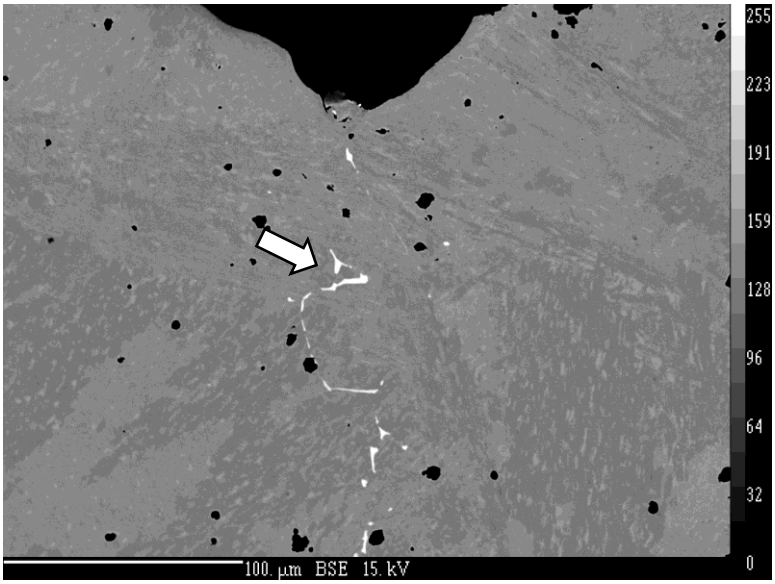

(a)

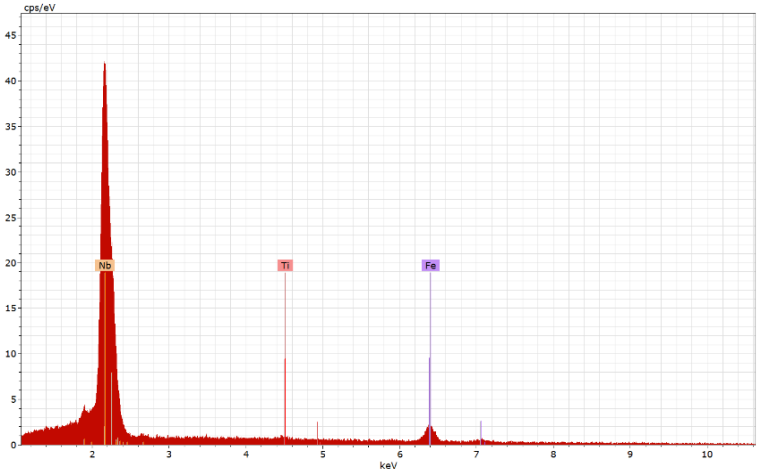

(b)

Figure 4.23 (a) BSE image of Nb precipitates at the centreline segregation area for slab E (MR=3) and (b) EDX spectrum of the precipitates in (a).

Nb precipitates were observed for both as-cast and homogenized samples, as shown in **Error! Reference source not found.**. Long rod-shaped precipitates were observed for the a s-cast Mannesmann 3 sample (circled in (a)) and the sample homogenized at 1300°C for 2 h (circled in **Error! Reference source not found.** (b)). Precipitate size measurements were d one using the relatively low magnification BSE images. From the preliminary measurements, the average length for Nb precipitates in the as-cast slab is 12.0 µm with a standard deviation

of 5.12 μm. The average width of the rod-shaped precipitates is 2.24 μm with a standard deviation of 0.47 μm.

After homogenization at 1300°C for 2 h, the average length of the precipitates decreased to 9.88 μm with a larger standard deviation of 6.43 μm. The average width was similar with a value of 2.50 μm and a standard deviation of 0.44 μm. Precipitates decreased in size and were spheroidized after homogenization at 1200°C for 16 h (circled in **Error! Reference s ource not found.** (c)). From the size measurement results, the spheroidized precipitates have an average diameter of 1.02 μm with a standard deviation of 0.39 μm.

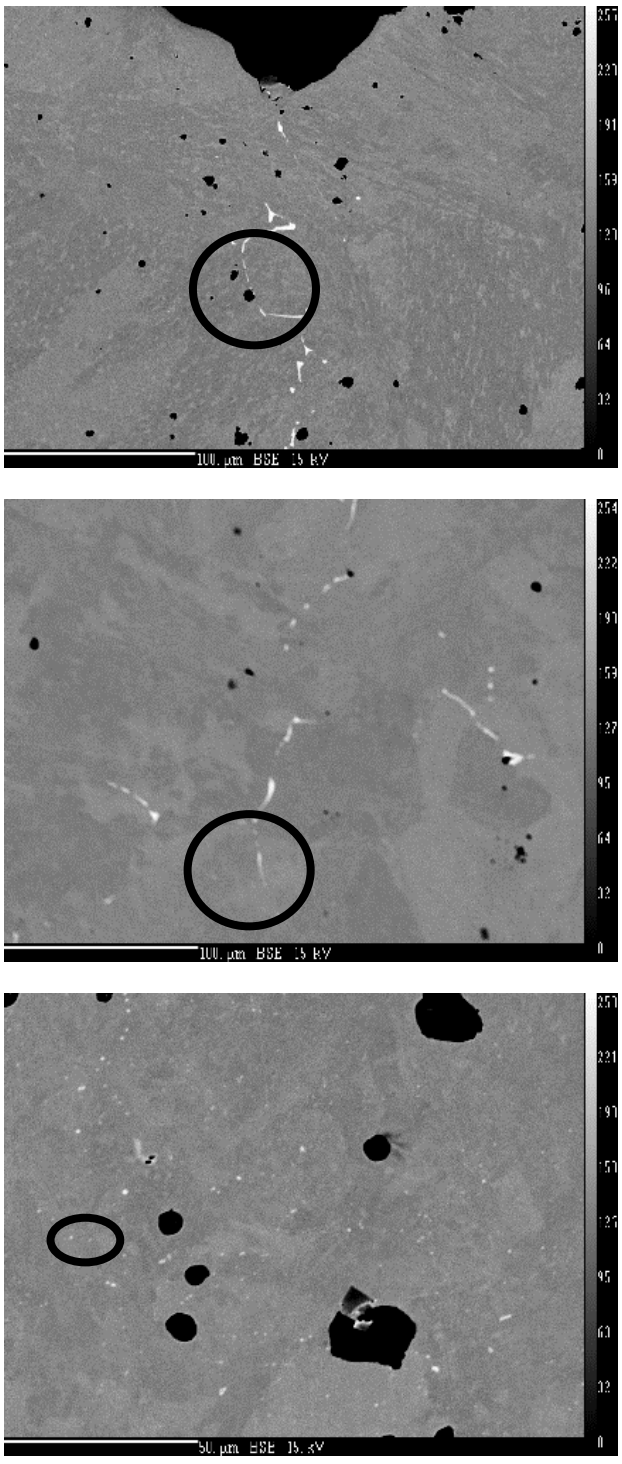

(a)

(b)

(c)

Figure 4.24 BSE images of Nb precipitates (circled white particles) in slab E (MR=3): (a) As-cast (b), 1300°C for 2 h and (c) 1200°C for 16 h.

To understand the Nb precipitates, future analysis about the formation and size distribution before and after homogenization is needed.

4.3.2 Mn Composition Comparison

This section compares the Mn reduction during homogenization at above three conditions using EMPA mapping and line scan techniques. Based on the line scan results, the effect of the complex Mn distribution of as-cast sample will be discussed.

4.3.2.1 Mn Maps

From the maps shown in Figure 4.25, it is evident that centreline segregation still exists after the homogenization process. Mn is concentrated at the centreline region (circled) and away from centreline (rectangle). There is a clear drop in Mn intensity rectangular area during homogenization at 1200°C for 16h.

The processed Mn maps shows a dispersed Mn segregation pattern at the centreline segregation region (circled in Figure 4.25). Mn enrichment at the centreline segregation is not continuous. The analyzed location is critical in comparing as-cast and homogenized Mn segregation. To compare the amount of Mn reduction at the centreline segregation region quantitatively, line traverses were conducted for both the as-cast and homogenized samples (mirror analyzing surface used to ensure EMPA analysis at the same location) at the highly-concentrated centreline region indicated by the dashed lines shown in Figure 4.25.

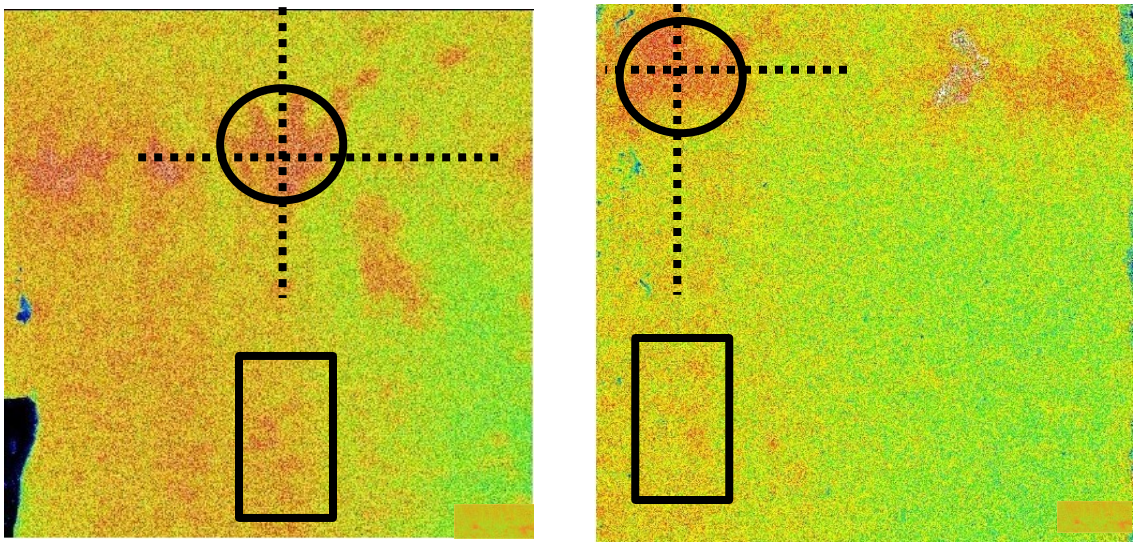

(a) (b)

Figure 4.25 Mn mapping of slab D (MR=2): (a) as-cast and (b) homogenized at 1200°C for 16h.

Mn concentration profiles through the centreline segregation band are compared in Figure 4.26. Peak adjust is the adjustment used to line up the centre of the segregation peak for comparison. (The distance between two dashed horizontal lines is the peak adjust distance.) Although the line scans were performed at the same location for two samples, there may have been a different start point for each scan compared with the centre of the segregation band. The Mn concentration decreases within the centreline segregation band after homogenization. The quantitative analysis results verify the existence of a Mn-rich zone.

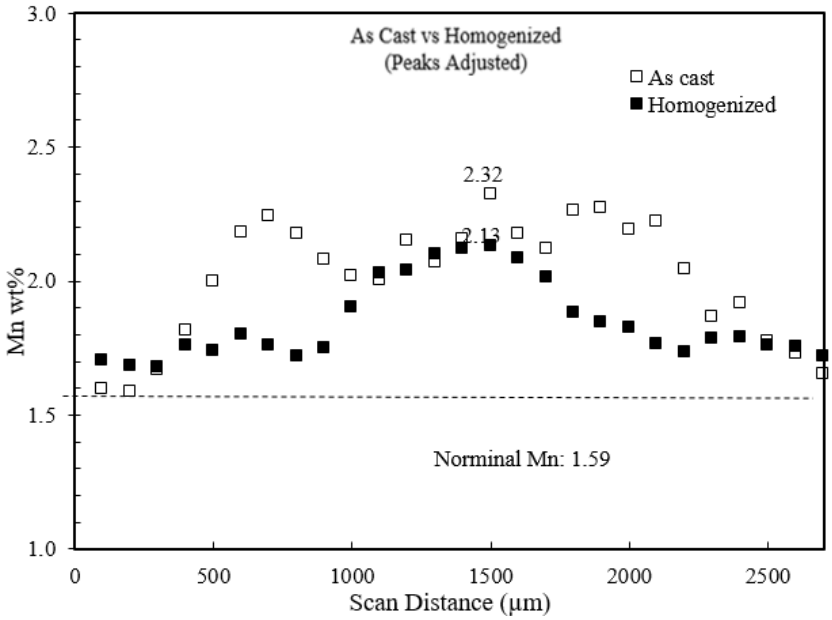

Figure 4.26 Mn concentration profiles before and after homogenization for slab D (MR=2); as-cast and homogenized at 1200°C for 16h.

4.3.2.2 Line Traverses Comparison

Figure 4.27 (a), (b), and (c) illustrate the Mn concentration at the centreline segregation region for samples homogenized at 1100°C for 16 h, 1200°C for 16 h, and 1300°C for 2 h, respectively. Included in the figures are vertical dashed lines representing the location of the segregation band in the cast slab samples. Again, line scans on the corresponding slab, and homogenized samples were taken at similar positions. The full scan of a 10 mm region could be found in Appendix G.

In Figure 4.27 (a), the Mn concentration decreases after homogenization across the whole sample and the peak Mn concentration at centreline segregation band decreases dramatically for the Mannesmann 2 steel. In all three samples, a significant decrease in the Mn concentration at the centreline segregation band was observed.

Within the centreline segregation band area, the Mn concentration of the Mannesmann 2 steel decreases after annealing at 1100°C for 16 h and 1200°C for 16 h. There are multiple segregation bands for the as-cast steel in Figure 4.27 (b) (three vertical dashed lines), and the minor bands were eliminated during homogenization at 1200°C for 16 h. As a result of the

multiple segregation bands, the major Mn segregation peak in the middle of the three bands was reduced even more relative to the 1100°C anneal for 16 h.

The Mn segregation ratio (S.R.) was reduced more for samples with a single segregation peak (Figure 4.27 (a) and (c)) compared with samples with multiple segregation peaks (Figure 4.27 (b)). The S.R. were reduced from 1.35 and 1.54 to 1.20 and 1.08 after homogenized at 1100°C for 16 h and 1300°C for 2 h, respectively. For 1200°C for 16 h, the S.R. was reduced from 1.46 to 1.34.

As shown in Figure 4.27 (c), the Mn segregation peak was almost eliminated during the homogenization treatment at 1300°C for 2 h. Thus, the effect of homogenization depends on the cast segregation profile. Homogenization is useful to reduce Mn segregation at the centreline region for a single peak situation, not for the multiple peak situation.

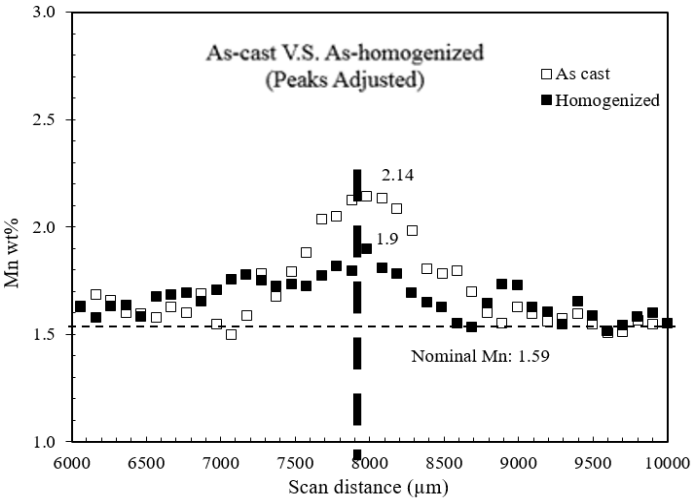

(a)

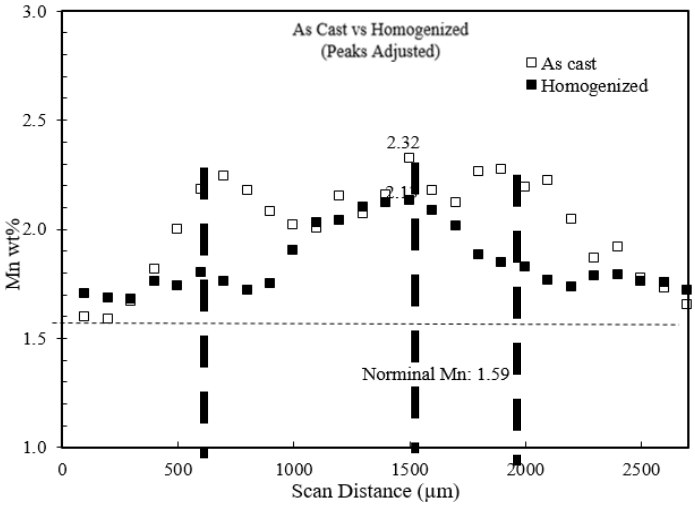

(b)

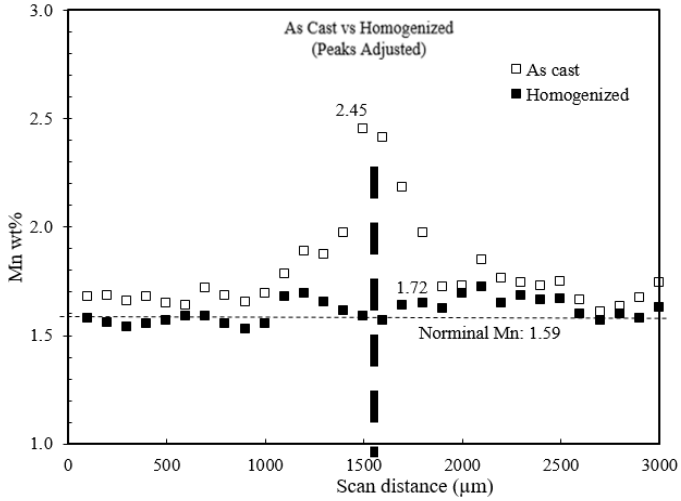

(c)

Figure 4.27 Mn composition profiles for slab D (MR=2) before and after homogenization. 1100°C for 16 h, (b) 1200°C for 16 h and (c) 1300°C for 2 h.

Figure 4.28 shows the Mn segregation pattern at the center position of the cast slab for Mannesmann 3 steels homogenized at different temperature and time conditions. Within the centreline segregation band area, a decrease in Mn concentration after homogenization is observed at all temperatures for the Mannesmann 3 steels. The multiple Mn segregation peaks for the as-cast samples are reduced after homogenization at 1100°C and 1200°C for 16 h. The multiple Mn segregation peaks are eliminated for the Mannesmann 3 samples after homogenization at 1300°C for 2 h.

Similar to the Mannesmann 2 samples, the segregation band peaks still exist after homogenization. The Mn segregation ratios at the peaks were all reduced after homogenization treatment at all three temperatures. The segregation pattern for Mn remains similar for the Mannesmann 3 steels before and after homogenization.

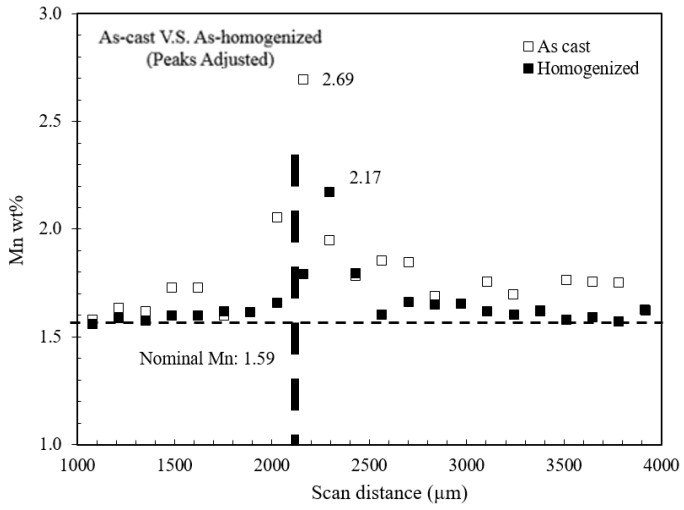

(a)

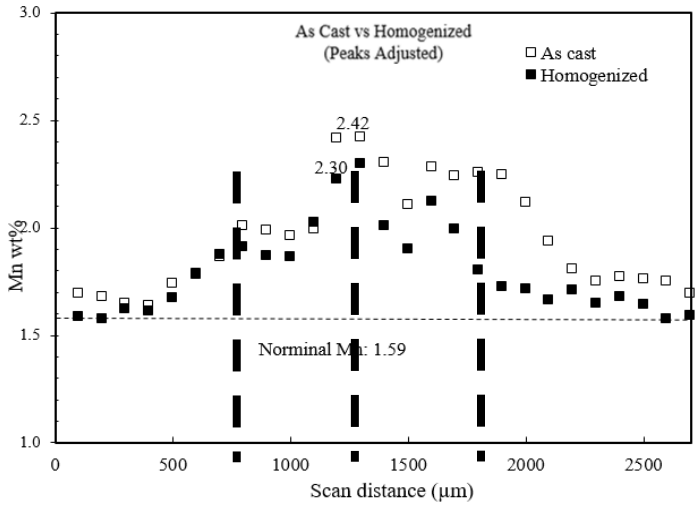

(b)

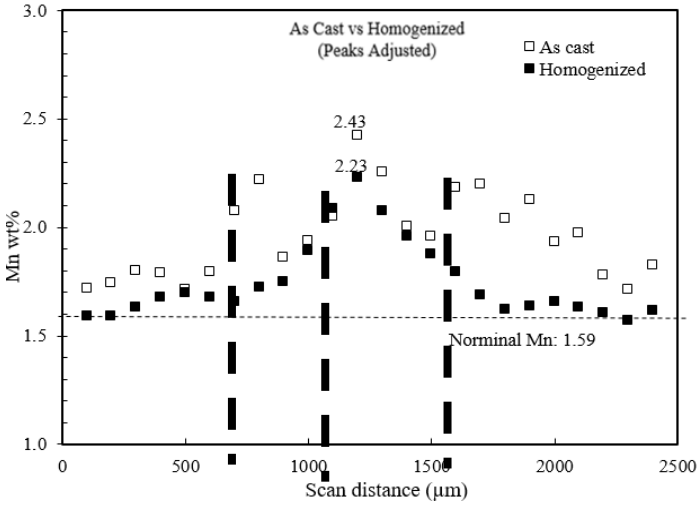

(c)

Figure 4.28 Mn composition of slab E (MR=3) before and after homogenization.

(a) 1100°C for 16 h, (b) 1200°C for 16 h and (c) 1300°C for 2 h.

From previous research work, Mn segregation at the centreline region for cast steels was reported with only one dominate segregation band with a different size as shown in Figure 4.15. Previous EMPA quantitative analyses on Mn segregation at the centreline segregation region were showing single Mn segregation peak for the centreline segregation of microalloyed steels. Both Den Boer and Aminorroaya-Yamini reported a dominant centreline segregation band with a width of 10 mm of HSLA steel. (Boer, 2013) (Aminorroaya-Yamini, 2008) The size of the segregation band varies with slab thickness and composition. Multiple Mn segregation bands were observed in this study.

Ferrite growth rate is reported to have a negative impact on Mn segregation. The lower the ferrite growth rate, the higher the level of Mn segregation. (Enomoto, 1999) As shown in Figure 4.29, Multiple Mn segregation bands are observed if the ferrite growth rate is low enough. Figure 4.29 (a) shows the schematic of the chemical potential at the α-γ interphase boundary region for a Fe-C-Mn steel. x is the horizontal distance across the α-γ interphase, and δ is half width of the α-γ interphase boundary.

Included in Figure 4.29 (b), V_{nom} represents a growth rate of ferrite during austenite-ferrite transformation for low-carbon steel, ranges from 20 μm/s to 0.02 μm/s.(Enomoto, 1999) As the growth rate decrease, the double Mn segregation peaks is started to form with 0.1 μm/s ferrite growth rate, and two dominate peaks are found with 0.02 μm/s growth rate. Thus, the local cooling rate contribute the Mn distribution for slabs. To understand the formation of the multiple Mn segregation peaks at the centre line, the local cooling condition needs to be studied. This includes both metallurgical and EMPA Mn mapping works. The microstructure study on slab samples correlates the Mn segregation need to be done in the future work.

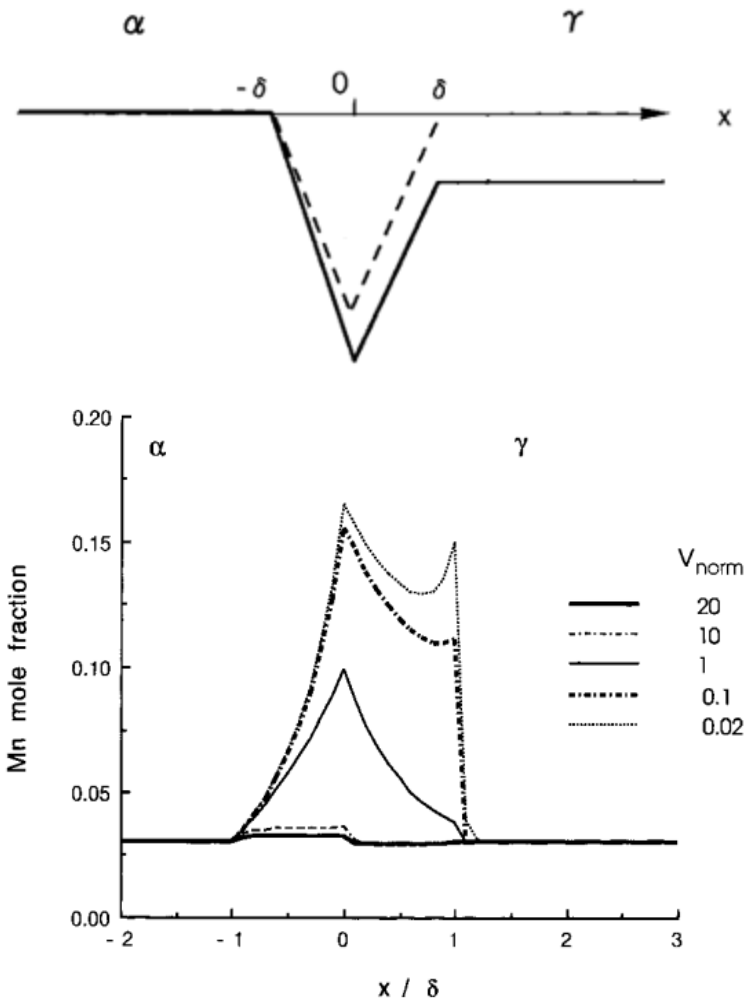

Figure 4.29 (a) α-γ interphase boundary region schematic and (b) Shape and size of Mn centreline segregation as a relation of ferrite growth rate. (Enomoto, 1999)

4.3.3 Mannesmann Comparison

Table 4-16 lists the peak Mn concentration and the average Mn concentration within the centreline segregation band found using "shot gun" analysis for both Mannesmann 2 and Mannesmann 3 samples before and after homogenization at 1200°C for 16 h at the same locations. The example results of this shot gun analysis could be found in Appendix I.

For the Mannesmann 2 sample, the highest Mn concentrations were reduced slightly from 2.32 wt% to 2.13 wt% during homogenization at 1200°C for 16 h. Similarly, for the Mannesmann 3 sample, the peak Mn concentration dropped from 2.66 wt% to 2.36 wt%. As

discussed above, the small concentration drops for both samples were expected since multiple centreline segregation bands were observed. For those samples with single centreline segregation bands, a larger reduction in Mn peak values was expected. To compare the effect of Mn reduction for multiple peaks samples, the average Mn concentration at the centreline segregation band was used.

From Table 4-16, the average Mn concentration for the Mannesmann 2 samples was 1.73 wt% after homogenization at 1200°C for 16 h with a standard deviation of 0.176 wt%. For the as-cast sample, the average Mn concentration was 1.76 wt% with a standard deviation of 0.209 wt%. There is a decrease in the average Mn composition for the Mannesmann 3 sample after homogenization at 1200°C for 16 h, from 2.32 wt% (standard deviation = 0.260 wt%) to 2.02 wt% (standard deviation = 0.076 wt%). This "shot gum" analysis confirms Mn reduction within the centreline segregation band during homogenization at 1200°C for 16 h for the multiple segregation bands situation.

Table 4-16 Mn Composition "shot gun" analysis before and after homogenization at 1200°C for 16 h for Mannesmann 2 and 3 samples.

	Mannesmann 2			Mannesmann 3		
	Peak Mn	Average Mn	Standard Deviation	Peak Mn	Average Mn	Standard Deviation
			(wt%)			
Nominal	1.59			1.59		
As-cast	2.32	1.76	0.209	2.66	2.32	0.260
Homogenized	2.13	1.73	0.176	2.36	2.02	0.076

From the comparison, the Mannesmann rating system reflects the difference in both Mannesmann 2 and 3 as-cast and pipe samples. From Table 4-16, the Mannesmann 3 slab sample exhibited higher Mn levels for both the peak and average cases at the centreline segregation band, as well as the standard deviation, than the Mannesmann 2 slab sample.

4.3.4 Summary

For the homogenization experiments, the average microhardness decreases for both Mannesmann samples. Higher microhardness values were found at the centreline segregation region than the bulk average value for both Mannesmann 2 and 3 homogenized samples. Nb precipitates were observed for both the as-cast and homogenized samples. Long rod-shaped precipitates were found in the as-cast slabs. Similar shaped precipitates, shorter in length, were found for the sample homogenized at 1300°C for 2 h. Spheroidized precipitates (smaller in size) were found for the sample after homogenization at 1200°C for 16 h.

Based on line scan measurements, the homogenization treatment effectively reduces the peak Mn concentration for samples with a single segregation band. For multiple segregation band samples, the homogenization treatment effectively reduces the concentration across the segregated bands, but less so at the peak of the segregation band. "Shot gun" analysis confirmed Mn composition reduction within the segregation band for the multiple segregation bands situation.

Homogenization was used to find the temperature and time that could induce the Mannesmann 3 samples to have the same level of centreline segregation as the Mannesmann 2 samples.

The EPMA analyses discussed above have limitations. One of which is related to sample preparation. For this analysis, a sample was cut into two halves and the mirror surfaces were analyzed in as-cast and homogenized conditions. Although the analyzed surfaces are supposed to be the same for both samples, Mn compositions might be different because both samples have been ground and polished before analysis. Therefore, the observed Mn reduction after homogenization can also be attributed to the variation of Mn composition in the as-cast state for both samples. Another approach in measurement is needed to validate the observations presented. To validate the micro analysis conclusions in a larger area, a macro analysis of a 5 mm thick area for each sample was carried out, and the results are compared and discussed in the next section.

4.4 Macro Analysis

The results of the micro analysis on Mannesmann 3 sample showed a higher value of Mn segregation ratio than Mannesmann 2 for both slabs and pipes. The comparisons above were based on the local measurements (line scans of microhardness and EMPA). The results from these local measurements varied with different locations.

A macro analysis was later carried out using the sum seg (SS) number, and was applied to microhardness test results, metallurgical measurements, microprobe analysis results, and image analysis results in order to compare the centreline segregation behaviour between Mannesmann 2 and Mannesmann 3. For each parameter (microhardness, Mn composition etc.), the results were separated into different classes as shown in Appendix L, and were used to calculate the SS numbers (the calculation method could be found in section 4.2.4.3). The macro analysis is based on each analysis data within a 5 mm wide measurement region at the centreline regions. The results provide the macro comparisons of the sum seg numbers between different analyzed categories for different Mannesmann 2 and Mannesmann 3 samples.

4.4.1 Slab and Pipe Comparison

The results of prior austenite grain size, microhardness, and Mn concentration were used for SS numbers. The detailed distribution of each parameter could be found in Appendix J. **Error! Reference source not found.** Figure 4.30 is the example of the microhardness value distributions for slab D (MR=2). Slab D has its highest percentage of microhardness value at 230 to 240 class. The SS number was calculated using equation 4-1, and compared with other parameters.

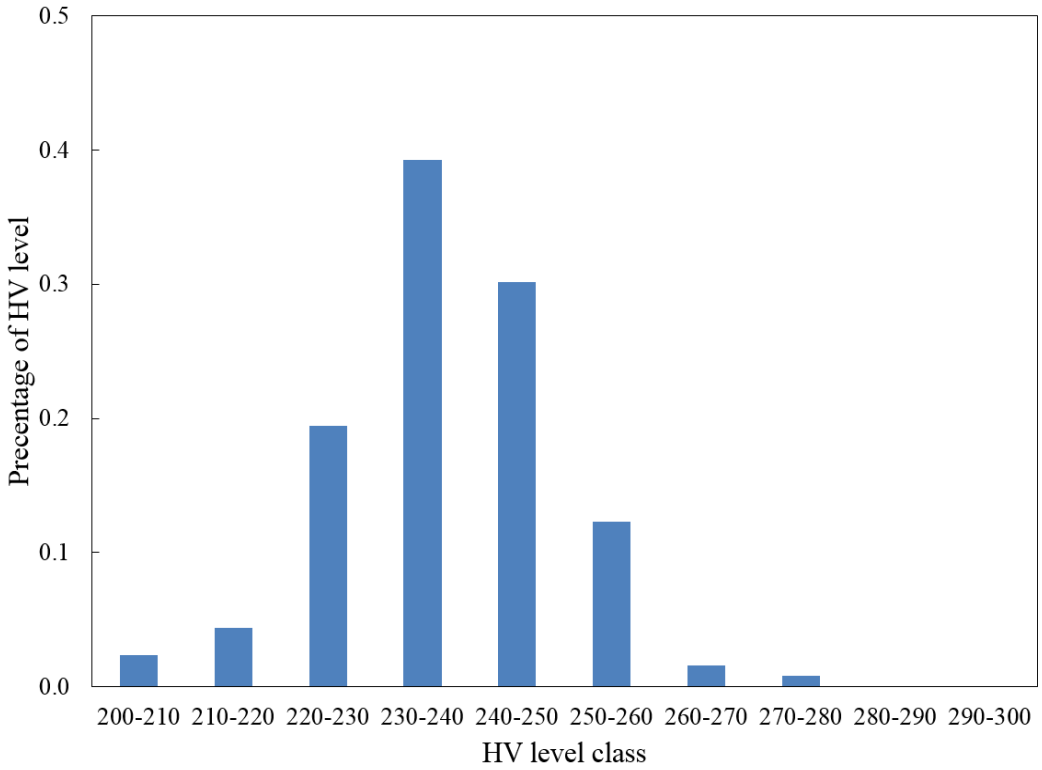

Figure 4.30 Microhardness value distribution for slab D (MR=2).

Figure 4.31**Error! Reference source not found.** compares the SS number of microhardness, ferrite grain size, and PAGS with image analysis results based on macro images and Mn maps for both Mannesmann 2 and Mannesmann 3 slabs. Mannesmann 3 slabs exhibit a higher SS number in microhardness (4.84% higher) and PAGS (7.58% higher) with a lower ferrite grain size (5.24% lower) than Mannesmann 2 slabs. The image analysis SS numbers are showing larger difference between Mannesmann 2 and 3 slabs. Mannesmann 3 slabs exhibit a 13.6% and 96.7% higher value for SS number calculated from macro images and EMPA Mn maps respectively.

There is no significant difference had been found in SS numbers for the PAGS (7.6%) and ferrite size (5.2%). This confirms micro analysis results of no difference between PAGS and ferrite size between Mannesmann 2 and 3 slab samples discussed in section 4.2.1. The difference for microhardness results (4.8%) between Mannesmann 2 and 3 slab samples was also small. As discussed in section 4.2.3, the microhardness difference between two different

Mannesmann rating slabs is small from microhardness line scans. This SS number confirms the minor difference in microhardness at centreline between Mannesmann 2 and 3 samples.

SS numbers from image analyses are showing more than 10% difference between Mannesmann 2 and 3 slabs. Mannesmann 3 slabs exhibit 13.6% higher values in SS number than Mannesmann 2 slabs from macro images, and 96.7% from EMPA Mn maps. These two big differences ensure the higher level of centreline segregation (found from micro analyses) for Mannesmann 3 slabs than Mannesmann 2 slabs. To distinguish this difference quantitatively, macro analysis on Mn line scans were done.

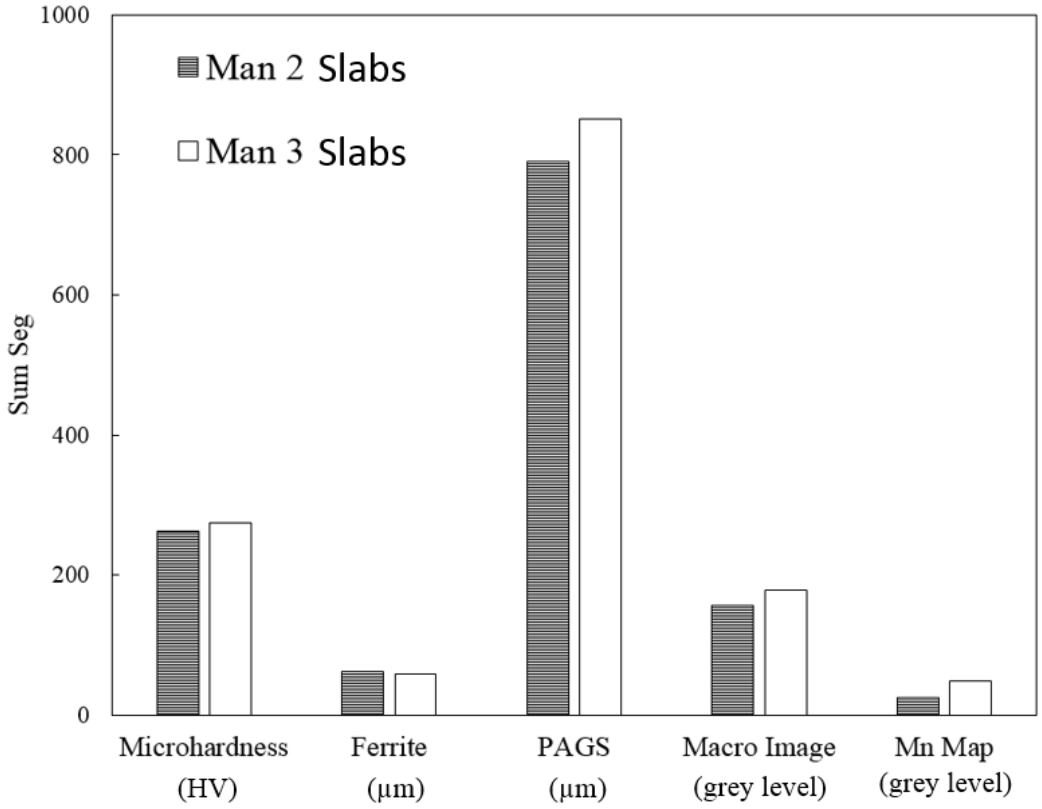

Figure 4.31 SS comparison of microhardness, ferrite, and PAG size for Mannesmann 2 and 3 slabs.

Error! Reference source not found. compares SS number of Mn line scan analysis results o n both slabs and pipes. For both, Mannesmann 3 samples have larger SS number than Mannesmann 2 samples (6.99% and 9.50% higher for slabs and pipe respectively), which indicate a higher level of Mn segregation in a macro view at the centreline segregation region.

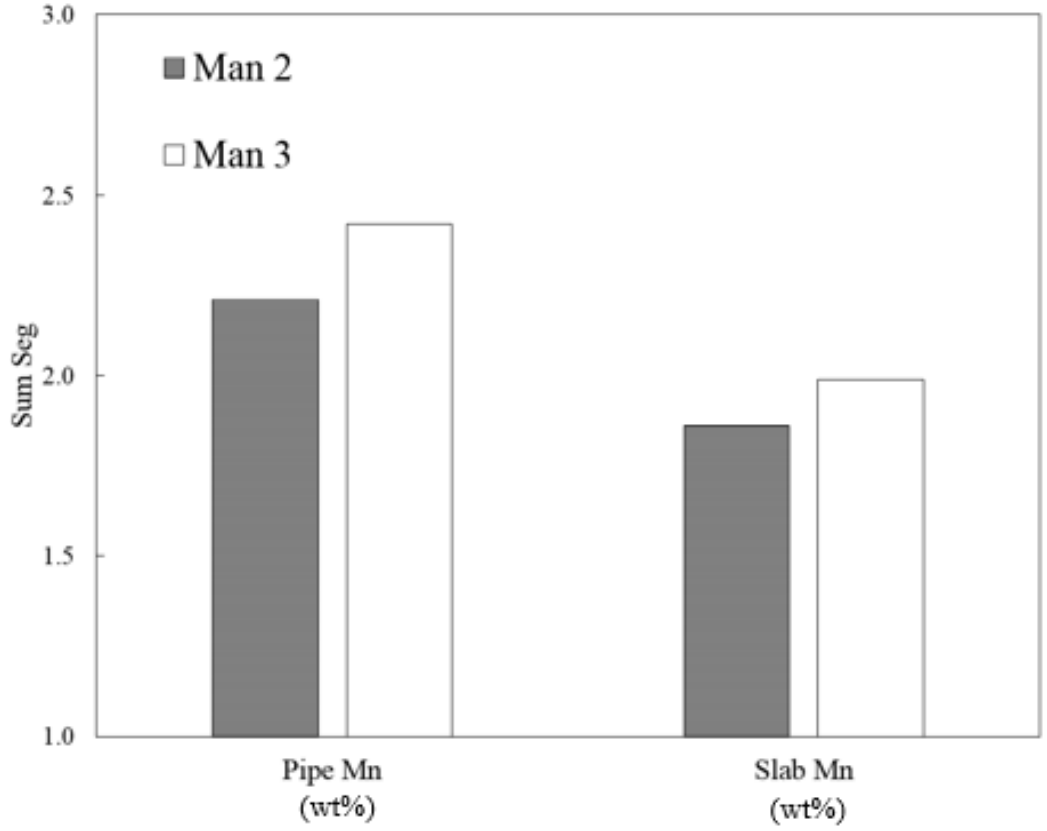

Figure 4.32 SS comparison of Mn point analysis for Mannesmann 2 and 3 slabs and pipes.

Both EMPA Mn maps and line scans measure the Mn intensity directly at the analyzing position, which should lead to a similar difference between Mannesmann samples in SS numbers. But, the difference between two Mannesmann slabs in SS number of Mn line scans (6.99%) is much less than the SS number calculated using EMPA Mn maps (96.7%). This unexpected disagreement emphasis the limitation of the EMPA Mn line scans. The line scans results are representing the Mn composition for the 5 mm region with a width of less than 15 μm per line, while each Mn map has a width of 10 mm. Thus, maps are more representative than line scans. The calibration of Mn maps with quantitative line scan data was proposed as the future work.

4.4.2 Homogenized sample Comparison

Figure 4.33 compares SS number of microhardness analysis for Mannesmann 2 and 3 slab samples and homogenized samples at 1100˚C for 16 h and 1200˚C for 16 h. Compared to slab samples, SS number for homogenized samples decreased from 250 to 200. This result consitants with decreasing in both average and peak microhardness values after homogenization founded in microhardness analysis. Both Mannesmann 2 and 3 samples homogenized at 1200˚C for 16 h have lower SS number than the sample homogenized at 1100˚C for 16 h. Mannesmann 3 samples have a slightly higher SS number than Mannesmann 2 samples for sample homogenized at 1100˚C for 16 h, while it is lower than Mannesmann 3 samples for sample homogenized at 1200˚C for 16 h. This macro analysis confirms the drop of the microhardness at the centreline segregation region after homogenization process.

Figure 4.34 compares the Mn segregation at the centreline segregation region before and after homogenization at 1100˚C for 16 h, 1200˚C for 16 h, and 1300˚C for 2 h. The SS number decreases for both Mannesmann 2 and 3 from samples homogenized at 1100˚C for 16 h to samples homogenized at 1200˚C for 16 h, and found lowest in samples homogenized at 1100˚C for 16 h. From EMPA line analysis on these homogenized samples, the results were affected by the location segregation pattern (single peak vs. multiple peaks). The SS analysis approves that homogenization at 1300˚C for 2 h has the highest efficiency within these three homogenization conditions.

For Mannesmann 2 samples, the SS number increases slightly after homogenized at 1100˚C for 16 h than slab samples. Also, it is found higher SS number in Mannesmann 2 sample than Mannesmann 3 sample after homogenized at 1200˚C for 16 h. These are limited by only one sample analyzed at this preliminary stage. More samples need to be analyzed in the future.

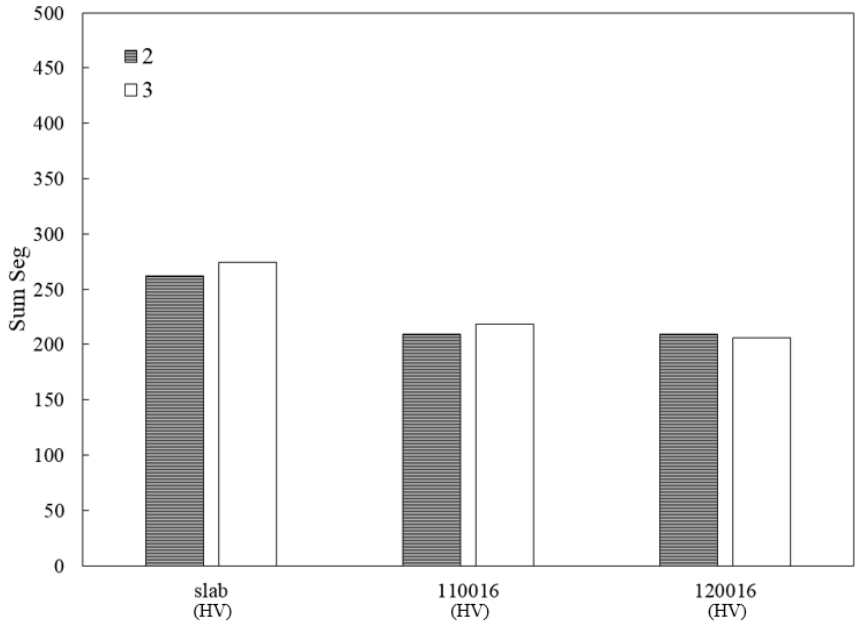

Figure 4.33 SS comparison of microhardness for Mannesmann 2 and 3 homogenized sample at 1100˚C16h and 1200˚C16h.

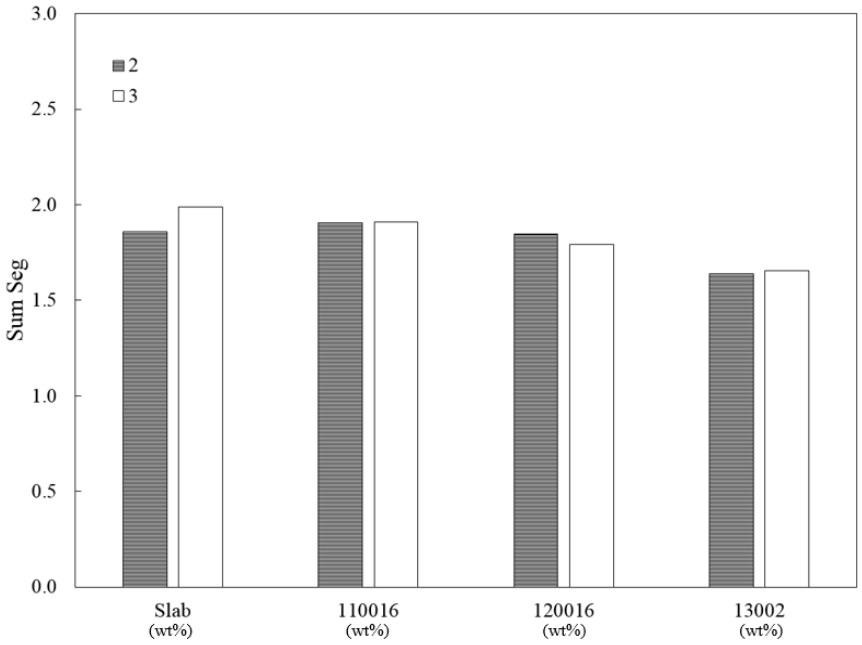

Figure 4.34 SS comparison of Mn point analysis for Mannesmann 2 and 3 homogenized sample at 1100˚C16h, 1200˚C16h, and 1300˚C2h.

4.4.3 Summary

The SS analysis indicates an increase in SS number from Mannesmann 2 sample to Mannesmann 3 sample in terms of slab appearance and Mn composition. Homogenization analysis results are showing a similar increasing trend from Mannesmann 2 to Mannesmann 3 samples with preliminary results. Segregation was found to be reduced mostly after homogenized at 1300˚C for 2 h.

In the future, the SS analysis needs to be optimized as to the size of the sampling area to be measured to relate the Mannesmann rating to metallurgical values. In addition, more samples should be analyzed in order to develop a database of segregation. This will enable the steelmaker to begin to diagnose the casting process parameters that lead to the different types of Mannesmann ratings. This clearly implies that the SS using imaging is the fastest and easiest to carry out and should be developed further for both research and industrial use.

5. Conclusion and Future work

A centreline segregation quantification methodology was developed and used to quantify the differences between centreline segregation in Mannesmann 2 and Mannesmann 3 samples. This methodology combines electron microprobe analysis (EMPA) mapping, EMPA line scans, microhardness tests, and microstructural analysis. Based on this methodology, Mannesmann 3 samples show a higher level of segregation at the centreline than Mannesmann 2 samples. Homogenization tests conducted at 1100 ˚C for 16 h, 1200 ˚C for 16 h, and 1300 ˚C for 2 h resulted in a reduction of Mn segregation to up to 30%. Macro analysis compared results from microhardness tests, ferrite grain size, prior austenite grain size, and Mn composition with the corresponding image analysis results. The sum seg (SS) number suggests a higher level of segregation at the centreline for Mannesmann 3 than Mannesmann 2 samples. Finally, future work on centreline segregation characterization is proposed.

5.1 Centreline Segregation Analysis of Mannesmann 2 and 3 Samples

1] An EMPA elemental mapping technique was developed to quantify elemental distributions over a relatively large region of the centreline segregation band for continuous cast slab samples. The elemental maps show non-uniformity in the elemental distribution along the centreline segregation band. In addition, EMPA mapping of Mn was used as a preliminary step for subsequent quantitative EMPA line scans of cast slab samples (i.e., aided in the selection of representative regions for each line scan).

2] Line scans conducted on both Mannesmann 2 and Mannesmann 3 slabs and pipes showed that the Mannesmann 3 steel exhibited higher Mn segregation ratio (S.R.) than the Mannesmann 2 steel. For slabs, the Mannesmann 3 sample had a Mn S.R. of 1.69, which was higher than the Mannesmann 2 sample with a S.R. of 1.35. For pipe samples, Mannesmann 3 exhibited a Mn S.R. of 1.44, which was higher than the Mannesmann 2 sample with 1.33.

3] The centreline segregation band width was measured from EMPA Mn line scans. The width of the segregated zone was larger in the Mannesmann 3 samples. For the slab samples, the average band width for the Mannesmann 3 steel was 2000 μm versus a width of 1600 μm

for the Mannesmann 2 samples. For the pipe samples, the average band width for the Mannesmann 3 steel was 50 μm versus a width of 42 μm for the Mannesmann 2 samples.

4] Optical microscopy measurements of the centreline segregation band width indicated a wider segregation band for Mannesmann 3 samples than Mannesmann 2 samples. For slabs, the Mannesmann 3 sample had an average band width of 644 μm, which is higher than band width for the Mannesmann 2 sample (514 μm). For pipes, the band widths were measured to be 40 μm and 22 μm for Mannesmann 3 and 2 steels, respectively.

5] Microhardness testing across the segregation band showed higher hardness values for the Mannesmann 3 sample relative to the Mannesmann 2 sample. For slabs, the Mannesmann 3 samples had a peak hardness value of 289 HV, which was higher than the Mannesmann 2 peak hardness of 263 HV. In addition, the Mannesmann 3 samples had a higher hardness peak to average hardness ratio (P/A) than the Mannesmann 2 samples. For Mannesmann 3 slabs, the P/A ratio was 1.15. For Mannesmann 2 slabs, the P/A ratio was 1.09. For pipes, the Mannesmann 3 samples had peak value of 303.7 HV with a P/A ratio of 1.55. The Mannesmann 2 sample had a peak value of 250.4 HV with a P/A ratio of 1.16.

5.2 Effect of Homogenization on Segregation

1] Experimental homogenization conditions of 1100˚C for 16 hrs, 1200˚C for 16 hrs and 1300˚C for 2 hrs were applied to both Mannesmann 2 and Mannesmann 3 slab samples.

For the Mannesmann 2 samples, the Mn S.R. decreased the most (from 1.54 to 1.08) for the sample homogenized at 1300˚C for 2 h. This decrease in S.R. was accompanied by a decrease in average hardness from 241 HV to 208 HV. The P/A ratio after homogenization increased slightly from 1.09 to 1.11.

For the Mannesmann 3 sample, the Mn S.R. decreased the most (from 1.69 to 1.36) for the sample homogenized at 1100˚C for 16 h. This decrease in S.R. was accompanied by a decrease in average hardness from 251 HV to 205 HV. The P/A ratio after homogenization increased from 1.15 to 1.20. This increase was attributed to the presence of stable precipitates in the centreline segregation zone.

For the homogenization conditions stated above, the S.R. decreased dramatically for single segregation band samples. However, for multiple segregation bands, there was a minimum reduction in S.R. for the above homogenization conditions.

2] Nb precipitates were observed in both as-cast and as-homogenized samples. Long rod shaped precipitates were found in as-cast slabs. Similar shaped precipitates were found after homogenization at 1300˚C for 2 h, but were smaller in length. Spheroidized precipitates were present after homogenization at 1200˚C for 16 h and were smaller in size.

5.3 Macro Analysis

The macro analysis results indicate an increasing value in the SS number from the Mannesmann 2 samples to the Mannesmann 3 samples in terms of microhardness, PAGS, and Mn composition. These results were found consistently for slabs, pipes and as-homogenized samples. The macro analysis concludes that higher segregation behaviour for Mannesmann 3 steels at the centreline region than Mannesmann 2 steels.

With more samples analyzed in the future, a database of SS number could be developed that relates the Mannesmann rating to metallurgical values. This provides a fast and easy way to diagnose the casting process parameters, which lead to different Mannesmann ratings, for both research and industrial use.

5.4 Future Work

For the future work, the development of the SS database is suggested. This development requires more image analysis, metallurgical analysis, precipitates analysis, and elemental segregation analysis.

More image analyses are needed for both macro images and EMPA maps. More Mannesmann rating samples (from 1 to 5) and elements (like Si, Cr, Mo, Nb, etc.) should be included in the analysis. The segregation of other elements (like P and C) at the centreline needs to be measured. The relation between microhardness and element segregation behaviour for pipe samples needs to be established.

PAGS based on the optical microscopy images need to be fully measured for all Mannesmann rating slab samples. Local secondary arm spacing need to be measured as well. The development of these measurement results could compare to with local elemental segregation behavior, and indicate the level of local segregation. Microstructure analysis at the centreline segregation region need to be done on slab samples to suggest the components at the centreline of the slab.

Measurement of the amount of martensite-austenite (MA) constituent at the centerline segregation region is needed. Nb precipitates before and after homogenization need to be identified as well. Quantitative X-ray fluorescence (XRF) may be used to analyze the composition of the precipitates. High magnification secondary electron images could help counting the fraction and the size of the precipitates for both slabs and samples homogenized under different conditions.

The combination of the above analysis results enriches the SS database, and will be used to relate the macro images to metallurgical values such as microhardness values, element compositions, PAGS, precipitates fractions, etc. This database will help both research and industrial understand the casting procedure better.

References

A.E. Giannakopoulos, P. L. (1994). Analysis of Vickers Indentation. *International Journal of Solids and Stuctures, 31*(19), 2679-2708.

Aboutalebi, M. R. (1995). Coupled Turbulent Flow, Heat, and Solute Transport in Continuous Casting Processes. *Metallurgical and Materials Transactions B, 26*(4), 731-744.

Adams, C. J. (1941). Hot Ductility and Strength of Strand Cast Steels up to Their Melting Points. *Open Hearth Processdings, TMS-AIME, 54*, 290-302.

Agren, J. (1982). Numerical Treatment of Diffusional Reactions in Multicomponent Alloys. *Journal of Physics and Chemistry of Solids, 43*(4), 385-391.

Anderson, C. A. (1966). Extension of Electron Microprobe Techniques to Biochemistry by the Use of Long Wavelength X-rays. *Proceedings of the Fourth International Conference on X-ray Optics and Microanalysis*, (pp. 310-327). Paris.

Andersson, J.-O. a. (1992). Models for Numerical Treatments ofMulticomponent Diffusion in Simple Phases. *Journal of Applied Physics, 72*(1), 1350-1355.

Andrews, K. W. (1965). Empirical Formulae for the Calculation of Some Transformation Temperatures. *JISI*, 721-727.

Azizi, G. M. (2015). Unraveling the Effect of Homogenization Treatment on Decomposition of Austenite and Mechanical Properties of Low-Alloyed TRIP Steel. *Steel Research International, 87*(7), 820-823.

Bain, E. C. (1939). Alloying Elements in Steels. In *ASM Handbook.* Cleveland .

Bearden, J. A. (1967). X-Ray Wavelengths. *Reviews of Modern physics, 39*(1), 78-124.

Beckermann, C. (2001). Macrosegregation. *Encyclopedia of Materials: Science and Technology*, 4733-4739.

Beidokhti, B. A. (2009). Effects of Alloying Elements and Microstructure On the Susceptibility of the Welded HSLA Steel to Hydropgen-Induced Cracking and Sulfide Stress Cracking. *Material Science and Engineering A, 507*, 167-173.

Birks, L. S. (1971). *Electron Probe Microanalysis.* (2, Ed.) New York: Wiley Interscience.

Buehler, W. (2015). *Vickers Micro-hardness User manual.*

Campbell, J. (2003). *Casting* (2 ed.). Oxford: Elsevier.

Capdevila, C., Caballero, F., & Garcra de Andre´s, C. (2003). Austenite Grain Size Effects on Isothermal Allotriomorphic Ferrite Formation in 0.37C–1.45Mn–0.11V Microalloyed Steel. *Materials Transactions, 44*(6), 1087 - 1095.

Coldren, A. P. (1969). Steel Strengthening Mechanisms. *Climax Molybdenum*.

Cosslett, V. E. (1956). Microanalysis by a Flying-spot X-ray Method. *Nature, 177*, 1172-1173.

Darken, L. S. (1949). Diffusion of Carbon in Austenite with a Discontinuity in Composition. *Transactions of the Metallurgical Society of AIME, 180*, 430-438.

Davis, C. L. (2009). Segregation Behavious in Nb Microalloyed Steels. *Materials Science and Technology, 25*(9), 1126-1133.

DeArdo, A. J. (1982). *Thermomechanical Processing of Microalloyed Austenite.* Warrendale, PA: Metallurgical Society of AIME.

Degarmo, E., Black, J., & Kohser, R. (2003). *Materials and Processes in Manufacturing* (9th ed.). John Wiley and Sons, Inc.

Devillers, L. K. (1988). H. A. Z. Toughness: Metallurgical and Mechanical Points of View. *Revue de Métallurgie*, 267-282.

Durand-Charre, M. (2004). *Microstructure of Steels and Cast Irons.* Spinger.

Elleman, T. a. (1974). Surface Effects on Tritium Diffusion in Niobium, Zirconium and Stainless Steel. *Journal of Nuclear Materials, 53*, 299-306.

Emi, T. a. (2005). High-Speed Continuous Casting of Peritectic Carbon. *Materials Science and Engineering A*, 2-9.

Eskandari, M. A. (2008). Effects of Homogenization Conditions and Hot Rolling Parameters on Grain Refinement of an As-Cast 301 Stainless Steel. *The Iron and Steel Institute of Japan, 5*(2), 21-28.

Everhart, T. E. (1972). Idealised Spatial Emission Distribution of Secondary Electrons. *Journal of Applied Physics, 43*(9), 3707-3711.

Examples, D. (2007). *Homogenisation of a Binary Fe-Ni Alloy.* Stockholm: Foundation for Computational Thermodynamics.

F. Kurosawa, a. I. (1990). Precipitation Behavior of Phosphides in the Centerline Segregation Zone of Continuously Cast Steel Slabs. *Materials Transactions, 31*(1), 51-60.

Farrar, R. A. (1993). The Effect of Prior Austenite Grain Size on the Transformation Behaviour of C-Mn-Ni Weld Metal. *Journal of Materials Science, 28*(5), 1385-1390.

Femandez, A., Uranga, P., Lopez, B., & Rodriguez-Ibabe, J. (2003). Dynamic Recrystallization Behavior Covering a Wide Austenite grain size range in Nb and Nb–Ti microalloyed steels. *Materails Science and Engineering: A, 361*(1), 367-376.

Fitzgerald, R. ,. (1968). Solid-state Energy Dispersion Spectrometer fo rElectron Microprobe X-ray Analysis. *Science, 159*, 528-530.

Flemings, M. (1979). *Solidification Processing.* New York: McGraw-Hill.

Fournelle, J. (2010). *Power Point of Trace Elements*. Retrieved from http://www.geology.wisc.edu/~johnf/g777/ppt/80_Trace_elements.ppt

Fredriksson, H. a. (2006). Heat Treatment and Plastic Forming. In *Materials Processing During Casting* (pp. 227-251). John Wiliey and Sons, L. td.

Friel, J. J. (2006). X-ray Mapping in Election-Beam Instruments. *Microscopy and Microanalysis, 12*, 1-24.

Ghosh, A. (2001). Segregation in Cast Products. *Sadhana, 26*, 5-24.

Gladman, T. I. (1972). Some Aspects of the Structure-Property Relationships in High-Carbon Ferrite-Pearlite Steels. *JISI, 210*, 916-930.

Goldstein, J. ,. (2012). *Scanning Election Microscopy and X-ray Microanalysis* (3 ed.). Springer Science and Business Media.

Goldstein, J. I. (1992). *Scanning Electron Microscopy and X-ray Microanalysis : A Text for Biologists, Materials Scientists, and Geologists.* (2, Ed.) New York: Plenum Press.

Gorokhova, N. S. (1986). Solubility of Titanium and Niobium Carbides in High-chromium Ferrite. *Metal Science and Heat Treatment, 28*(4), 276-279.

Hafner, B. (2007). Scanning Electron Microscopy Primer. *Characterization Facility, University of MInnesota*.

Hall, C. E. (1966). *Introduction to Electron Microscopy.* (2, Ed.) New York: McGraw-Hill.

Hashemi, S. H. (2009). On the Relation of Microstructure and Impact Toughness Charateristics of DSAW Steel of Grade API X70. *Fatigue and Fracture of Engineering Materials and Structures, 32*, 33-40.

Hoglund, L. (1997). Internal Report Trita-Man-0605. *Divisioin of Physical Metallurgy, Royal Institute of Technology Stockholm*.

Howe, A. A. (1991). *Segregation and Phase Distribution during Solidification of Carbon.* European Commission.

Indentec. (2015, Feb). *Vickers Hardness Test*. Retrieved from http://www.indentec.com/downloads/info_vickers_test.pdf

Inox, E. (2015, June). *Hardness Testing.* Retrieved from http://www.euro-inox.org/pdf/map/HardnessTesting_EN.pdf

Irvine, K. J. (1957). Low-carbon Baintic Steels. *JISI*, 292-309.

Kerrick, D. M. (1973). The Role of Carbon Film Thickness in Electron Microprobe Analysis. *American MIceralogist, 58*, 910-925.

Kirkaldy, J. S. (1978). Thermodynamic Prediction of Ae3 temperature of steels with additions of Mn, Si,Cr,Mo,Cu. *Metallurgical Transactions A: Phisical Metallury and Materials Science 9(4)*, 495-501.

Kostryzhev, A. G. (2010). Bauschinger Effect in Microalloyed Steels: Part I. Dependence on Dislocation-particle Interaction. *Metallurgical and Materials Transactions A:, 41*(6), 1399-1408.

Kotler, G. K. (1972). Experimental Observations of Dendritic Growth. *Metallurgical Transactions, 3*(3), 723-726.

Kou, S. (2003). *Welding Metallurgy* (2nd ed.). Hoboken, New Jersey: John Wiley and Sons, Inc.

Krauss, G. (1990). *Steels: Heat Treatment and Processing Principles.* ASM Int. .

Kuisma-Kursula, P. (2000). Accuracy, Precision and Detection Limits of SEM-WDS, SEM-EDS and PIXE in the Multi-Elemental Analysis of Medieval Glass. *X-Ray Spectrometry, 29*, 111-118.

Kurosawa, F. I. (1980). Observation and Analysis of Phosphides in Steels using a Non-aqueous Electrolyte-Potentiostatic Etching Method. *Journal of The Japan institute of Metals, 44*(5), 539-548.

Kurosawa, F. I. (1981). Observation and Analysis of Precipitates Formed in Steels at Elevated-Temperatures using the Non-aqueous Elevtrolyte-potentiostatic Etching Method. *Journal of the Japan Institute of Metals, 45*(1), 72-81.

Kurz, W. a. (1981). Dendritic Growth and Limit of Stability Tip Radius and Spacing. *Acta Metallurgica, 29*, 11-20.

Laboratory, E. M. (2015). *Abount the Electron Microprobe Lavoratory (EML)*. Retrieved from http://www.eas.ualberta.ca/eml/?page=home

Laboratory, E. M. (2015). *Analytical Crystals Available*. Retrieved from http://www.eas.ualberta.ca/eml/?page=crystals

Lesoult, G. (2005). Macrosegregation in Steel Strands and Ingots: Characterization, Formation and Consequences. *Materials Science and Engineering: A, 413-414*, 19-29.

Lippard, H. E. (1998). Microsegregation Behavior during Solidification and Homogenization of AerMet100 Steel. *Metallurgical and Materials Transactions B, 29B*, 205-210.

Lippard, H. E. (1998). Microsegregation Behavior during Solidification and Homogenization of AerMet100 Steel. *Metallurgical and Materials Transactions B, 29B*, 205-210.

Locock, A. (2015, 11 10). *about the Electron Microprobe Laboratory (EML)*. Retrieved from Electron Microprobe Laboratory: http://www.eas.ualberta.ca/eml/?page=resources

Long, J. V. (1995). Microanalysis from 1950 to the 1990s. In *Microprobe Techniques in the Earth Sciences* (Vol. 6, pp. 1-48). New York: Chapman and Hall.

Lynch, P. C. (2011). *the Development of Ultrahigh Strength Low Alloy Cast Steels with Increased Toughness.* The Pennsylvania State University.

Marinenko, R. B. (1987). Digital Compositional Mapping with Standard Map Corrections for Wavelength-Dispersive Spectrometry Defocusing. *Journal of Microscopy, 145*, 207-223.

Martiny, A. A. (2008). SEM/EDS Analysis and Characterization of Gunshot Residues from Brazilian Lead-free Ammunition. *Forensic Science International, 177*(1), e9-e17.

Mason, J. T. (1982). Primary Dendrite Spacing. I. Experimental Studies. *Journal of Crystal Growth, 59*, 516-524.

Meyer, H.-P. (2015). *Electron probe micro-analyser (EPMA)*. Retrieved from http://www.rzuser.uni-heidelberg.de/~hb6/labor/ems/index_en.html

Mustaffa, N. A. (2004/2005). *Material Characterization and Engineering of Super-heater Tube of Boilers.* University fo Malaya.

Nayak, S. S. (2008). Microstructure and Properties of Low Manganese and Niobium Containing HIC Pipeline steel. *Materials Science and Engineering A, 494*, 456-463.

Newbury, D. E. (1990). Compositional Mapping with the Electron Probe Microanalyzer. *Analytical Chemistry, 62*, 1159A-1166A.

Okamoto, K. a. (1975). Dendritic Structure in Unidirectionally Solidified Cyclohexanol. *J. Crystal Growth, 29*(2), 131-136.

Onsager, L. (1931). Reciprocal RElations in Irreversible Process I. *Physical Review, 37*, 405-426.

Palmiere, E. J. (1994). Compositional and Microstructural Changes which Attend Reheating and Grain Coarsening in Steels Containing Niobium. *Metallurgical and Materials Transactions A, 25*(2), 277-286.

Pandi, R. (1998). *Modelling of Austenite-to-Ferrite Transformation Begaviour in Low Carbon Steels during Run-out Table Cooling.* University of Vritish Columbia.

Park, J. S. (2007). Determination of Nb (C, N) Dissolution Temperature by Electrical Resistivity Measurement in a Low-carbon Microalloyed Steel. *Scripta materialia, 56*(3), 225-228.

Pickering, B. G. (1988). Effect of Pearlite Morphology on Imapct Toughness of Eutectoid Steel Containing Vanadium. *Materials Science and Technology, 4*, 328-334.

Pinard, P. T. (2013). Charaterization of Dual-Phase Steel Microstructure by Combined Submicrometer EBSD and EPMA Carbon Measurements. *Microscopy and Microanalysis, 19*, 996-1006.

Pollack, H. (1988). *Materials Science and Metallurgy.* Prentice-Hall.

Potts, P. J. (1987). *A Handbook of Silicat Rock Analysis.* Blackie.

Preblinger, H. S. (2006). Methods for Assessment of Alab Centre Segregation as a Tool to Control Slab Continuous Casting with Soft Reduction. *The Iron and Steel Institute of Japan, 46*(12), 1845-1851.

Priestner, R. a. (2000). Processing of Steel for Ultrafine Ferrite Grain Structures. *Materials Science and Technology, 16*, 1267-1272.

Puppet, S. (2015, Oct). *File: CCt curve steel*. Retrieved from https://en.wikipedia.org/wiki/File:CCT_curve_steel.svg

Purdy, S. M. (2004). Macroetching. In A. International, *ASM Handbook* (Vol. Metallography and Microstructures, pp. 313-324). ASM International. doi:10.1361

Rapp, S. (2010). Requirements of the MAOP Rule and its Implications to Pipe Procerement. *INGAA Foundation*.

Reed, S. J. (1972). Electron Microprobe Analysis at Low Operating Voltage: Discussion. *American Mineralogist, 27*, 1550-1551.

Reed, S. J. (1996). *Electron Microbe Analysis and Scanning Electron Microscopy in Geoloy.* Cambridge University Press.

Reger M., B. V. (2014). Control of Centerline Segregation in Slab Casting. *Acta Polytechnica Hungarica*, 119-137.

Salmon Cox, P. H. (1967). The origin and Significance of Banding in 18Ni (25) Maraging Steel. *Transactions of the Metallurgical Society of AIME, 239*, 1809-1817.

Samll, K. D. (2008). Etching Specialty Alloys. *Advanced Materials & Processes*, 32-37.

Samuels, L. E. (1986). Microindentation Techniques in Materials Science and Engineering. (a. B. P. J. Blau, Ed.) *ASTM STP 889*, 5-25.

Shahdad, S. A. (2007). Hardness Measured with Traditional Vickers and Martens Hardness Methods. *Dental Materials, 23*(9), 1079-1085.

Siwecki, T. W. (1995). Recrystallization Controlled Rolling of HSLA Steels. In I. C. Microalloying, *Microalloying 95* (pp. 197-211). Pittsburgh: Iron and Steel Society.

Sprope, L. a. (1988). Experimental and Theoretical Studies of Gas Consumption in the Gas Carburizing Process. *Journal of Heat Treating, 6*(1), 9-19.

Su, L., Li, H., & Lu, C. (2013). The Assessment of Centrelien Segregation in Continuously Cast Line Pipe Steel Slabs using Image Analysis. *6th International Pipeline Technology Conference*, (pp. S27-01). Ostend.

Suzuki, S., Abiko, K., & Kimura, H. (1983). The Influence of Molybdenum on the Solubility of Phosphorus in a-ferrite. *Materials Science and Engineering, 60*, L17-L21.

Sweatman, T. R. (1969). Quantitative Electron-Probe Microanalysis of Rock-forming Minerals. *Journal of Petrology*, 332-379.

T. Lyman, H. B. (1973). *Metals Handbook* (8 ed.). Metal Park, OH: ASM.

Taguchi, K. F. (1990). Precipitation Behavior of Phosphides in the Centerline Segregation Zone of Continuously Cast Steel Slabs. *Materisl Transactions , JIM, 31*(1), 51-60.

Taha, M. A. (1986). Influence of Solidification Parameters on Dendrite Arm Spacings in Low Carbon Steels. *Journal of Materials Science Letters* , 307-310.

Takahashi, T. d. (2007). Investigation of Orientation Gradients in Pearlite in Hypoeutectoid Steel by use of Orentation Imaging Microscopy. *Steel Reasearch International, 78*(1), 38-44.

Thelning, K. E. (1984). *Steels and its Heat Treatment* (2 ed.). Linacre House, Jordan Hill, Oxford: Butterworth-Heinemann.

Thewlis, G. (1994). Transformation Kinetics of Ferrous Weld Metals. *Materials Science and Technology, 10*, 110-125.

Thomas, B. G. (2001). Continuous Casting. In K.-O. Yu, *Modeling for Casting and Solidification Processing* (p. 499). CRC Press.

Tsuchinda, Y. M. (1984). Behavior of Semi-macroscopic Segregation in Continuously Cast Slabs and Technique for Reducing the Segregation. *The Iron and Steel Institute of Japan*, 899-907.

Tsukatani, I. H. (1991). Effects of Silicon and Manganese Addition on Mechanical Properties of High-strength Hot-rolled Sheet Steel Containing Retained Austenite. *The Iron and Stel Institute of Japan, 31*(9), 992-1000.

Ul-Hamid, A. H.-J. (2006). Quantitative WDS Analysis Using Electron Probe Microanalyzer. *Materials Characterization, 56*, 192-199.

Valek, L. P. (2011). The Quality Results of Slabs at Segregation Area. *Metal*, 137-142.

VerltA, M. R. (1994). X-ray Microanalysis of Ancient Glassy Materials: a Comparative Study of Wavelength Dispersive and Energy Dispersive. *Archaeometry, 26*(2), 241-251.

W.F. Lange, M. E. (1988, March). The Kinetics of Ferrite Nucleantion at Austentie Grain Boundaries in Fe-C Alloys. *Metallurgical Transactions A, 19A*, 427-440.

Walls, M. J. (1998). *Applied Dental Materials.* Oxford: Blackwell Science.

Wang, R. C. (2005). The Microstruture Evolution of Nb, Ti Complex Microalloyed Steel During the CSP Process. *Materials Science Forum, 500-501*, 229-236.

Weng, Y. (2003). Microstructure Refinement of Structural Steel in China. *The Iron and Steel Institute of Japan International, 43*(11), 1675-1682.

Westrich, R. M. (1986). Microindenetation Techniques in Materials Science and Engineering. (P. a. Blau, Ed.) *ASTM STP 889*, 196-205.

Williams, J. C. (1995). In *Microalloying 95* (p. 117).

Won, Y. a. (2010). Simple Model of Microsegregation during Solidification of Steels. *Metallurgical and Materials Transanction A, 32A*, 1755-1767.

Won, Y., & Thomas, B. (2001). Simple Model of Microsegregation during Solidification of Steels. *Metallurgical adn Materials Transactions A, 32A*, 1755-1767.

Zajac, S. T. (1991). Recrystallization Controlled Rolling and Accelerated Cooling for High Strength and Toughness in V-Ti-N Steels. *Metallurgical Transactions A, 22*, 2681-2694.

Zhao, M. K. (2003). Continuous Cooling Transformation of Undeformed and Deformed Low Carbon Pipeline Steels. *Materials Science and Engineering: A, 355*(1-2), 126-136.

Zhou, T. (2010). Control of Microstructure During Solidification & Homogenization of Thin-Slab Cast Direct-Rolling (TSCDR) Microalloyed Steels. *Dorcor of Philosophy Thesis*.

Appendix

A. Picric Acid Etching

Saturated picric acid aqueous solution etching for prior austenite grain was tested in this study. It required a teeth brush cleaning during etching process, and additional polishing after etching. Images below compares the difference before and after polishing.

In Figure A.1 (a), there are clear dark lines from teeth brush. These steins had been removed in Figure A.1 (b) after careful polishing with 0.05 μm paste.

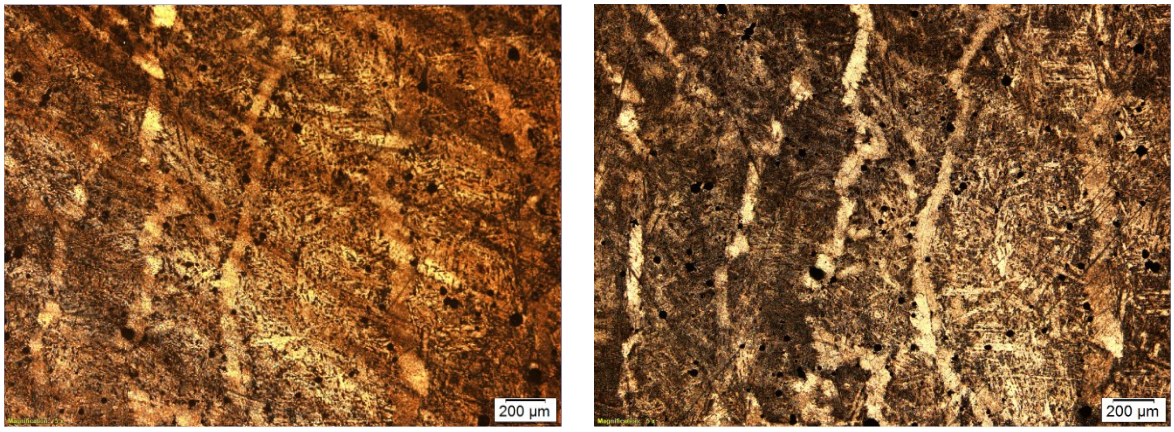

(a) (b)

Figure A.1 Picric acid etching at 65˚C-35min (a) before polishing (b) after polishing

B. PAG Size Measurement

Prior austenite grain size was measured by using ImageJ on the 4% Picral solution with additional HCl as shown in Figure B.1. There were prior austenite grain size, ferrite grain size and second phase width measurements in this study. The long solid lines were measuring the average size of the prior austenite grain. The short solid lines on light parts were measuring the width of ferrite. The short solid lines on darker parts were measuring the width the second phase near the centerline segregation region.

Figure B.1 PAG size measurement example- slab D (MR=2)

Table B-1 below is an example of the measurement for Mannesmann 2 and Mannesmann 3 samples.

Table B-1 PAG size measurement example.

Mannesmann 2 Sample			Mannesmann 3 Sample		
PAGB size	Second Phase Width	PAG ferrite size	PAGB size	Second Phase Width	PAG ferrite size
um	um	um	um	mm	um
402.0	405.1	53.7	1197.2	428.2	62.5
417.0	163.6	56.6	709.6	456.5	50.2
614.0	385.3	44.0	1862.4	608.1	89.3
1425.0	911.4	47.9	1338.4	498.7	65.7
528.0	844.9	59.0	769.2	735.6	39.3
955.0	770.1	68.7	300.8	492.4	123.1
790.0	505.0	32.1	690.8	570.1	91.7
818.0	146.4	100.6	436.4	661.8	53.3
377.0	463.6	161.5	710.8	891.8	62.2
430.0	673.4	166.9	1058.0	810.7	86.2
1162.0	637.0	67.1	1062.4	935.3	44.8
908.0	267.0	58.9	658.4		58.2
985.0		51.5	446.4		69.0
233.0		43.2	370.0		53.7
363.0		50.3	629.2		53.5
452.0		112.9	341.2		84.1
386.0		82.0	783.2		74.2
394.0		86.2	550.4		30.2
839.0		70.4			28.4
1523.0		67.3			36.6
989.0		74.5			52.8
590.0		55.3			37.9
614.0		45.0			36.3
764.0		59.4			35.2
608.0		80.5			113.1
688.0		54.2			73.1
823.0		94.9			77.8
414.0		17.2			71.7
959.0		26.8			82.5
		72.1			67.5
		51.9			83.1
		63.4			74.2
		57.6			100.0
		90.3			106.3
		88.8			92.0
		64.0			78.5
		34.5			34.5
		49.4			52.1
		74.2			41.5
		63.5			31.8
		74.2			29.4
		55.6			34.5

C. EMPA Condition Analysis Position

As shown in Figure C.1, the locations of the EMPA line scans were perpendicular to the microhardness scans. To compare the different operational conditions for quantitative microprobe analysis, two different setups were tested. Point spacing was compared at closed position as showing in the following Figure. The upper line has smaller point spacing (4 μm) than the lower one (10 μm).

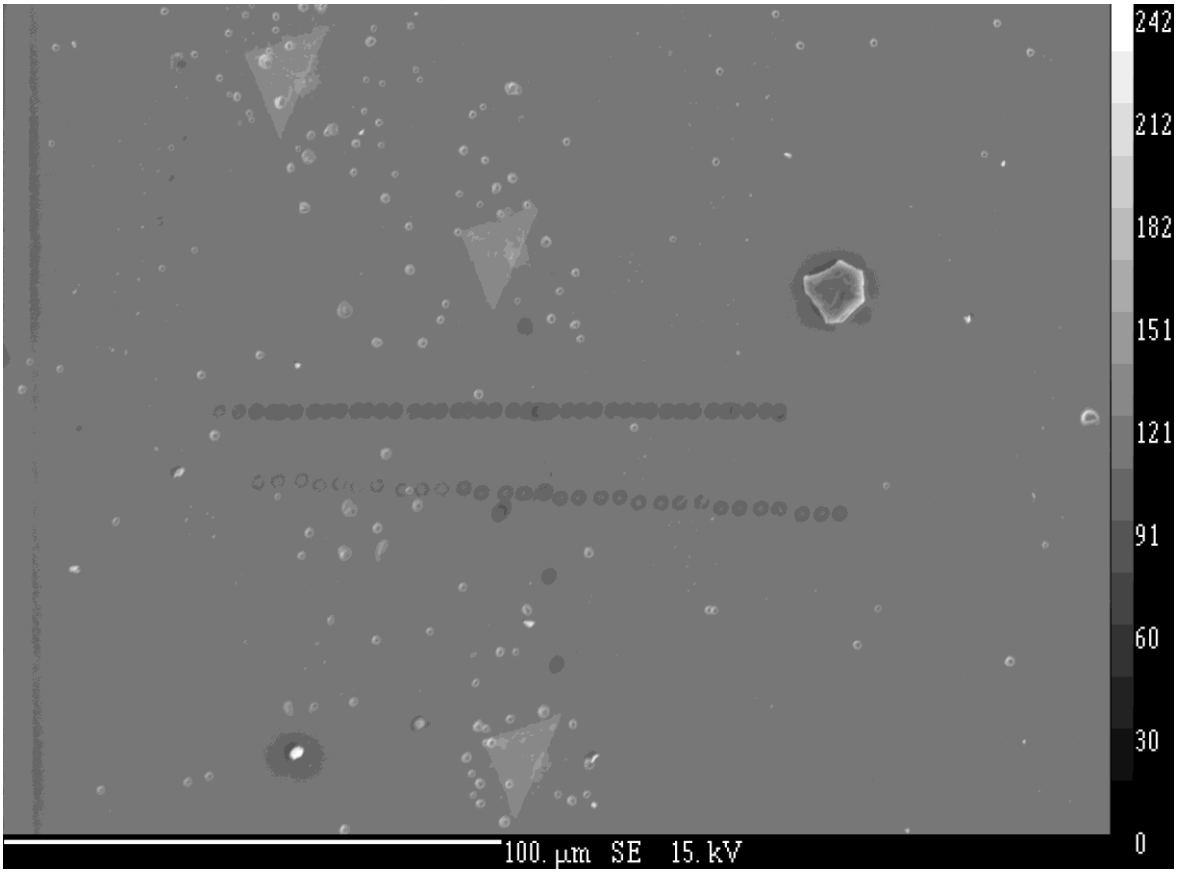

Figure C.1 EMPA point spacing comparison with fully focused beam Pipe B (MR=3).

D. EMPA Quantitative Results Example

Table D-1 is an example of the EMPA line scan results, which includes operational condition, element concentration, detection limit, relative error, XYZ position, diffraction crystal, counting time, number of counts, standard used, etc. The current used here was 30 nA, which is for demonstration.

Table D-1 EMPA results example.

SAMPLE	B3S left full line	B3S left full line	B3S left full line	B3S left full line
NUMBER	2	2	2	2
TAKEOFF	40	40	40	40
KILOVOLT	15	15	15	15
CURRENT	30	30	30	30
BEAMSIZE	10	10	10	10
LINE	21	22	23	24
REL. LINE	1	2	3	4
Si WT%	0.28925	0.283333	0.270356	0.263709
Mo WT%	0.150432	0.101021	0.107067	0.13615
Mn WT%	1.72885	1.80524	1.65434	1.68517
Cr WT%	0.215908	0.231596	0.224372	0.216177
Mn WT%	0	0	0	0
Fe WT%	97.5	97.5	97.5	97.5
TOTAL	99.8845	99.9212	99.7561	99.8012
Si AT%	0.57428	0.56223	0.537462	0.52411
Mo AT%	0.087434	0.058684	0.06231	0.079214
Mn AT%	1.75479	1.83133	1.68133	1.71221
Cr AT%	0.231547	0.248237	0.240935	0.232075
Mn AT%	0	0	0	0
Fe AT%	97.352	97.2995	97.478	97.4524
TOTAL	100	100	100	100
Si CDL99	0.006452	0.006407	0.006454	0.006437
Mo CDL99	0.032485	0.033915	0.033997	0.03343
Mn CDL99	0.008891	0.008833	0.008794	0.008763
Cr CDL99	0.014697	0.01469	0.014654	0.014711
Mn CDL99	0	0	0	0
Si %ERR	1.32509	1.34166	1.40075	1.42738
Mo %ERR	11.8376	17.4589	16.5931	13.2022
Mn %ERR	0.535881	0.521465	0.549023	0.54255

Cr %ERR	3.71877	3.49753	3.58829	3.71709
Mn %ERR	0	0	0	0
X-POS	8322	8322	8322	8322
Y-POS	15383	15283	15183	15083
Z-POS	84	84	84	85
RELDIST	0	100	200	300
BEAMCURR	30.2148	30.2163	30.2163	30.2163
BEAMCURR2	30.2209	30.2194	30.2179	30.2209
Si ka (1,LTAP) ONTIM	80	80	80	80
Mo la (2,PET) ONTIM	80	80	80	80
Mn ka (3,LLIF) ONTIM	80	80	80	80
Cr ka (4,PET) ONTIM	80	80	80	80
Mn ka (5,LLIF) ONTIM	0	0	0	0
Si ka (1,LTAP) HITIM	40	40	40	40
Mo la (2,PET) HITIM	40	40	40	40
Mn ka (3,LLIF) HITIM	40	40	40	40
Cr ka (4,PET) HITIM	40	40	40	40
Mn ka (5,LLIF) HITIM	0	0	0	0
Si ka (1,LTAP) LOTIM	40	40	40	40
Mo la (2,PET) LOTIM	40	40	40	40
Mn ka (3,LLIF) LOTIM	40	40	40	40
Cr ka (4,PET) LOTIM	40	40	40	40
Mn ka (5,LLIF) LOTIM	0	0	0	0
Si ka (1,LTAP) ONCNT	15.7001	15.4241	15.1452	14.9149
Mo la (2,PET) ONCNT	0.36569	0.335353	0.342532	0.364026
Mn ka (3,LLIF) ONCNT	13.3587	13.7883	12.7725	13.0217
Cr ka (4,PET) ONCNT	3.83792	3.95052	3.8899	3.84666
Mn ka (5,LLIF) ONCNT	13.9011	14.4961	13.3828	13.5419
Si ka (1,LTAP) OFCNT	7.21549	7.11382	7.21661	7.18071
Mo la (2,PET) OFCNT	0.214557	0.233862	0.234971	0.227238
Mn ka (3,LLIF) OFCNT	3.10788	3.06674	3.04112	3.01937
Cr ka (4,PET) OFCNT	2.27627	2.27506	2.26599	2.28243
Mn ka (5,LLIF) OFCNT	0	0	0	0
Si ka (1,LTAP) NECNT	8.48465	8.31031	7.9286	7.73423
Mo la (2,PET) NECNT	0.151133	0.101491	0.107561	0.136788
Mn ka (3,LLIF) NECNT	24.152	25.2177	23.1142	23.5443
Cr ka (4,PET) NECNT	1.56165	1.67545	1.62391	1.56422
Mn ka (5,LLIF) NECNT	0	0	0	0
Si ka (1,LTAP) K-RAW	0.008081	0.007915	0.007551	0.007366
Mo la (2,PET) K-RAW	0.001256	0.000843	0.000894	0.001137
Mn ka (3,LLIF) K-RAW	0.017484	0.018255	0.016732	0.017044

Cr ka (4,PET) K-RAW	0.002962	0.003177	0.00308	0.002967
Mn ka (5,LLIF) K-RAW	0	0	0	0
DATETIME	42268.70907	42268.71088	42268.71266	42268.71446
Si Z-COR	0.8888	0.8888	0.8888	0.8888
Mo Z-COR	1.0851	1.0851	1.0851	1.0851
Mn Z-COR	1.0183	1.0183	1.0183	1.0182
Cr Z-COR	0.9996	0.9996	0.9996	0.9995
Mn Z-COR	0	0	0	0
Si A-COR	1.6429	1.643	1.6432	1.6432
Mo A-COR	1.1044	1.1044	1.1044	1.1044
Mn A-COR	1.0022	1.0022	1.0022	1.0022
Cr A-COR	1.006	1.006	1.006	1.006
Mn A-COR	0	0	0	0
Si F-COR	0.9989	0.9989	0.9989	0.9989
Mo F-COR	0.9999	0.9999	0.9999	0.9999
Mn F-COR	0.9689	0.969	0.9688	0.9689
Cr F-COR	0.7281	0.728	0.7277	0.7279
Mn F-COR	0	0	0	0
Si ZAF	1.4586	1.4587	1.4589	1.4588
Mo ZAF	1.1983	1.1983	1.1983	1.1982
Mn ZAF	0.9888	0.9889	0.9887	0.9887
Cr ZAF	0.7322	0.7321	0.7317	0.7319
Mn ZAF	0	0	0	0
Si MAC	2289.642	2290.787	2287.635	2288.479
Mo MAC	1111.294	1111.72	1109.976	1110.272
Mn MAC	83.53062	83.41969	83.30726	83.41349
Cr MAC	108.0834	107.9397	107.7948	107.9317
Mn MAC	0	0	0	0
Si ka (1,LTAP) KRAT	1.98E-03	1.94E-03	1.85E-03	1.81E-03
Mo la (2,PET) KRAT	1.26E-03	8.43E-04	8.93E-04	1.14E-03
Mn ka (3,LLIF) KRAT	1.75E-02	1.83E-02	1.67E-02	1.70E-02
Cr ka (4,PET) KRAT	0.0029487	3.16E-03	3.07E-03	2.95E-03
Mn ka (5,LLIF) KRAT	0	0	0	0
Si STD_NUM	10	10	10	10
Mo STD_NUM	29	29	29	29
Mn STD_NUM	19	19	19	19
Cr STD_NUM	27	27	27	27
Mn STD_NUM	19	19	19	19
Si STD_NAM	Sanidine	Sanidine	Sanidine	Sanidine
Mo STD_NAM	Mo metal	Mo metal	Mo metal	Mo metal
Mn STD_NAM	Mn metal	Mn metal	Mn metal	Mn metal

Cr STD_NAM	Cr inclusions	Cr inclusions	Cr inclusions	Cr inclusions
Mn STD_NAM	Mn metal	Mn metal	Mn metal	Mn metal

E. EMPA MapsJ Macro

The EMPA maps were processed by using ImageJ, and the macro file was developed based on the EAS colourXray macro v3.0. (Locock, 2015)

```
"// This macro will try to process all files in a "source" folder
// and convert them into TIF format and store them in a "target" folder.
// Note: The macro converts the files to 8-bit grayscale prior to colouring.

dir1 = getDirectory("Choose Source Directory ");
dir2 = getDirectory("Choose Destination Directory ");
list = getFileList(dir1);
setBatchMode(true);
for (i=0; i<list.length; i++) {
        showProgress(i+1, list.length);
        filename = dir1 + list[i];
        run("Open...", "open="+dir1+list[i]+" image=[16-bit Unsigned] offset=0 number=1 gap=0");
        run("8-bit");
        run("16_Colors");
        run("Enhance Contrast", "Saturated pixels=[0.4] Normalize");
        saveAs("Jpeg", dir2+list[i]);
        close();
}
Dialog.create("Process done");
Dialog.addMessage(i+" files have been processed.\nYou can find the converted files in:\n"+dir2);
Dialog.show();"
```

F. MATLAB Code for Image Analysis

Main program:

```
Start_frame = 1;
End_frame = 1;

T_min =[0 20];
T_max = [20 40];

Name_frame = 'man1c-';
Output_name = 'Area_fraction.txt';

Area_fraction_main_multiple_temperature( Start_frame, End_frame, T_min,
T_max, Name_frame, Output_name);
open('Area_fraction.txt');
```

Function:

```
function Area_fraction_main_multiple_temperature( Start_frame, End_frame,
T_min, T_max, Name_frame, Output_name )

n = End_frame - Start_frame + 1 ;

n_multi = size(T_min,2);

for i = 1 : n
    N_frame( i, 1 ) = Start_frame + ( i - 1 ) ;
    filename = [ Name_frame num2str( N_frame(i,1) ) '.txt' ] ;
    T( :, : ) = load( filename ) ;
    for j = 1:n_multi
        fraction( i, j ) = Area_fraction( T, T_min(1,j), T_max(1,j) ) /
100 ;
    end
end

ratio = [ N_frame fraction ];


% plot( N_frame, fraction, 'o' )

a = ['Frame  - T min - ' num2str(T_min)];
b = ['number - T max - ' num2str(T_max)];
c = num2str(ratio);

fid = fopen(Output_name, 'w'); % w for write
fprintf(fid, '%s\r\n', a);
fprintf(fid, '%s\r\n', b);
fprintf(fid, '%s\r\n', c);
fclose(fid);

% save( 'Area_fraction.txt', 'ratio', '-ASCII')
```

```
function ratio = Area_fraction( T, T1, T2 )

number = 0 ;

b = length( T( 1, : ) ) ;
a = length( T( :, 1 ) ) ;


for i = 1 : a
    for j = 1 : b
        if( T( i, j ) >= T1 && T( i, j ) < T2)
           number = number + 1;
        else
           number = number + 0;
        end
    end
end

ratio = ( number / ( a * b ) ) * 100 ;
```

G. Mn Concentration Comparison for Homogenized Sample

Figure and Figure below are the example of Mn composition through the segregation band at the whole sample width before and after homogenization at 1100˚C and 16 h for Mannesmann 2 and Mannesmann 3 samples respectively.

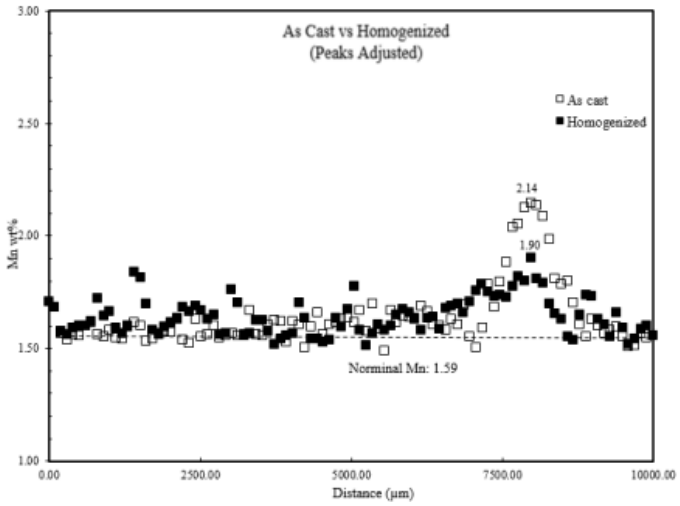

Figure G.1 Mn concentration before and after homogenization for MR 2 as-cast and as-homogenized at 1100˚C-16h.

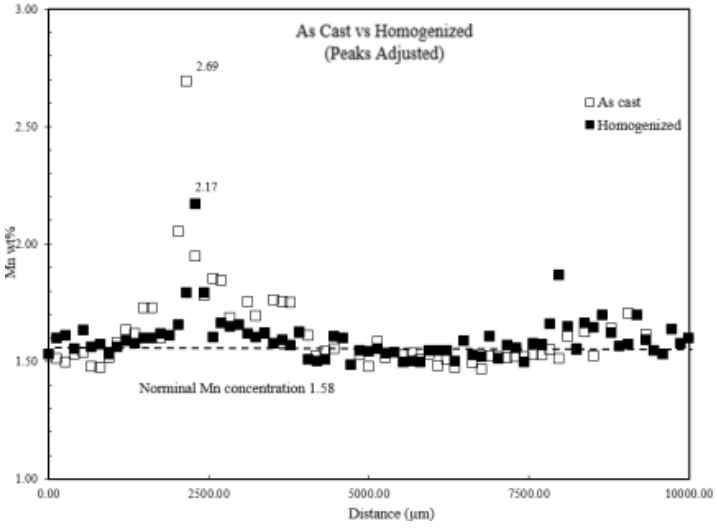

Figure G.2 Mn concentration before and after homogenization for MR 3 as-cast and as-homogenized at 1100˚C-16h.

H. EMPA Background

H.1 Interaction Volume

Interaction volume of electron beam in the solid is the region between the solid and the beam. It is caused by the effect of elastic and inelastic interactions of the electron beam in the solid. (Everhart, 1972) As shown in Figure , The size of interaction volume is called effective electron beam size that affects the microprobe analyzing setups.

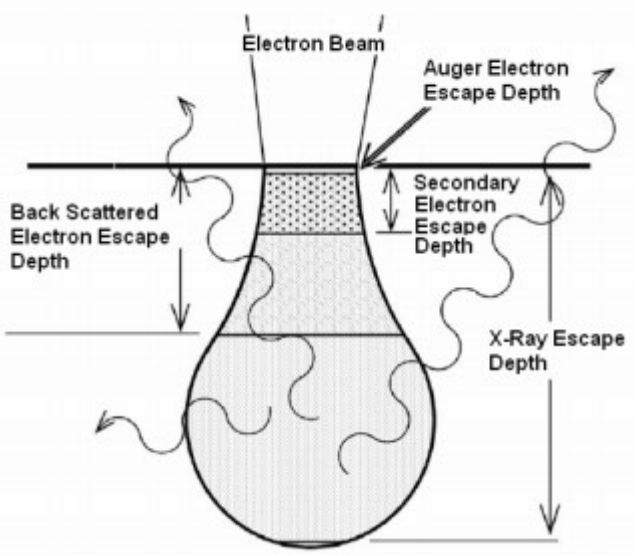

Figure H.1 Schematic diagram of interaction volume. (Hafner, 2007)

$$x\ (\mu m) = \frac{0.1\ E_0^{\ 1.5}}{\rho} \qquad \text{H-1}$$

$$y\ (\mu m) = \frac{0.077\ E_0^{\ 1.5}}{\rho} \qquad \text{H-2}$$

Equation H-1 and H-2 are the calculation formula for the depth and width of the effective beam size, respectively, (Potts, 1987) where x and y are the depth of electron penetration and width of the excited volume, respectively; E_0 is the accelerating voltage of the electron beam (keV); and ρ is the density of the analyzing solid (g/cm^3).

H.2 Diffraction Crystal

WDS has higher detection limit than EDS due to the improved spectral resolution, sensitivity and the ability to detect light elements. (Ul-Hamid, 2006) Using a diffraction crystal to select the specified wavelength makes WDS a quantitative analysis for element detection.

As shown in Figure , X-rays will be diffracted by the designed crystal and X-ray detector is placed at the calculated distance for the target element from Bragg's Law.

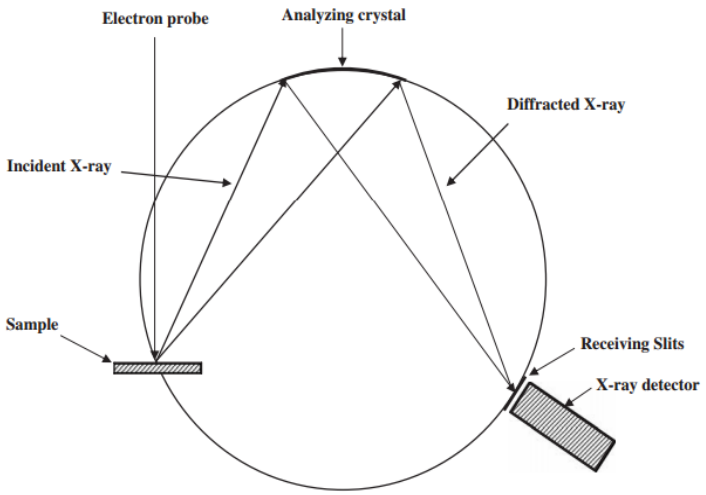

Figure H.2 Schematic diagram of WDS setup. (Ul-Hamid, 2006)

The selection of the crystal is based on its capability of resolving peaks. The selection is based on the lattice spacing of the crystal (2d) and an example of crystal selection could be found in Table . The Kα line is used as default since it is the most intensive line for detection. The Kα is the major line used in this study. (Bearden, 1967)

Table H-1 Diffraction crystal selection example. (Laboratory, 2015)

Name	Crystal Description	2d (Å)	Kα	Lα
TAP	Thallium Acid Phthalate	25.756	F – P	Mn - Nb
PET	Pentaerythritol	8.745	Si – Fe	Sr – Tb
LIF	Lithium Fluoride	4.027	Ca – Rb	Te – U
LDE1	Layered Dispersion Element	60	C – Ne	Cl – Zn
LDE2	Layered Dispersion Element	98	B – O	P – Mn

I. Shot Gun Analysis Example Results

Summary of shot gun analysis results for slab D and E were prepared in Table and I-2 respectively. A shot gun analysis is one where a number of elemental analyses are carried out in a region of interest. In this region, the elemental analysis is measured along a line using data collected every 50 μm. In this work 4 to 5 lines were used for the 'shot gun; analysis in a given region of interest. Comparing the results in Tables 7.4 for the as cast and homogenized sample, there does not appear to be a significant difference between measured values. The contrary applies in the case of the MR=3 samples

Table I-1 Elements average before and after homogenization slab D (MR=2) at 1200 °C-16h.

	Si	Mo	Nb	Cr	Mn
Nominal wt%	0.26	0.138	0.09	0.22	1.59
As-cast wt%	0.295	0.112	0.102	0.226	1.761
Standard Deviation	0.032	0.023	0.133	0.033	0.209
As-homo wt%	0.291	0.104	0.139	0.224	1.733
Standard Deviation	0.026	0.032	0.234	0.011	0.176

Table I-2 Elements average before and after homogenization slab E (MR=3) at 1200 °C-16h.

	Si	Mo	Nb	Cr	Mn
Nominal wt%	0.24	0.137	0.089	0.24	1.58
As-cast wt%	0.348	0.076	0.585	0.279	2.32
Standard Deviation	0.033	0.053	0.481	0.029	0.26
As-homo wt%	0.341	0.105	0.34	0.273	2.018
Standard Deviation	0.07	0.019	0.291	0.018	0.076

J. Sum Seg Analysis

Microhardness distribution example

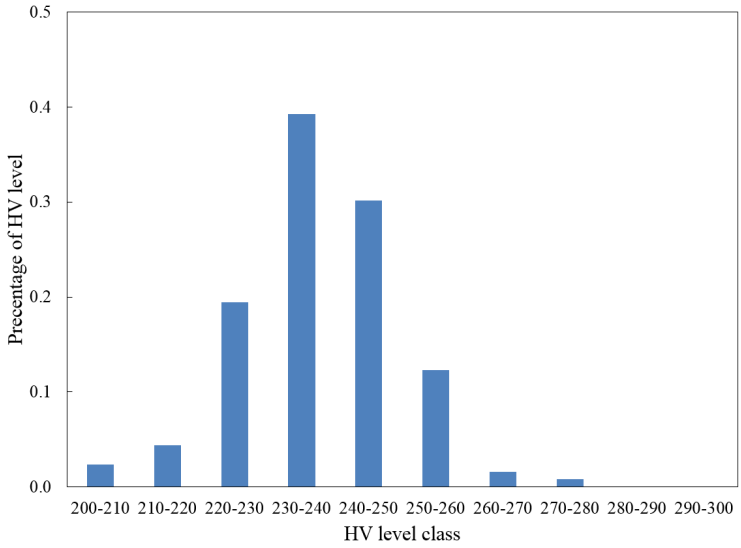

Figure J.1 Microhardness distribution of slab D (MR=2).

PAGS distribution example

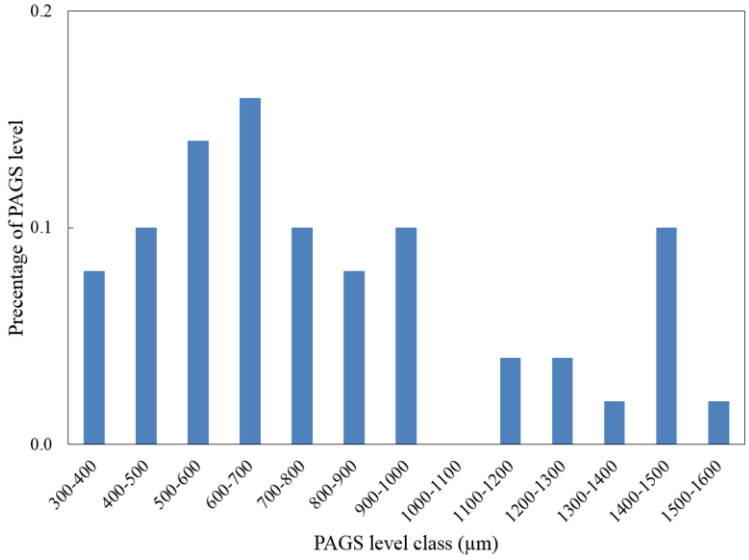

Figure J.2 PAGS distribution of slab D (MR=2).

Mn composition distribution example:

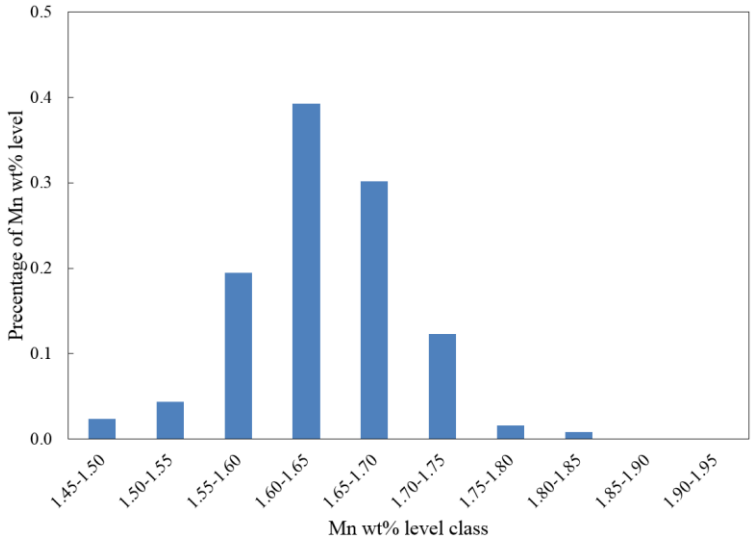

Figure J.3 Mn composition distribution of slab D (MR=2).